Sheffield Hallam University

A Sheffield Hallam University thesis

FT-infrared and pyroelectric studies on

calix[8]arene Langmuir-Blodgett films

Pierre Anthony Rees Oliviere

A thesis submitted in partial fulfilment of the requirements of

Sheffield Hallam University

for the degree of Doctor of Philosophy

July 2001

Collaborating Organisation: University of Sheffield

Abstract

Pierre Anthony Rees Oliviere
Thesis submitted for the degree of Doctor of Philosophy
July 2001

FT-infrared and pyroelectric studies on calix[8]arene Langmuir-Blodgett films

Pyroelectric activity is exhibited by materials which possess a spontaneous temperature-dependent electric polarisation. These materials generate a current as their temperature is changed. Many classes of organic materials exhibit pyroelectric activity but only if processed in such a way that a non-centrosymmetric arrangement of dipole results. When deposited as alternate layers by the Langmuir-Blodgett (LB) technique a macroscopically polar assembly is formed. To date, the best performance has been achieved by alternately depositing two materials, one containing acid groups and the other containing amine groups. Calixarenes are one family of materials which are particularly good vehicles for the acid and amine groups. Alternate layer LB films of acid- and amine-substituted calixarenes have high pyroelectric coefficients and form extremely robust films.

Fourier transform infrared (FTIR) spectroscopy is a useful tool in examining the properties of thin film samples. Using the FTIR techniques of attenuated total reflection (ATR) and reflection-absorption infrared spectroscopy (RAIRS) it is possible to study the behaviour of the acid and amine groups within the pyroelectric samples.

This thesis describes the pyroelectric properties of a series of calix[8]arenes. The dependence of the pyroelectric coefficient on temperature, film thickness and substituent chain length is analysed. The infrared spectra show that the acid and amine groups interact by proton transfer but also that the remaining acid groups form either facing dimers with the amine or sideways dimers between themselves. The spectra do not change with temperature. This demonstrates that the films are thermally stable. Additionally, this invariance shows that the pyroelectric activity in these films does not arise from a change in the proton transfer as has been previously postulated. Theoretical calculations undertaken predict that the source of the dipole change required for the level of pyroelectric activity seen is likely to be a change in distance between the acid and amine groups. Further observations, quantitatively examined by curve fitting techniques, show that the greater the number of proton-transferred pairs, the lower the pyroelectric coefficient. Thus, only the temperature-dependent separation of the acid and amine pairs which have not undergone proton transfer is responsible for the pyroelectric activity in these systems.

Acknowledgements

1. INTRODUCTION

2. LANGMUIR-BLODGETT DEPOSITION 15

4. PYROELECTRIC ANALYSIS

5. ROOM TEMPERATURE INFRARED ANALYSIS

6. VARIABLE TEMPERATURE INFRARED ANALYSIS 100

xi

FT-infrared and pyroelectric studies on calix[8]arene Langmuir-Blodgett films

1. Introduction

1.1 Aims

Calixarenes are a family of materials which have a wide range of potential applications[1,2] and thus are the subject of a great deal of research. Additionally, much progress has been made in the field of organic heat sensors, especially using films of materials containing acid and amine groups.

The focus of this study is a group of specially synthesised calixarenes containing such moieties. These materials have been made to allow them to be deposited as thin films by the Langmuir-Blodgett (LB) technique. Films of these calixarenes, when deposited in an alternate layer structure, have already been shown to be pyroelectric.[3,4]

The main aim of this project is to investigate the structural and electrical properties of thin multilayered films of these carboxylic acid- and amine-substituted calix[8]arenes. The pyroelectric nature of these calixarene assemblies will be assessed for the various combinations of materials available. This is the first step in understanding the pyroelectric mechanism since any variations in the pyroelectric effect due to small variations in the molecular structure will be revealed.

The next stage in understanding these systems is the use of the Fourier-transform infrared (FTIR) methods of attenuated total reflection (ATR) and reflection-absorption infrared spectroscopy (RAIRS). It is the interaction between the acid and amine groups which is thought to be the main mechanism for pyroelectricity. The FTIR spectroscopic techniques of ATR and RAIRS make it possible to observe the carboxylic acid and amine bands in these types of thin films.[5] By monitoring the behaviour of these bands

2

under various conditions, an insight into the pyroelectric effect can be gained.

Firstly, a picture of the systems at room temperature can be built up in order to understand the structure of the films as well as the state of the acid and amine bands at a fixed temperature. Secondly, the behaviour of the relevant bands can be monitored whilst the temperature of the film is varied. Hence, the correspondence between the measured pyroelectric coefficient and the acid and amine moieties can be analysed. An added benefit of using FTIR is that any other changes in films structure can also be examined and hence any secondary mechanisms of pyroelectricity may also come to light.

1.2 Pyroelectric LB films

In order for a material to display pyroelectric properties, it must possess a temperature-dependent polarisation. In the case of organic materials, this requirement means that there must be an overall dipole across the sample in one preferred direction. Generally, for materials in which the molecules are arranged randomly, there will be no net polarisation across the sample. Therefore, a way of arranging the molecules in a non-centrosymmetric manner is needed to ensure that there will be an overall polarisation across the sample. The Langmuir-Blodgett deposition technique provides the means to manufacture thin films of organic materials in a highly ordered way.

Extensive research has been undertaken into the pyroelectric behaviour of organic Langmuir-Blodgett films. A variety of systems have been studied, such as ion complexes,[6,7] molecules displaying a large internal dipole,[8] polymers,[9] even biological molecules[10] as well as alternate layer structures of two different materials.[11,12] The greatest success has been obtained by using alternate-layer structures of materials in

3

which carboxylic acid and amine groups on different molecules are brought together by alternate layer LB deposition. Various carrier molecules have been used, from simple straight chain systems[11,13] to polymeric siloxanes.[14] It has been found that while it is the acid and amine pairing which provide the source of the pyroelectric activity in such systems, the form of the molecules used has a significant effect on the resultant pyroelectric coefficient. To date, calixarenes have been shown to be the best vehicles for the acid and amine moieties.[15]

1.2.1 The pyroelectric coefficient

A pyroelectric material has a net polarisation in one direction. At a constant temperature, this polarisation is masked by surface charges. For a sample with parallel plate type electrodes, the surface charges induce image charges.[7] When a change in temperature, δT, occurs, a change in polarisation perpendicular to the plates, δP_3, results. This in turn gives rise to a change in surface charge, δQ, on the electrodes, described by the following relationship:

$$\frac{\delta Q}{\delta T} = \frac{\delta(P_3 A)}{\delta T}$$

Equation 1-1

where A is the electrode area.

The pyroelectric coefficient, Γ, is defined as the rate of change of polarisation with temperature.[16] It has components in all directions but only the component perpendicular to the plane of the electrodes, Γ_3, is usually measured. Assuming that the sample experiences constant stress, σ, (i.e. it is free to expand) the pyroelectric coefficient is then:

4

$$\Gamma_3 = \frac{1}{A}\left(\frac{\partial Q}{\partial T}\right)_\sigma + \frac{Q}{A^2}\left(\frac{\partial A}{\partial T}\right)_\sigma$$

Equation 1-2

The second term in this relationship arises from the thermal expansion of the sample, since all pyroelectric materials are also piezoelectric. However, in the case of the thin film samples under analysis, the change in electrode area on heating is negligible. In addition, alternate layer acid/amine LB systems have been found to display particularly low piezoelectric coefficients.[17] Therefore, the second term is effectively zero and can be ignored, leaving:

$$\Gamma = \frac{1}{A}\left(\frac{\partial Q}{\partial T}\right)_\sigma$$

Equation 1-3

The subscript on the pyroelectric coefficient will be omitted for brevity from now on since pyroelectric measurements are invariably made using a parallel plate electrode system. Therefore, all pyroelectric coefficients quoted can be assumed to be the Γ_3 components of the pyroelectric vector.

It should be noted that equation 1-3 combines the primary and secondary pyroelectric contributions. These are the temperature dependent spontaneous polarisation and the change in polarisation due to the mechanical deformations of the material respectively. Further analysis is required to separate these components but this will not be discussed here. The interested reader is referred elsewhere.[18]

1.3 Materials

The main focus of the project is on calixarenes but other materials have been used to provide a base from which to study the calixarenes. A description of all the materials used is given here.

1.3.1 Straight chain materials

The straight chain materials used were stearic acid and octadecylamine (Aldrich >99.5%) [Figure 1-1]. The abbreviations SA for stearic acid and ODA for octadecylamine will be used from now on. These materials were used to provide a background before moving onto calixarenes.
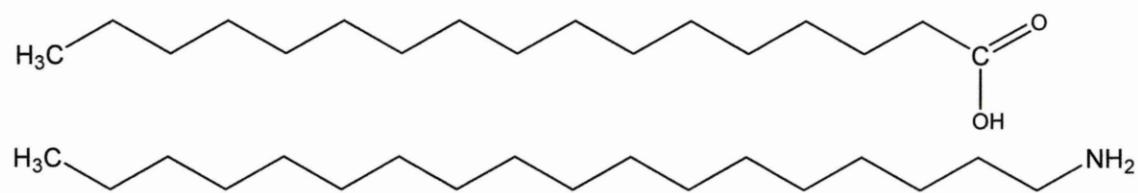
Figure 1-1: Stearic acid (SA, top) and octadecylamine (ODA, bottom).

1.3.2 Calixarenes

Calixarenes, as a family of chemicals, have shown much potential in a variety of applications.[1,2] Most importantly for this work, LB films of substituted calixarenes can be used in heat sensing devices.[19] Indeed, a number of the applications of calixarenes arise because their chemical structure may be modified to a significant degree while still allowing their deposition in the form of LB films.[20] The LB technique is essential for the realisation of a wide variety of functional devices;[21] calixarenes are thus an ideal family of materials to use in such contexts. An illustration of this is that nanoparticles have been made using LB films of the same calixarenes used in this work.[22]

Chemical sensing is a wide field in which the calixarene family of materials have shown great promise. Again, LB films have been used in the construction of sensors.[23,24]

6

However, calixarenes may also be incorporated into sensing devices by various other means and have been shown to be useful in a huge range of detection applications.[25] Their chemical versatility is such that, with suitable modification, selective complexes may be formed with a vast number of ionic species.[26] This is the first stage in the development of ion-selective sensors such as for the detection of sodium,[27] calcium,[28] lead[29] or organic amides among many others.[30] Calixarenes have also been used in the form of self-assembled systems to detect organic compounds in water[31] and volatile organic compounds.[32] In addition to the range of species which may be detected by calixarenes, their usefulness as sensing materials is increased by the fact that they can provide several different transduction modes.[33]

The name, meaning a cuplike (calix) aromatic hydrocarbon (-arene), is derived from the Greek, kalux, meaning husk, shell or pod and refers to the most common shape adopted by the molecules. The monomer of the basic calixarene consists of a benzene ring with a hydroxyl group adjacent to a CH_2 "link". At least four of these monomers form a ring to give rise to the calixarene oligomer, for example eight units for a calix[8]arene [Figure 1-2].
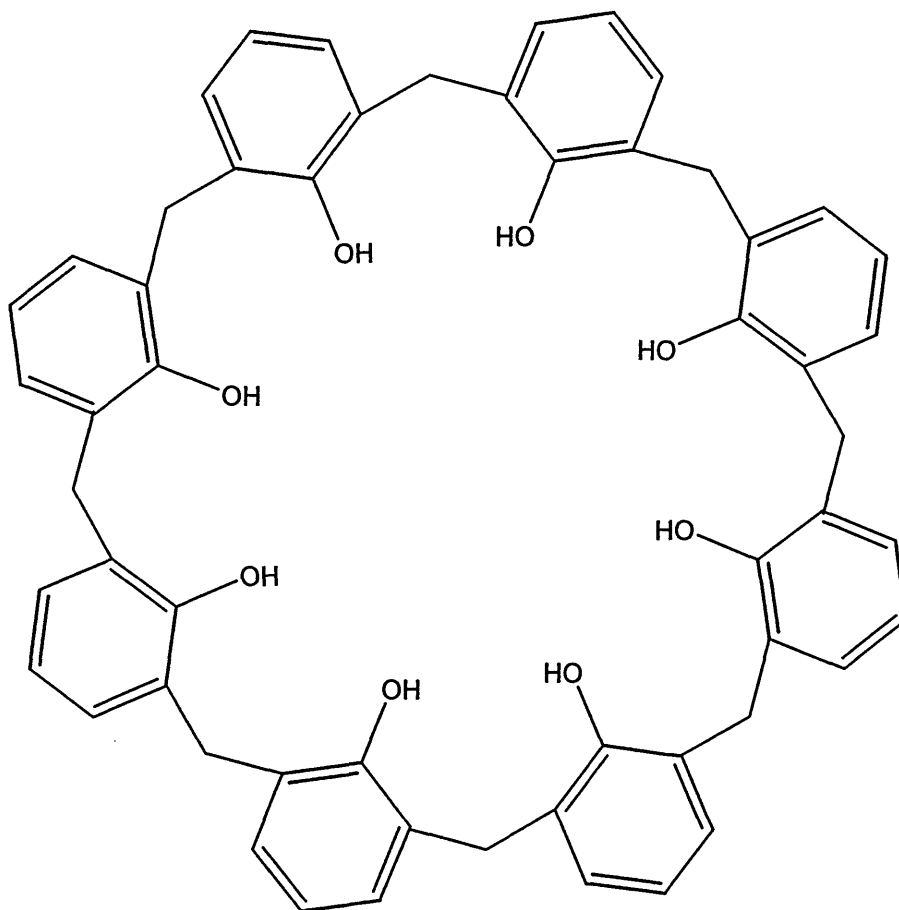
Figure 1-2: Calix[8]arene.

When drawn in this manner the true shape is not obvious. In reality, the conformation of the molecule is such that the hydroxyl groups are at the lower part of a bowl formed by the benzene rings. Figure 1-3 is an example of the form of these molecules. The bowl shape can clearly be seen in this projection.
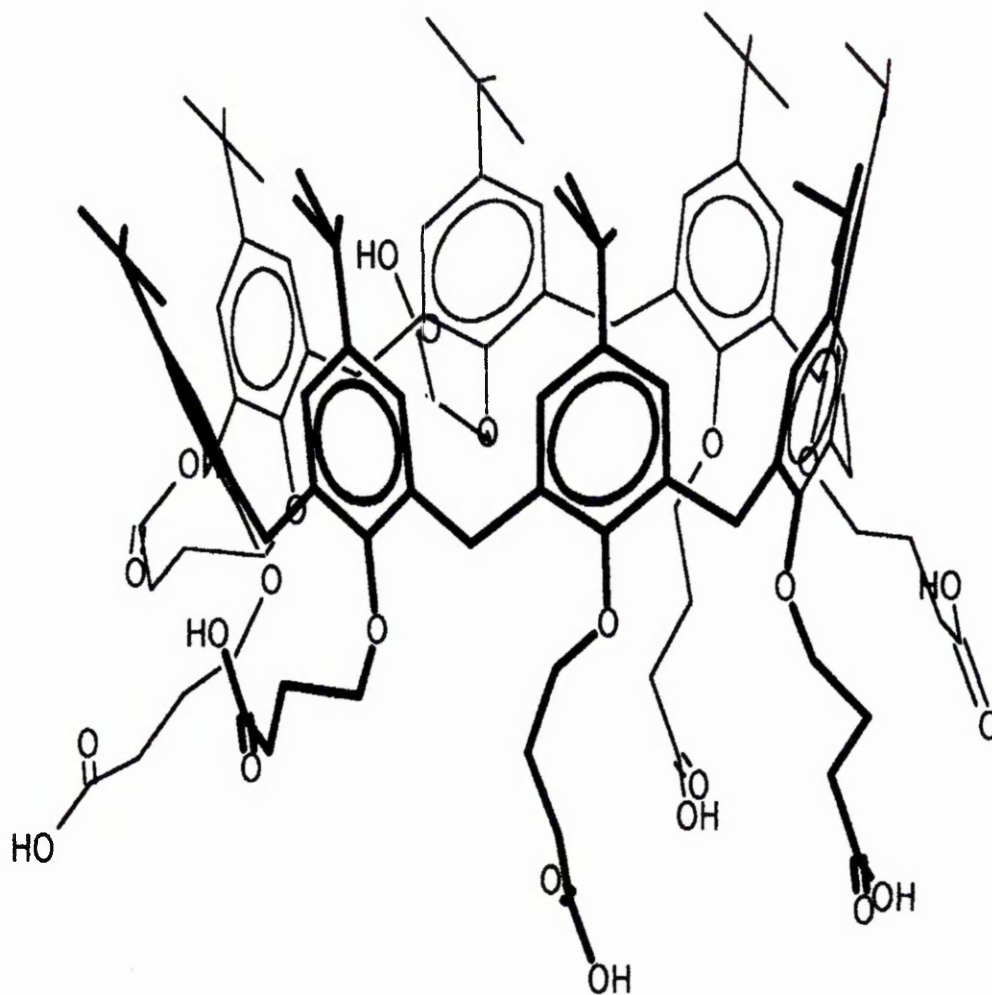
Figure 1-3: Side view of C3 molecule.

In order to display pyroelectric activity, the calixarenes must be modified. Firstly, carboxylic acid and amine groups must be introduced and secondly the molecules must be capable of forming Langmuir-Blodgett assemblies. To satisfy the first condition the hydroxyl groups on the lower rim have been substituted for a short alkyl chain terminated by either a carboxylic acid or amine moiety. Subsequently, the hydrogen atoms on the top rim have been replaced by a t-butyl group to allow LB deposition. The changes made are summarised in Figure 1-4 and Table 1-1 along with the abbreviations used throughout this thesis.

9
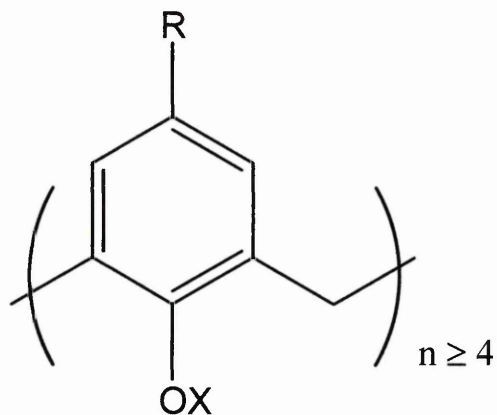
Figure 1-4: General form of substituted calixarene.

Material	Abbreviation	R	X
Amine-substituted calix[8]arene	AM	t-butyl	$(CH_2)_3NH_2$
Acid-substituted calix[8]arene	C1	t-butyl	CH_2COOH
Acid-substituted calix[8]arene	C3	t-butyl	$(CH_2)_3COOH$
Acid-substituted calix[8]arene	C5	t-butyl	$(CH_2)_5 COOH$

Table 1-1: Substituent groups and abbreviations used.

1.4 Résumé of thesis

The background to the pyroelectric effect has been covered in this chapter. A description of the aliphatic materials, used for the background work, as well as the calix[8]arenes under analysis in this project has been given.

Chapter 2 concerns the technique of Langmuir-Blodgett deposition. The preparation of films is described, starting with those containing a single material before going on to look at the method of making alternate layer structures. The different types of

10

assemblies obtainable by LB deposition are shown, with emphasis on those which result in the non-centrosymmetry required for pyroelectric behaviour.

The infrared techniques used to study the thin films under analysis in this thesis are covered in chapter 3. Firstly, a general background to FTIR spectroscopy is given, followed by a description of ATR and RAIRS. The reasons for choosing these methods to study LB films are outlined.

The pyroelectric analysis of the calixarene systems is the subject of chapter 4. Initially, the measured physical properties of the materials on the water surface are discussed. Then the system used to make the pyroelectric measurements is presented. Finally, the pyroelectric results obtained are shown and analysed along with some suggested theories regarding the possible mechanisms of the pyroelectric effect in the calixarene films.

The FT-infrared results obtained at room temperature form chapter 5. Firstly, the spectra obtained of the aliphatic systems are shown and the pertinent bands identified. This is followed by the ATR and RAIRS results obtained for the calixarene assemblies, both individually and as alternate layer systems.

Chapter 6 starts by examining the *ex situ* spectra taken of the alternate layer calixarene films at room temperature and at an elevated temperature. This is followed by a description of the specially designed apparatus used to obtain FTIR spectra at different temperatures *in situ*. The results obtained from the *in situ* measurements are then presented and their implications discussed, in particular with respect to the pyroelectric measurements obtained in chapter 4.

Chapter 7 summarises the important results and conclusions and finishes with some suggestion for continuing the research in future.

1.5 References

[1] C. D. Gutsche, Calixarenes, The Royal Society of Chemistry, 1989.

[2] C. D. Gutsche, Calixarenes revisited, The Royal Society of Chemistry, 1998.

[3] T. Richardson, M. B. Greenwood, F. Davis, C. J. M. Stirling, Pyroelectric Molecular Baskets: Temperature-Dependent Polarization from Substituted Calix(8)arene Langmuir-Blodgett Films, Langmuir, 1995, 11, 4623-4625.

[4] T. Richardson, M. B. Greenwood, F. Davis, C. J. M. Stirling, Calix(8)arene LB superlattices: Pyroelectric molecular baskets, IEE Proceedings-circuits devices and systems, 1997, 144, 2, 108-110.

[5] W. H. Abd. Majid, T. H. Richardson, D. Lacey, A. Topacli, Qualitative evaluation of pyroelectric mechanisms in Langmuir-Blodgett films containing a cyclic polysiloxane substituted with aliphatic side chains using Fourier transform infrared (FTIR) spectroscopy, Thin Solid Films, 2000, 376, 225-231.

[6] R. Colbrook, T. Richardson, M. W. Poulter, G. G. Roberts, M. E. C. Polywka, S. G. Davies, Pyroelectric organo-ruthenium Langmuir-Blodgett superlattices, Materials Science and Engineering, 1990, B7, 189-193.

[7] R. Colbrook, D.Phil. Thesis, Pyroelectric Langmuir-Blodgett Films, University of Oxford, 1990.

[8] T. Kamata, J. Umemura, T. Takenaka, N. Koizumi, Relationship between pyroelectricity and molecular orientation in alternate Langmuir-Blodgett films, Journal of Physical Chemistry, 1991, 95, 4092-4098.

[9] K. A. Fiebig, E. Dormann, Dielectric and pyroelectric properties of Langmuir-Blodgett film capacitors, Applied Physics A, 1991, 52, 268-272.

[10] M. Petty, J. Tsibouklis, M. C. Petty, W. J. Feast, Pyroelectric behaviour of synthetic biomembrane structures, Thin Solid Films, 1992, 210/211, 320-323.

[11] C. A. Jones, M. C. Petty, G. G. Roberts, G. Davies, J. Yarwood, N. M. Ratcliffe, J. W. Barton, IR studies of pyroelectric Langmuir-Blodgett films, Thin Solid Films, 1987, 155, 187-195.

[12] M. B. Greenwood, T. Richardson, D. W. Bruce, D. M. Taylor, D. Lacey, J. Yarwood, Characterisation of LB multilayers and ABABA alternate layer superlattices incorporating iridium alkoxystilbazoles, Thin Solid Films, 1996, 284-285, 46-48.

[13] G. H. Davies, J. Yarwood, M. C. Petty, C. A. Jones, Fourier transform IR studies of alternate layer acid-amine Langmuir-Blodgett films with pyroelectric properties, Thin solid films, 1988, 159, 461-467.

[14] D. Lacey, S. J. Holder, W. H. A. Majid, R. Capan, T. Richardson, High pyroelectric sensitivity in alternate layer Langmuir-Blodgett superlattices, Materials Science & Engineering C-Biomimetic Materials Sensors And Systems, 1995, 3(3-4), 197-203.

[15] C. M. McCartney, PhD thesis, Electrical and structural properties of calixarenes, University of Sheffield, 1998.

[16] S. B. Lang, Sourcebook of Pyroelectricity, Gordon and Breach, 1974.

[17] P. E. Dunn, M. W. Poulter, G, G, Roberts, The measurement of the piezoelectric effect in Langmuir-Blodgett films, Thin Solid Films, 1992, 210, 338-340.

[18] R. Çapan, PhD thesis, The Pyroelectric Effect in Langmuir-Blodgett Films Containing Linear Polysiloxanes, University of Sheffield, 1998.

[19] C. M. McCartney, T. Richardson, M. A. Pavier, F. Davis, C. J. M. Stirling, The temporal and thermal stability of pyroelectric calix[8]arene Langmuir-Blodgett films, Thin Solid Films, 1998, 329, 431-434.

[20] F. Davis, A. J. Lucke, K. A. Smith, C. J. M. Stirling, Order and Structure in Langmuir-Blodgett Mono- and Multilayers of Resorcarenes, Langmuir, 1998, 14, 4180-4185.

[21] G. G. Roberts, Langmuir-Blodgett Films, Plenum Press, New York, 1990.

[22] A. V. Nabok, T. Richardson, C. McCartney, N. Cowlam, F. Davis, C. J. M. Stirling, A. K. Ray, V. Gacem, A. Gibaud, Size-quantization in extremely small CdS clusters formed in calixarene LB films, Thin Solid Films, 1998, 327-329, 510-514.

[23] A. V. Nabok, N. V. Lavrik, Z. I. Kazantseva, B. A. Nesterenko, L. N. Markovskiy, V. I. Kalchenko, A. N. Shivaniuk, Complexing properties of calix[4]resorcinolarene LB films, Thin Solid Films, 1995, 259, 244-247.

[24] A. K. Hassan, A. V. Nabok, A. K. Ray, F. Davis, C. J. M. Stirling, Complexation of metal ions with Langmuir-Blodgett films of novel calixarene azo-derivative, Thin Solid Films, 1998, 329, 686-689.

[25] D. Diamond, K. Nolan, Calixarenes: Designer Ligands for Chemical Sensors, Analytical Chemistry, 2001, 73, 22A-29A.

[26] R. Ludwig, Calixarenes in analytical and separation chemistry, Fresenius Journal of Analytical

Chemistry, 2000, 367, 103-128.

[27] J. A. J. Brunink, J. R. Haak, J. G. Bohmer, D. N. Reinhoudt, M. A. McKervey, S. J. Harris, Chemically modified field-effect transistors; a sodium ion selective sensor based on calix[4]arene receptor molecules, Analytica Chimica Acta, 1991, 254, 75-80.

[28] T. McKittrick, D. Diamond, D. J. Marrs, P. O'Hagan, M. A. McKervey, Calcium-selective electrode based on a calix[4]arene tetraphosphine oxide, Talanta, 1996, 43, 1145-1148.

[29] F. Cadogan, P. Kane, M. A. McKervey, D. Diamond, Lead-Selective Electrodes Based on Calixarene Phosphine Oxides Derivatives, Analytical Chemistry, 1999, 71, 5544-5550.

[30] K. M. O'Connor, D. W. M. Arrigan, G. Svehla, Calixarenes in Electroanalysis, Electroanalysis. 1995, 7, 205-215.

[31] C. Marenco, C. J. M. Stirling, J. Yarwood, Thiacalixarene self assembled monolayers on roughened gold surfaces and their potential as SERS-based chemical sensors, Journal of Raman Spectroscopy, 2001, 32, 183-194.

[32] D. L. Dermondy, R. M. Crooks, T. Kim, Interactions between organised, surface confined monolayers and vapour-phase probe molecules. 11. Synthesis, characterization and chemical sensitivity of self-assembled polydiacetylene/calix[n]arene bilayers, Journal of the American Chemical Society, 1996, 118, 11912-11917.

[33] D. Diamond, M. A. McKervey, Calixarene-based Sensing Agents, Chemical Society Reviews, 1996, 15-24.

2. Langmuir-Blodgett deposition

2.1 Introduction

This chapter introduces the technique of Langmuir-Blodgett (LB) deposition. Following a brief historical background, a general overview of the equipment used is given. The formation of floating monolayers, their transfer onto solid substrates and the multilayer morphologies obtainable are explained. Finally the alternate layer deposition of calixarenes, which gives rise to films displaying pyroelectric activity, is described. The description given here is necessarily specific to this project. For a broader background to the LB technique, the interested reader is referred elsewhere.[1,2,3]

2.2 Background

The Langmuir-Blodgett technique dates from the early part of the last century and stems from work by Irvine Langmuir and Katherine Blodgett. Based on previous studies by Lord Rayleigh[4] on floating oil layers and Agnes Pockels' detailed investigations of surface tension,[5,6] Langmuir proved that such layers were just one single molecule thick.[7] Blodgett achieved the next important step in transferring the floating Langmuir layer onto a solid substrate.[8]

The LB technique uses the fact that amphiphilic molecules spread to a single molecular thickness on a water surface. When bounded by a moveable barrier, this layer can be compressed such that a two dimensional solid is formed. It is this solid layer which is transferred to a substrate forming a Langmuir-Blodgett film.

2.3 Materials

Materials must have certain properties if they are to be used to form Langmuir-Blodgett films. Firstly, they must be insoluble in water and thus form a floating monolayer at the water surface. Secondly, they need to be readily soluble in a suitable solvent so that they may be spread easily onto the water surface. Additionally, there is often a requirement that the material will arrange itself such that all the molecules are orientated in the same direction. The latter is achieved by using molecules which are amphiphiles, that is, have both hydrophobic and hydrophilic parts.

The most common hydrophilic groups are hydroxyl (-OH), amine ($-NH_2$) and carboxylic acid (-COOH), the latter two being useful for the generation of pyroelectricity. The hydrophobic part is generally a unit containing aliphatic chains, aromatic rings or a combination of these. This portion of the molecule also ensures that the first requirement, of insolubility in water, is fulfilled. Two groups of materials were used in this study; straight chain molecules and calixarenes. Both of these sets of molecules were described in Chapter 1.

2.4 The Langmuir trough

The basic piece of equipment used to make LB films is the Langmuir trough [Figure 2-1]. The apparatus is made up of a PTFE trough (not shown) filled with ultra pure water, known as the subphase. The barrier is a PTFE-coated fabric belt which is stretched around six PTFE rollers. This is then half submerged into the water so that there is a confined surface area within the barrier. This arrangement is known as a constant-perimeter system[9] as the area within the barrier can be adjusted while the perimeter

16

length remains unchanged. The area is controlled automatically during deposition using a feedback mechanism operating between the Wilhelmy balance and the barrier motors, in order to maintain a constant pre-set surface pressure [section 2.5.1]. The final part is the deposition system which allows the substrate to be passed up and down through the air-water interface at a controlled speed. This is very important as the speed of deposition can affect the final morphology of an LB film.[10]
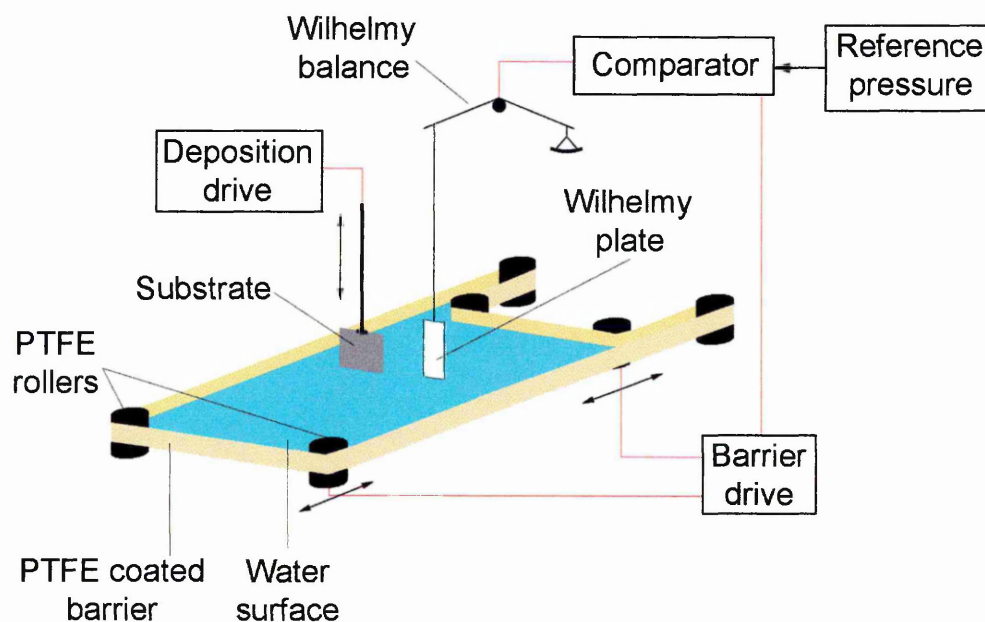
Figure 2-1: The components of a Langmuir trough.

2.5 Monolayer formation

The material to be used must first be dissolved in a suitable solvent; chloroform has been used for all the materials in this project. The solution is then spread over the water surface, drop by drop, while the area within the barrier is maintained at maximum.
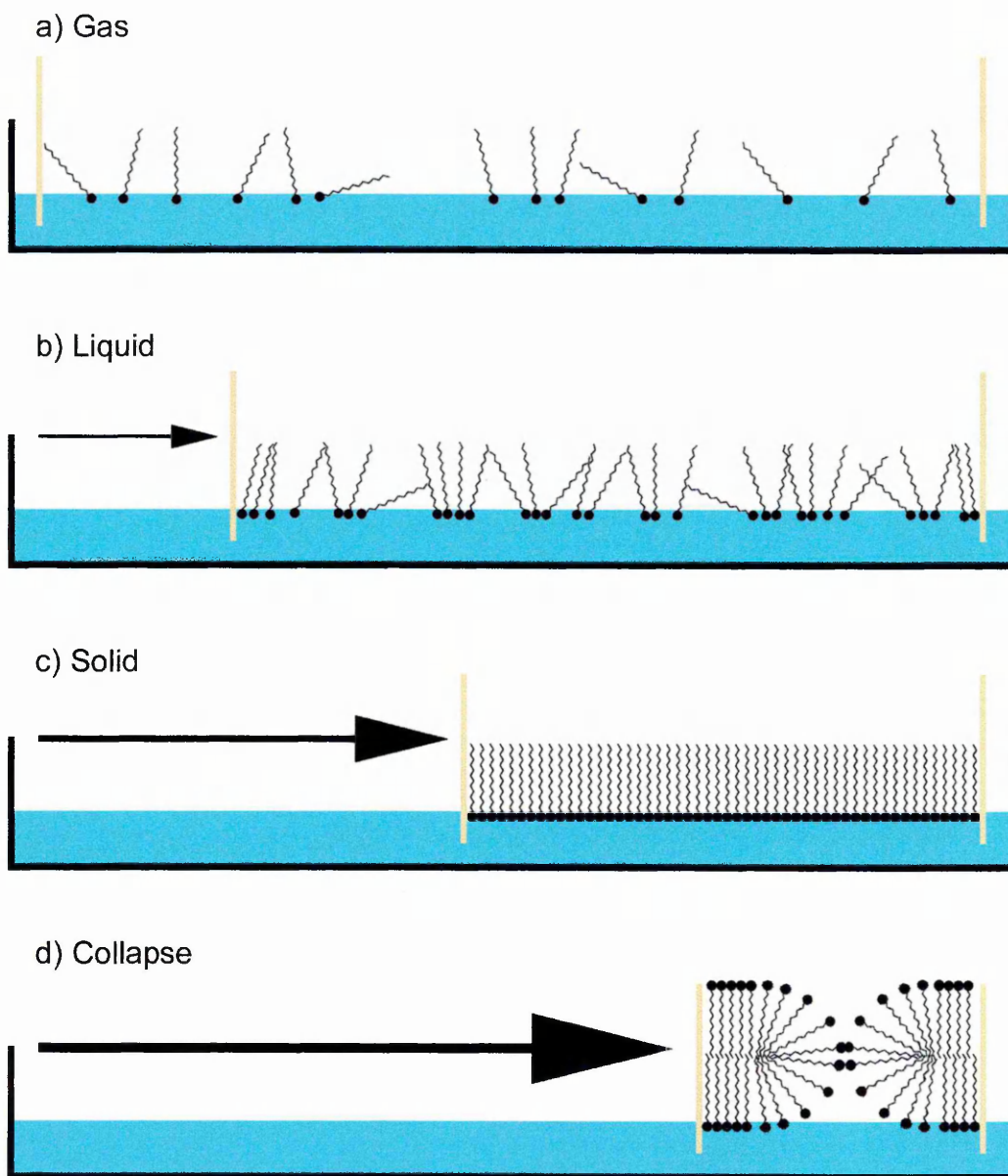
Figure 2-2: Phases of a floating monolayer.

After the solvent has been allowed to evaporate, the molecules on the surface are well separated with no significant interaction between molecules. This can be thought of as a two-dimensional equivalent of a gas [Figure 2-2a]. The barrier is then gradually closed, reducing the available surface area. At some point, the monolayer enters a liquid phase [Figure 2-2b] where the molecules interact but retain a great deal of molecular freedom. Eventually, as the available area is reduced further, a solid phase is reached

18

[Figure 2-2c]. A true monolayer has now been formed and the molecules are closely packed and highly ordered. If the monolayer is compressed further, the film will collapse forming crystallites or multilayered domains [Figure 2-2d].

2.5.1 The Wilhelmy method

The phases described above can be defined in terms of surface pressure. As previously mentioned, a Wilhelmy plate is used to monitor the surface pressure. This consists of a piece of filter paper which is hung from an electrobalance such that it dips into the subphase [Figure 2-3].
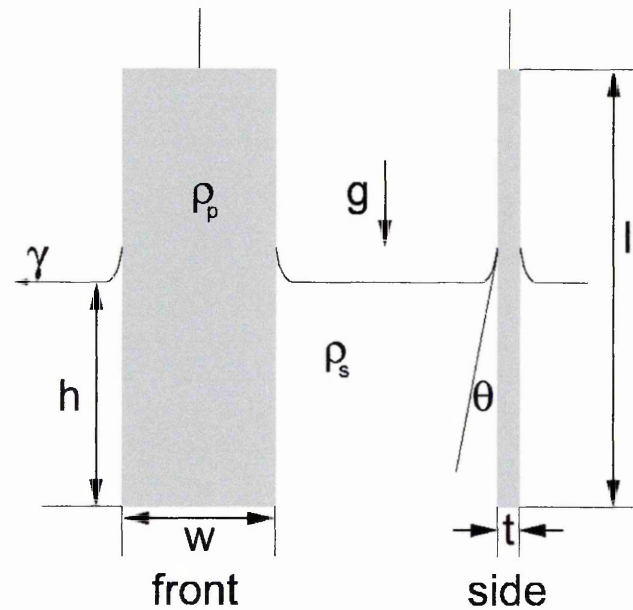
Figure 2-3: The Wilhelmy plate.

The overall force on the plate when it is in the water is the resultant of the downward forces of gravity and surface tension and the upward force due to the buoyancy of the plate. This can be expressed as:

$$F = \rho_p glwt + 2\gamma(t + w)\cos\theta - \rho_s ghwt \qquad \textbf{Equation 2-1}$$

where l, w and t are the plate dimensions,

ρ_p and ρ_s are the densities of the plate and the subphase respectively,

h is the depth of immersion,

γ is the surface tension,

θ is the contact angle of the subphase on the plate and

g is the acceleration due to gravity.

When material is spread onto the surface it causes a decrease in the surface tension and thus a change in the force on the plate. Measurements are made when the Wilhelmy plate is completely wetted and as the plate is chromatography paper, θ is small so $\cos\theta \approx 1$ and $w \gg t$ so $w + t \approx w$. Therefore, the change in the force acting on the plate ΔF is:

$$\Delta F = 2w\Delta\gamma \qquad \textbf{Equation 2-2}$$

where $\Delta\gamma$ is the change in surface tension or the surface pressure. This is given the symbol Π and so:

$$\Pi = \frac{\Delta F}{2w} \qquad \textbf{Equation 2-3}$$

Expressed in units of mNm^{-1}, the surface pressure is a very important parameter in the LB deposition process. It is used to ensure that deposition takes place with the material in the desired phase, usually when the monolayer is a solid.

2.5.2 Isotherms

The measurement of surface pressure is not solely used to control the barrier during deposition. If it is recorded while the barrier is gradually closed the result is a pressure-area (Π-A) isotherm, that is a plot of the surface pressure against the area available to the material [Figure 2-4]. An isotherm can yield a lot of important information about the material concerned. The regions where the material is in the gaseous, liquid and solid phases can be identified, as well as the point of collapse (these are marked on Figure 2-4 as a, b, c and d corresponding to the equivalent parts of Figure 2-2). LB film forming materials show a variety of different behaviours on the water surface and this can be seen in their differing isotherms. The different phases are not always seen [Figure 2-4i] or there may be plateaux [Figure 2-4ii] depending on the shape of the molecule.
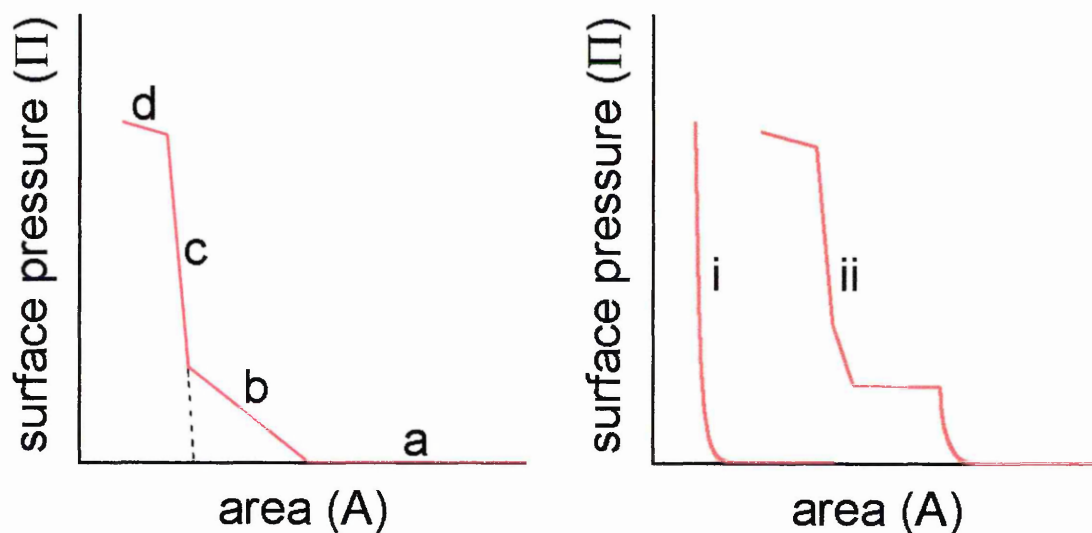
Figure 2-4: An ideal isotherm (left) and some example isotherms (right).

An important feature of isotherms is that they provide a direct measure of cross-sectional molecular area. Extrapolation of the solid phase back to the x-axis (as shown in Figure 2-4) yields the area taken up by the molecules on the surface, A. From this and

knowing the volume, v, and concentration, c, of the solution spread on the water surface, the area per molecule, A_m, is:

$$A_m = \frac{Am}{vcN_A}$$
Equation 2-4

where m is the molecular mass

and N_A is Avagadro's number.

Finally the compressibility of a material can be obtained by measuring the gradient of the relevant part of the isotherm. This can reveal further details regarding the arrangement and packing of molecules on the water surface.

2.6 Deposition

Once the monolayer has been formed at the air-water interface, the next step is to transfer the material onto a substrate. Prior to deposition the substrate to be used must be meticulously cleaned. The silicon ATR crystals were first placed in an ultrasonic bath under chloroform. This was followed by refluxing in pure isopropyl alcohol (IPA) for a minimum of six hours. The latter has the dual benefit of ensuring the cleanliness of the surface and also rendering it somewhat hydrophilic, which aids the transfer of the materials used here. The aluminium-coated glass slides were always freshly made, in the same manner as for the bottom contacts of the pyroelectric devices [chapter 4, section 4.3.1] and then also underwent refluxing in IPA before use.

Deposition is achieved by passing the substrate through the interface. The result is that the molecules adhere to the surface of the substrate, forming an LB monolayer. Multilayers can be built up through repeated transfers in this manner. Depending on the

nature of the material and substrate used, different types of LB films result. The following describes the possible film morphologies when a single material is deposited.

2.6.1 X-, Y- and Z-type deposition

An LB film of a single material can fall into one of three categories: X-; Y- or Z-type. The three possible arrangements arise because material can be deposited in two ways. The substrate can be moved through the floating monolayer from the water to the air (an upstroke, Figure 2-5) or from the air to the water (a downstroke, Figure 2-6). Subsequent layers can then be deposited by repeating the process in the same direction or the other direction.
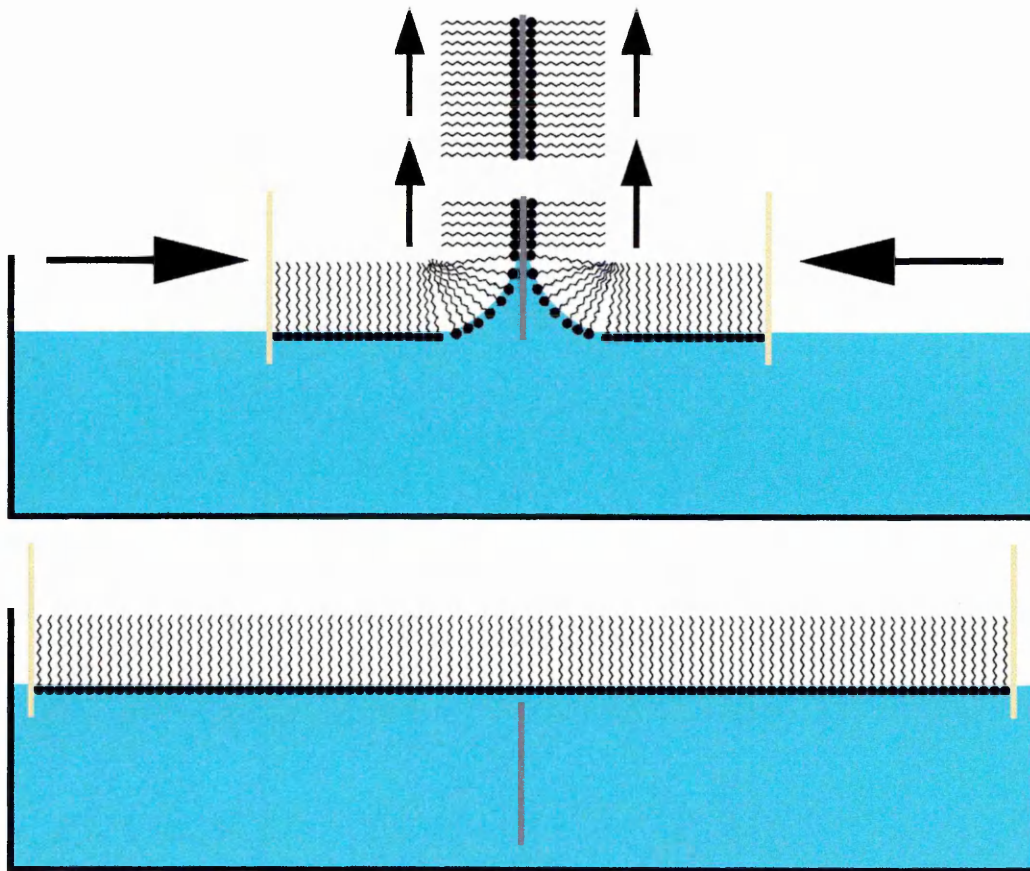
Figure 2-5: Langmuir-Blodgett deposition of one monolayer on an upstroke.

23

If deposition only occurs during the downstroke, an X-type film results [Figure 2-7a]. Likewise, deposition only during the upstroke produces a Z-type film [Figure 2-7c]. A Y-type structure is achieved when a monolayer is transferred both on the upstroke and the downstroke [Figure 2-7b].
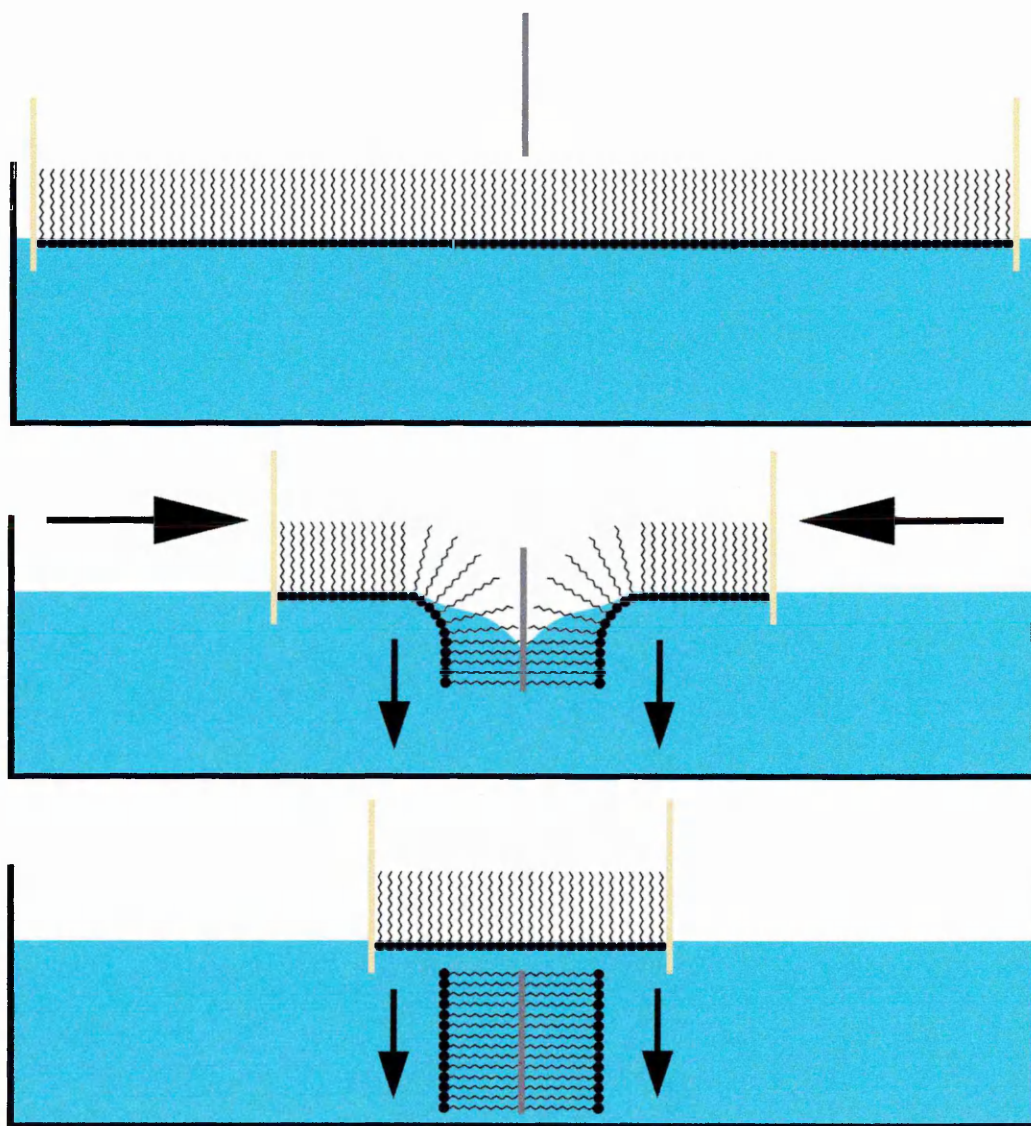
Figure 2-6: Langmuir-Blodgett deposition of one monolayer on a downstroke.

Which film structure is obtained in practice depends on the material itself, the type of substrate used and the design of the trough. Thus, a degree of control over the nature of the LB film is afforded the experimenter. This is important for certain applications, such as pyroelectricity or second harmonic generation, where an overall dipole moment is required. Any molecular dipoles present are cancelled out in a centrosymmetric arrangement such as a Y-type film so a non-centrosymmetric, X- or Z-type film is needed.
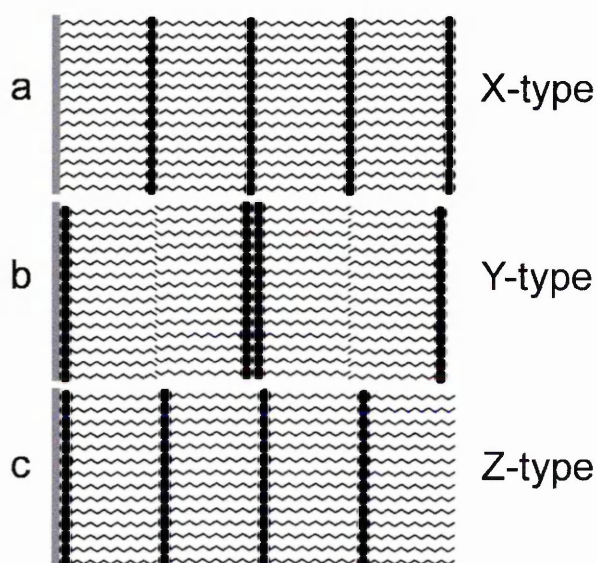
Figure 2-7: Langmuir-Blodgett film structures.

2.7 The alternate layer trough

The pyroelectric LB films described in this thesis consist of two different materials. These systems have been made using a specially designed double trough.[11] This trough has many similarities with that described in section 2.4. The Wilhelmy method is used to measure the surface pressure and the barriers are controlled by the same feedback system. The alternate layer trough is also of the constant perimeter type but the area

within the movable barrier is split by a fixed PTFE barrier. This barrier incorporates the dipping mechanism and sample holder [Figure 2-8]. Each compartment of the trough (A and B) has a separate pressure monitor and barrier drive so each can be independently controlled. This allows the deposition of alternate layers at different pressures.

The dipping mechanism consists of a rotating drum onto which the substrate is mounted. This passes the substrate up through one side and down through the other as it rotates at a controlled speed. With this system, the sample may be rotated in either direction and also the deposition rate can be altered for each section. Therefore, deposition from each compartment of the trough may be made as an upstroke or downstroke and importantly at a different rate from one side to the other. This ensures that each material can be deposited with the optimum parameters needed for a high quality film.
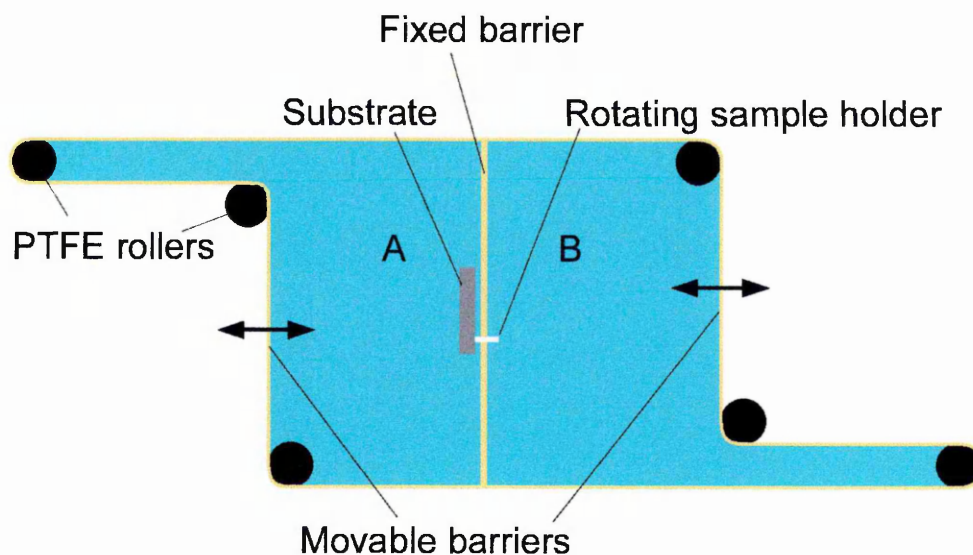
Figure 2-8: Top view of alternate layer trough.

2.7.1 Deposition

The films produced by the alternate layer trough consist of two different materials and so their morphology is not the same as for films made with one material only. As the substrate is passed through each side in turn, layers are built up in the sequence A/B/A/B/A/B ... [Figure 2-9]. The result is that although the structure is similar to the Y-type previously described, as it is composed of two different materials it is non-centrosymmetric.
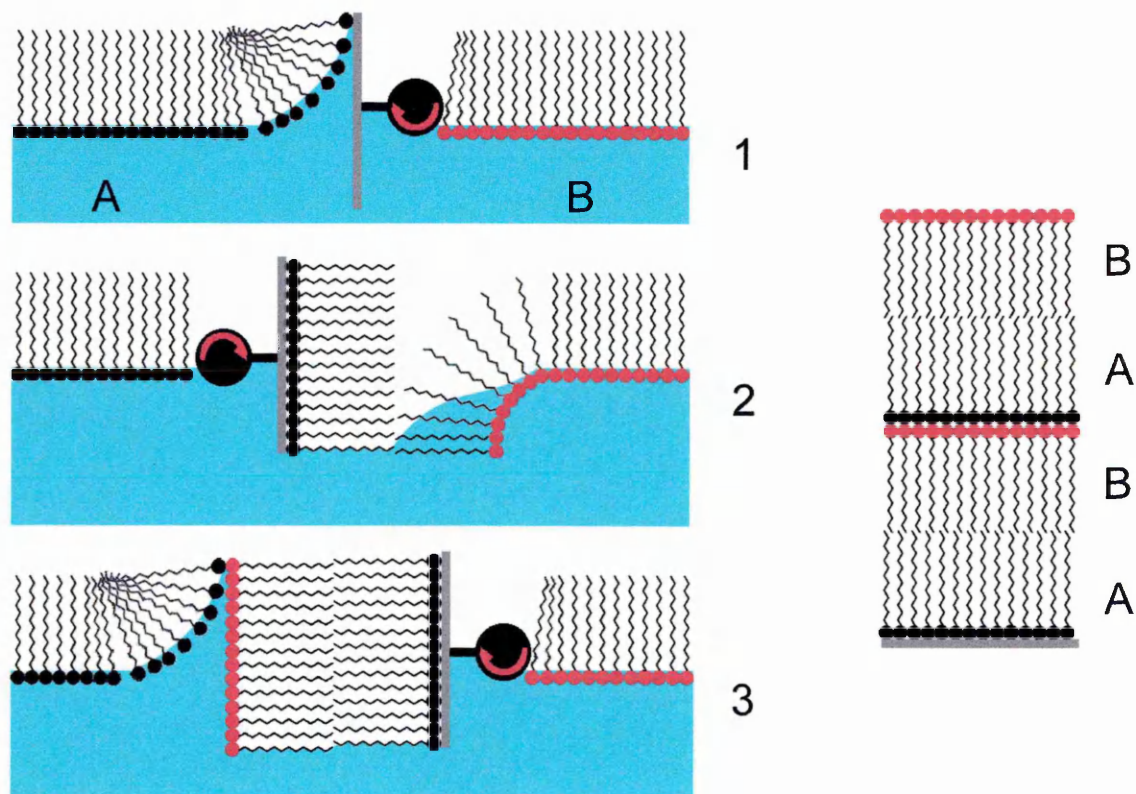
Figure 2-9: Alternate layer deposition (left) and resulting film structure (right).

If the materials are chosen so that their dipoles do not cancel out, a macroscopically polar LB film is produced. In the case of the calixarenes used here, the dipoles in the acid-substituted and amine-substituted materials point in opposite directions with

27

respect to the pendant alkyl chains. Therefore, when such materials are deposited as alternate layer films, their dipoles point in the same direction and a non-zero polarisation results [Figure 2-10]. In this case, there is a temperature-dependent change in the dipole and the films exhibit pyroelectric activity which forms the basis of the research presented in this thesis.
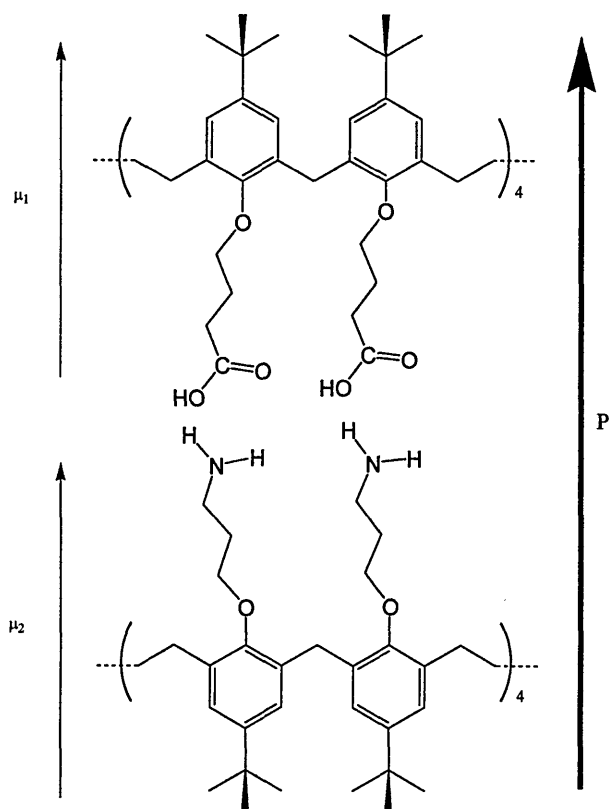
Figure 2-10: Polarisation in an alternate layer LB film.

2.8 Summary

The concept of Langmuir-Blodgett films has been introduced. An overview of the manufacture of monolayer and multilayered systems has been given. This included the methods of measuring the surface pressure and obtaining isotherms of the materials on the water surface. There followed a description of the technique used to make the pyroelectric alternate layer assemblies under investigation here. The reasons behind the need for alternating and thus non-centrosymmetric structures were outlined.

2.9 References

[1] M. C. Petty, Langmuir-Blodgett Films, Cambridge University Press, 1996.

[2] G. Roberts, Langmuir-Blodgett Films, Plenum Press, 1990.

[3] A. Ulman, An introduction to ultrathin organic films: from Langmuir-Blodgett to self assembly, Academic Press, London, 1991.

[4] Lord Rayleigh, Measurements of the Amount of Oil necessary in order to check the Motions of Camphor upon Water, Proceedings of the Royal Society of London, 1890, 47, 364-367.

[5] A. Pockels, Surface tension (Letter to the editor), Nature, 1891, 43, 437-439.

[6] A. Pockels, On the relative contamination of the water-surface by equal quantities of different substances, Nature, 1892, 46, 418-419.

[7] I. Langmuir, The mechanism of the surface phenomena of floatation, Transactions of the Faraday Society, 1920, 15, 62-74.

[8] K. B. Blodgett, Films Built by Depositing Successive Monomolecular Layers on a Solid Substrate, Journal of the American Chemistry Society, 1935, 57, 1007-1022.

[9] L. Blight, C. W. N. Cumper, V. Kyte, Manipulation of insoluble films at an oil/water interface, Journal of Colloid Science, 1965, 20, 393-399.

[10] F. R. Rana, S. Widayati, B. W. Gregory, R. A. Dluhy, Metastability in Monolayer Films Transferred onto Solid Substrates by the Langmuir-Blodgett Method: IR Evidence for Transfer-Induced Phase Transitions, Applied Spectroscopy, 1994, 48, 10, 1196-1203.

[11] B. Holcroft, M. C. Petty, G. G. Roberts, G. J. Russell, A Langmuir trough for the production of organic superlattices, Thin solid films, 1985, 134, 83-88.

3. Infrared Spectroscopy

3.1 Introduction

This chapter describes the theory of infrared spectroscopy. A general background of the technique is given, followed by a more detailed account of Fourier Transform infrared (FTIR) spectroscopy. Finally, the methods of attenuated total reflection (ATR) and reflection-absorption infrared spectroscopy (RAIRS), used for the analysis of the thin films in this project, are covered.

3.2 Background

Infrared radiation was discovered by Sir William Herschel two centuries ago. In the electromagnetic spectrum, it lies beyond the red portion of the visible spectrum in the wavelength range 0.78-1000μm [Figure 3-1]. Infrared radiation is commonly referred to in 'frequency' units of wavenumbers, cm^{-1}, which will be used from now on. Thus the range given above corresponds to ~12800-10cm^{-1}. This generally is divided into three parts: near- (~12800-4000cm^{-1}); mid- (~4000-650cm^{-1}) and far-infrared (~650-10cm^{-1}). Infrared radiation induces transitions between quantized vibrational energy levels and this forms the basis for infrared spectroscopy. The theory of infrared spectroscopy has been amply covered elsewhere[1,2,3,4,5] so only the pertinent aspects will be presented here.
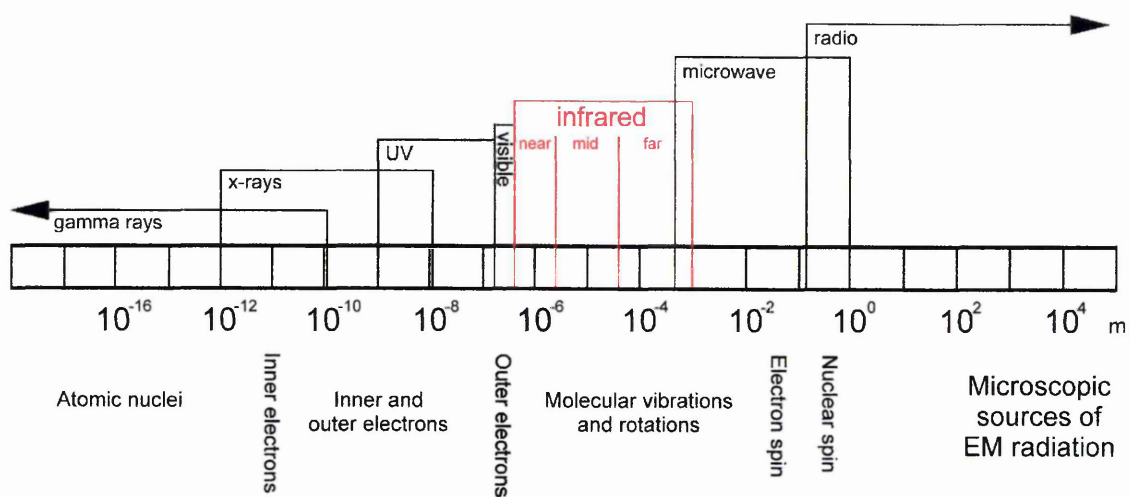
Figure 3-1: The electromagnetic spectrum.
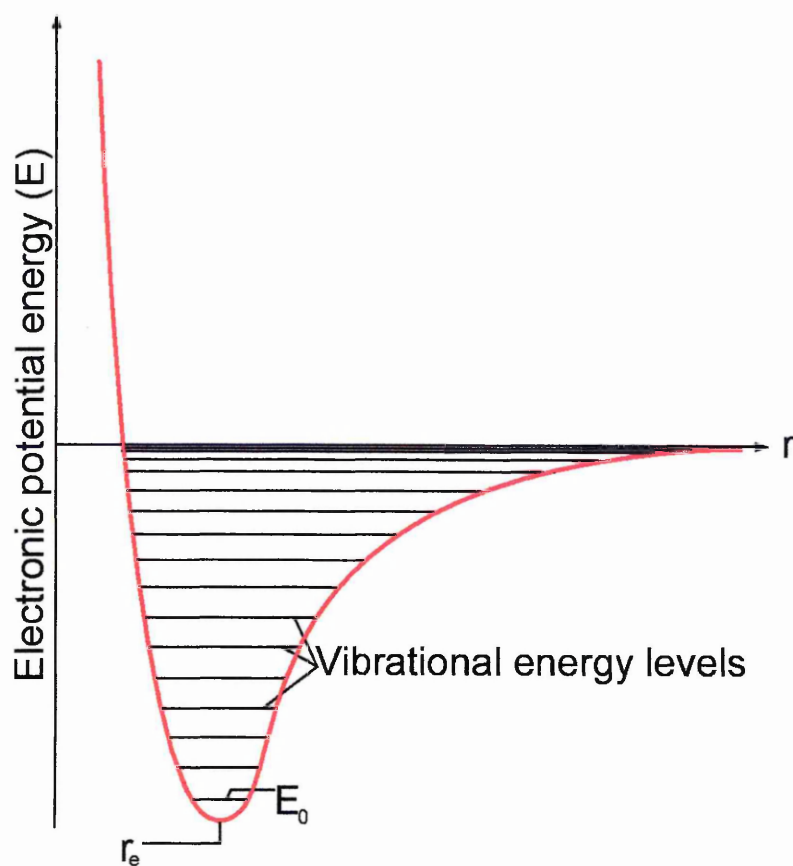
Figure 3-2: The Morse curve, an anharmonic potential for a diatomic molecule.

3.2.1 Interaction of infrared radiation with matter

Electromagnetic radiation interacts with matter across a broad range of energies, with different results. In the case of infrared spectroscopy, this interaction is in the energy range of molecular vibrations and rotations. For electromagnetic radiation, such as infrared, to be able to interact with matter, certain conditions must be met.

Consider the simple case of two atoms joined by a bond. For such a system, the potential energy, E, can be approximated to a Morse curve [Figure 3-2] given by the function:

$$E = D_e \left(1 - \exp[a(r_e - r)]\right)^2 \qquad \textbf{Equation 3-1}$$

where: D_e is the energy of dis-association of the molecule,

r is the internuclear distance,

r_e is the equilibrium distance, i.e. the bond length

and a is a constant.

Applying the Morse function in the Schrödinger equation gives the permitted energy levels as:

$$E_n = h\nu\left(n + \frac{1}{2}\right) - h\nu x_e\left(n - \frac{1}{2}\right)^2 \qquad \textbf{Equation 3-2}$$

where x_e is the anharmonicity constant $= \dfrac{\hbar\omega}{4D_e}$

and n = 0, 1, 2, 3, …

Therefore, for a transition to occur, just the right amount of energy must be absorbed (or emitted) to exactly reach another vibrational state. Thus the selection rule is Δn = +/- 1, +/- 2, +/- 3, …

Additionally, if a molecule is to absorb (or emit) radiation [Figure 3-3a] it must have an associated transition dipole. This means that a change in the dipole moment, μ, [Figure 3-3b] due to a vibration must occur, that is:

$$\frac{\partial \mu}{\partial r} \neq 0 \qquad\qquad\qquad \textbf{Equation 3-3}$$

where r is the molecular separation.

For a non-polar diatomic molecule consisting of two identical atoms (i.e. N_2) $\frac{\partial \mu}{\partial r} = 0$ and there is no infrared spectrum. However, for polyatomic molecules, infrared radiation can be absorbed even though no permanent dipole exists (e.g. benzene) as transition dipoles can occur.
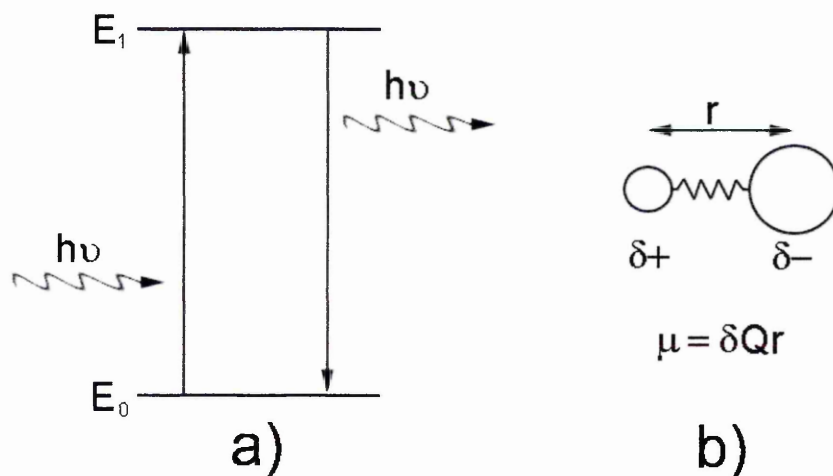
Figure 3-3: Absorption and emission (a) and a molecular dipole (b).

3.2.2 Molecular vibrations

Since the vibrational frequency of a given band is dependent on the atomic masses and bond involved, different molecular groups can be identified by their particular

34

adsorption frequencies. For a molecule of N atoms, 3N-6 separate vibrations can occur. This is because each atom has 3 degrees of freedom, less 3 translation modes (all atoms moving along the same axis) and 3 rotation modes (all atoms rotating around a common axis). Some examples of possible vibrational modes are shown in Figure 3-4.

Generally, the fundamental frequency of a particular vibration is observed, that is an energy change corresponding to $\Delta n = +/- 1$. Other transitions of $\Delta n = +/-2, +/-3$ … are known as overtones and occur at frequencies of twice (first overtone) and three times (second overtone) etc. that of the fundamental vibration. Further types of bands are known as combination and difference bands. These arise from the addition or subtraction respectively of two or more fundamental or overtone bands. At room temperature, overtones and combinations are generally weak and only the fundamental bands are seen.
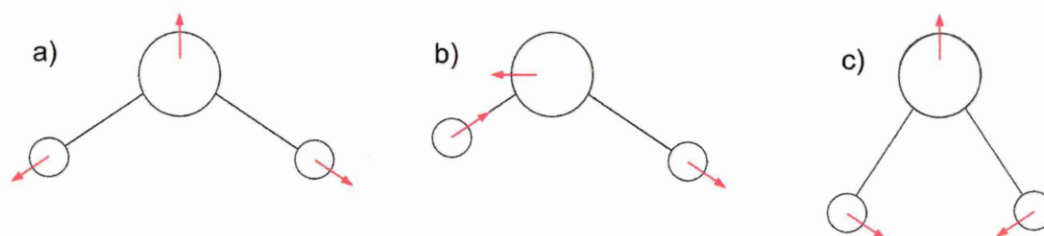
Figure 3-4: Some possible molecular vibrations: a) symmetric stretch; b) antisymmetric stretch; c) bending.

3.2.3 Environmental factors

FTIR spectroscopy does more than indicate which chemical groups and modes are present in a given sample. The absorption bands are affected by a number of factors,

giving rise to tremendous variations in the measured band shape. This can be used to glean information about the environment occupied by any give absorption mode.

The first important effect on the absorption band of any given infrared active mode is the position it occupies within a molecule. Neighbouring atoms or groups can cause other vibrations to be shifted to higher or lower energies or cause bands to have increased or decreased intensities. These effects, however, simply tend to make band assignments more difficult and do not result in useful information when the chemical structure of the material under analysis is already known, as in this case.

The next main cause of variations in the form of absorption bands is from the chemical environment surrounding the group in question. This is particularly important for material in solid film form where a wide range of different states can occur. These include differing orientations of the molecules, various crystalline forms and interactions with neighbouring molecules. An important observation which can be made is that the absorption band width depends on the degree of orientational order found in a sample. In a highly ordered structure, as can be expected in LB films, a band will tend to be narrower than for the same mode in a randomly arranged state. Similarly, for materials adopting crystalline states, bands can be narrowed in this way. A further effect on an absorption band can arise from the crystal field, this can cause one band to be split into two or more for example.

A final point to note is that the instrument and parameters used to obtain the infrared spectrum also have an effect on the band width. This can potentially cause problems when quantitatively comparing data from different machines. Thus it is important to ensure that the same instrument parameters are always used in order that different spectra may be accurately compared.

3.3 Dispersive infrared spectroscopy

The traditional infrared spectrometer is of the dispersive type. The infrared source would ideally be a blackbody emitter but most commonly a Globar (a SiC rod electrically heated to 1750K) source is used. The infrared radiation is directed using mirrors into two beams, one of which passes through the sample to be analysed. The beams are then split into their component frequencies by a dispersive element such as a prism or grating and the intensities are measured and compared sequentially by a detector.

3.4 FTIR spectroscopy

Fourier transform infrared (FTIR) spectroscopy is an alternative method of measuring infrared spectra [Figure 3-5]. The principle difference between the conventional and the FT method is that the dispersive element is replaced by an interferometer. This results in an interferogram being measured at the detector which must be Fourier-transformed to obtain a spectrum.
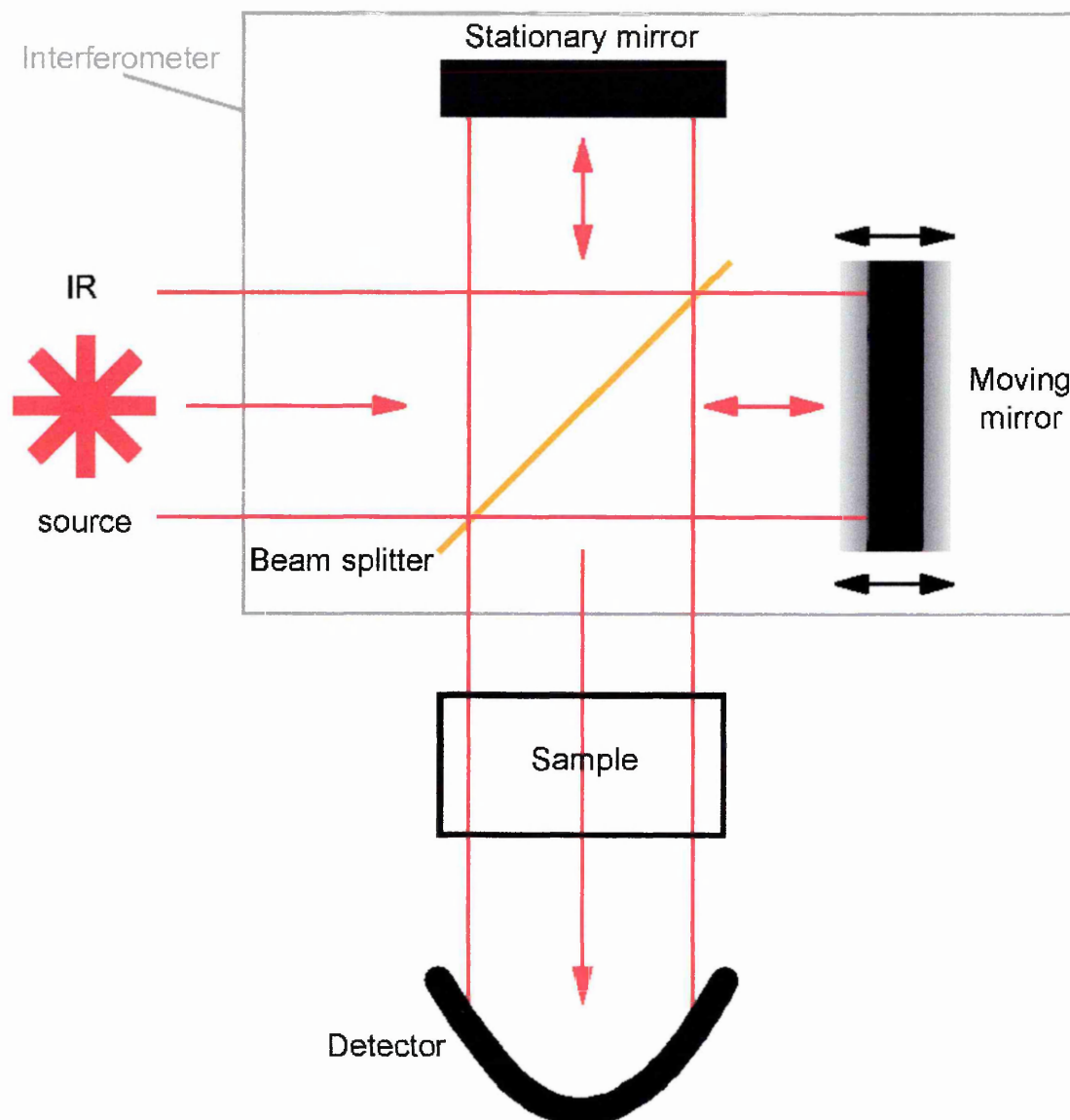
Figure 3-5: Schematic diagram of a FTIR spectrometer.

3.4.1 The Michelson interferometer

The interferometer used in FTIR is of the Michelson type. This consists of a beam splitter (KBr) and two mirrors; one which is fixed and one which moves back and forth. The infrared beam from a polychromatic source (Globar) is collimated by mirrors and is then passed through the beam splitter which is angled at 45°. Thus 50% of the beam is transmitted to the moving mirror and 50% reflected to the stationary mirror. The

reflected beams recombine at the beam splitter and are directed through the sample to the detector. The moving mirror introduces a path difference or retardation, x, between the two recombined beams. When both mirrors are equidistant from the beam splitter, there is zero path difference (ZPD) and constructive interference occurs for all wavelengths. At a particular wavelength, λ, when the moving mirror moves by $\frac{1}{4}$, the path difference is $\frac{1}{2}$ so the recombined beams will interfere destructively. As the moving mirror oscillates about the ZPD position, an interference pattern is produced for each wavelength and the sum of all such patterns produces the final interferogram measured by the detector, since the source is polychromatic [Figure 3-6].
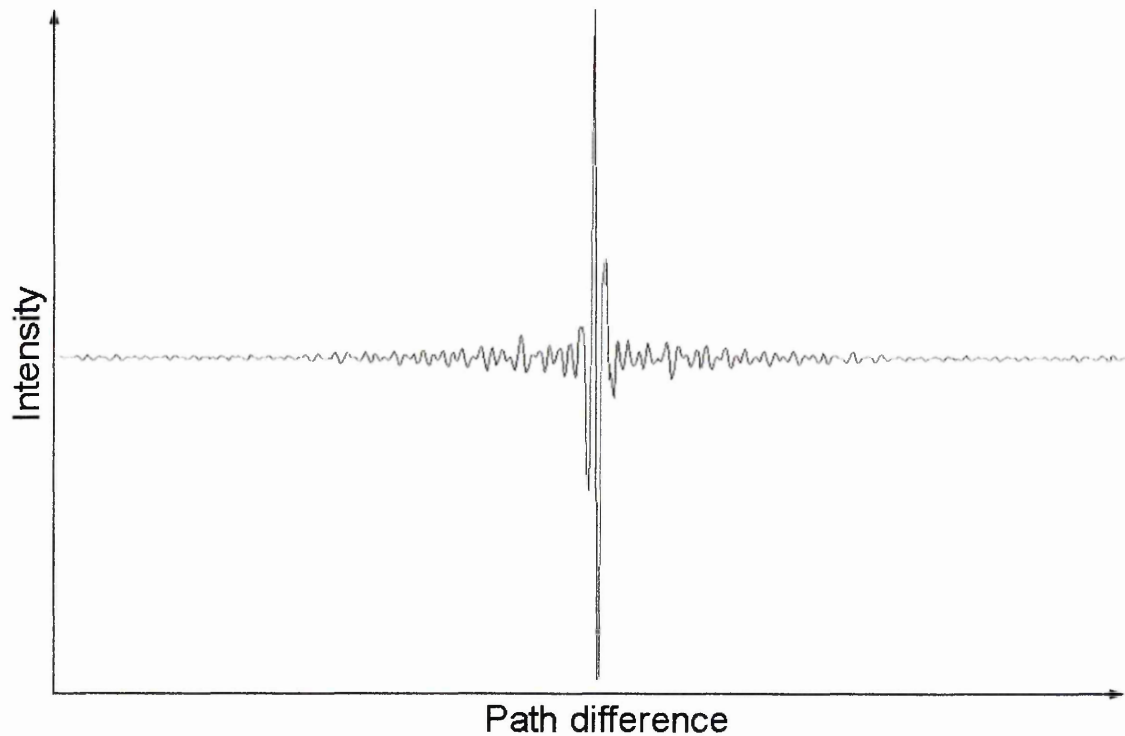
Figure 3-6: A typical interferogram.

The interferogram as detected is clearly not a spectrum and further processing is required in the form of a Fourier transform.

39

The intensity of radiation at the detector as a function of path difference, x, can be expressed as:

$$I_{(x)} = \int_{0}^{\infty} S_{(\bar{v})} \cos(2\pi\bar{v}x)d\bar{v}$$ **Equation 3-4**

where $I_{(x)}$ is the intensity of the interferogram at x,

$S_{(\bar{v})}$ is the spectral density amplitude at $\bar{v}$,

x is the retardation,

and $\bar{v}$ is the frequency in cm^{-1}.

Since the Fourier transform is to be computed numerically, the signal must be digitised. This is achieved by measuring the signal at fixed distances of mirror travel, known as the sampling interval, Δx. A laser in the machine is used as a reference, usually a HeNe laser emitting at 632.8nm. Thus the amplitude of the real part of each frequency element is:

$$S_{(\bar{v})} = \sum_{x=0}^{D} I_{(x)} \cos(2\pi\bar{v}x)\Delta x$$ **Equation 3-5**

The product of the sampling interval, Δx, and the number of samples taken, N, give the path difference, x. N is usually in the range 500 to 10,000.

A side effect of discrete sampling intervals is the possibility of aliasing. This occurs when there is the possibility of more than half a wavelength passing between sampling intervals, that is when:

$$\Delta x \leq \frac{\lambda}{2}$$ **Equation 3-6**

this gives a maximum frequency which may be studied of:

$$\overline{v}_{max} = \frac{1}{2\Delta x}$$ **Equation 3-7**

Sampling every laser wavelength, for a HeNe laser, results in a maximum frequency of $7901 cm^{-1}$. This is above the transmission window of the KBr beam splitter used in mid-infrared instruments and thus aliasing is automatically avoided.

3.4.2 Advantages

FTIR spectroscopy offers several advantages over the dispersive method.

3.4.2.1 The Fellgett advantage

The Fellgett, or multiplex advantage,[6,7] arises since all spectral elements are measured simultaneously. The signal to noise ratio, S_N, for thermal detectors depends on the square root of the observation time of each element. The number of spectral elements in a digitised spectrum, N, is the frequency range divided by the resolution. Thus for a dispersive instrument:

$$S_N \propto \frac{T^{\frac{1}{2}}}{N^{\frac{1}{2}}}$$ **Equation 3-8**

where T is the total experiment time.

However, for an FT instrument, all elements are observed for the whole experiment time so:

$$S_N \propto T^{\frac{1}{2}}$$ **Equation 3-9**

This means an improvement in S_N by a factor of $N^{1/2}$ for the same experiment time. This is a great advantage for the study of thin film samples such as the calixarene assemblies under analysis in this project. It should be noted that this advantage only applies when the greatest source of noise is from the detector (see section 3.4.3).

3.4.2.2 The Jaquinot advantage

The Jaquinot, or throughput advantage,[8] occurs as there are no slits to attenuate the infrared beam in an FTIR spectrometer. Therefore a much greater signal reaches the detector than in the case of a dispersive instrument. The ratio of optical throughputs of an interferometer, $G_{\bar{v}}^I$, to that of a grating, $G_{\bar{v}}^G$, assuming equal collimated beam areas, has been shown to be:

$$\frac{G_{\bar{v}}^I}{G_{\bar{v}}^G} = \frac{2\pi f}{h} \qquad \textbf{Equation 3-10}$$

where f is the focal length of the collimator

and h the height of the entrance slit of the grating.

In a sensitive grating spectrometer f/h can be >30 giving an optical throughput more than 190 times greater in the FTIR machine. This results in a significant improvement in the signal to noise ratio. However, in the case of ATR, the beam throughput is limited by the thickness of the crystal used so this advantage is not as great as it might otherwise be.

3.4.2.3 The Connes advantage

The Connes advantage[9] results from the frequency scale being known extremely accurately. As the distance or time domain of the interferogram is fixed precisely by the laser wavelength, when the Fourier transform is applied the result is an exact wavelength scale. This offers the benefit that spectra can easily be added to or subtracted from each other.

The first case is used to improve signal to noise as the spectra from many individual scans can be co-added. This is equivalent to an increase in the experiment time. Thus, the signal to noise ratio is improved proportionally to the square root of the number of co-added scans [Equation 3-9]. This is important for the analysis of thin samples such as the LB films of calixarenes under investigation in this project. The ability to subtract one spectrum from another is very useful for the analysis of various samples where weak bands are involved. Additionally, this can be used to improve the quality of spectra by removing unwanted bands, for example due to water vapour and CO_2.

3.4.3 Disadvantages

The disadvantages of FTIR spectroscopy are by far outweighed by the advantages. In the past, the principle problem was that FTIR instruments measure interferograms and do not directly yield spectra. The resulting computer analysis needed a lot of computing power and time. However with modern desktop computers the necessary Fourier transform can now be performed in no more than seconds.

More troublesome is the fact that FTIR spectrometers are of the single beam type while dispersive instruments tend to be double beam. This means that a reference background is not taken at the same time as the spectrum of the sample. The problem here is that

atmospheric components such as CO_2 and water vapour are very strong infrared absorbers. Thus a small variation in atmospheric conditions between background and sample scans can result in absorptions from CO_2 and H_2O appearing in the spectrum, possibly masking bands of interest. This problem can be overcome in two ways: either the spectrometer can be purged with dry CO_2-free air or dry nitrogen, or the offending bands can be digitally subtracted from the spectrum by computer [section 3.4.2.3].

A final problem only applies to certain machines; those which are source noise-limited. In these cases, the Fellgett disadvantage applies because all frequencies are observed simultaneously. If there is noise in a particular part (i.e. frequency range) of the radiation emitted by the source when the Fourier transform is applied it will affect the whole spectrum. However, this is only really a problem for far-infrared machines since mid-infrared machines are detector-noise limited and the Fellgett advantage applies.

3.5 Sampling techniques

There are many methods of obtaining infrared spectra from samples. The techniques chosen depend on the characteristics of the sample to be analysed and on the information required. In this project, attenuated total reflection (ATR) and reflection-absorption infrared spectroscopy (RAIRS) were used. These are briefly discussed in the following sections along with transmission infrared (TIR) for comparison.

3.5.1 Transmission

This is the simplest method in which the infrared beam is passed directly through the sample [Figure 3-5]. Although it is easy to set up, sampling by TIR has several disadvantages. Samples which are very thick or strongly absorbing cannot be studied.

Additionally, it is difficult to obtain spectra of weakly absorbing or, importantly for this work, very thin samples as TIR is not a very sensitive technique. Finally, only transition dipoles which have a component parallel to the substrate surface are sampled [Figure 3-7].
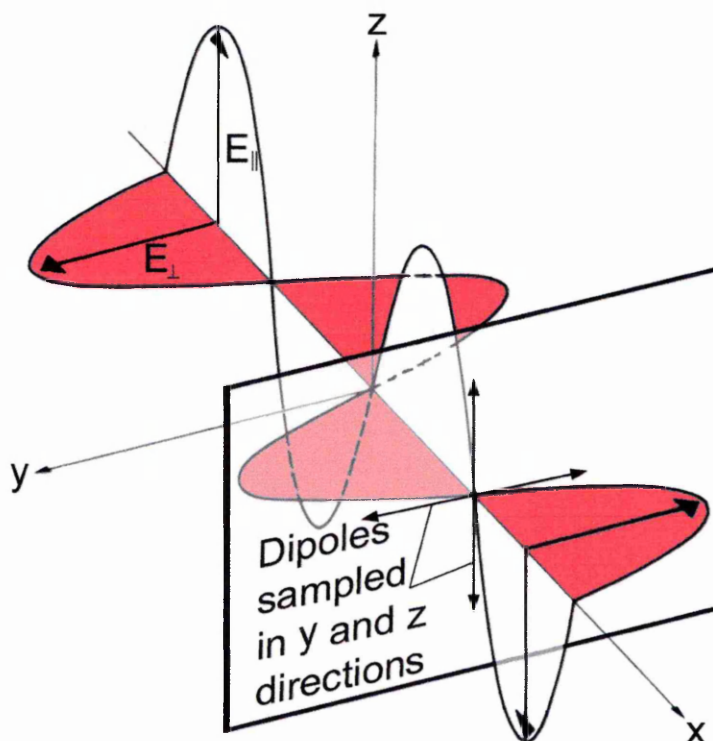
Figure 3-7: Polarisations in transmission infrared spectroscopy.

3.5.2 Attenuated total reflection

The method of attenuated total reflection (ATR) depends entirely on the phenomenon of the evanescent wave. Newton observed the penetration of the electromagnetic field into an optically rarer medium during total internal reflection within an optically denser medium in the early 1800s[10]. This effect was used in the 1960s to produce infrared spectra for the first time.[11,12] It was shortly after applied to the study of monolayers[13] and is now a widely used sampling technique[14,15] [Figure 3-8].

45

The sample to be analysed is placed in contact with an optically denser crystal or internal reflection element (IRE). The infrared beam is then directed into the IRE such that the angle of incidence at the interface with the sample is greater than the critical angle. This results in total internal reflection, attenuated by the material under investigation via the evanescent field. The form of the IRE can be chosen so that several internal reflections occur, each one adding to the intensity of the evanescent field and thus to the sensitivity of the measurement. The IRE used in this project is parallelepipedal and made of intrinsic silicon and gives approximately 40 reflections ($n = 3.4$, $\theta_i = 45°$).
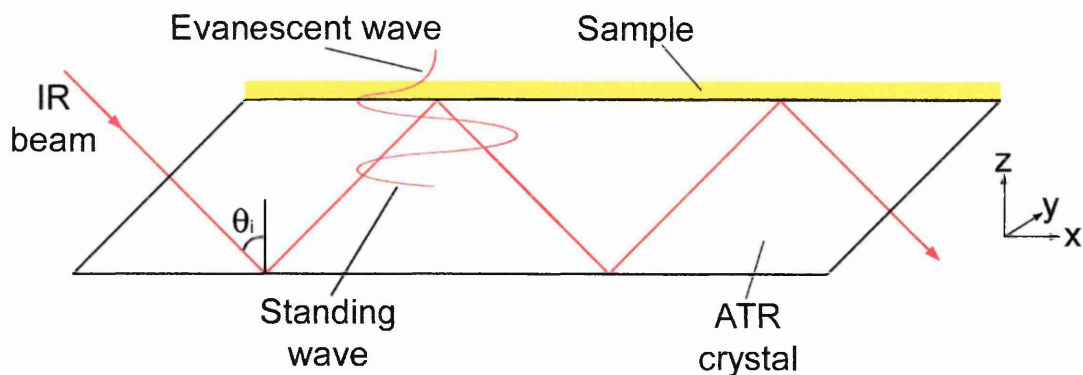
Figure 3-8: The ATR experiment (not to scale).

The most important component of an ATR experiment is the evanescent field since it is this which interacts with the samples to obtain a spectrum. It has some important properties which are that:

The field is confined to the interface and decreases in intensity with increasing distance into the rare medium, normal to the interface (along the z-axis);

The field intensity in the rare medium is non-zero but there is an instantaneous normal component of energy flow across the interface with a time average equal to zero. Therefore there is no energy loss at the interface and total internal reflection occurs;

The field has components in all spatial directions and thus interacts with transition dipoles in any orientation;

There is a non-zero energy flow parallel to the surface (along the x-axis) resulting in the incident and reflected waves being displaced. This effect is the Goos-Hänchen shift.[16]

The first point determines how much of the rare medium is sampled. The decay in the evanescent field is exponential and can be written as:[17]

$$E = E_0 \exp\left[\frac{-2\pi}{\lambda_1}\left(\sin^2\theta_i - n_{21}^2\right)^{\frac{1}{2}} z\right]$$
Equation 3-11

where E is the electric field amplitude,

E_0 is the value of E at the interface (z = 0),

$\lambda_1 = \lambda/n_1$ is the wavelength of the radiation in the dense medium,

θ_i is the angle if incidence,

$n_{21} = n_2/n_1$, the ratio of refractive indices of the rare medium to the dense medium

and z is the distance normal to the interface.

3.5.2.1 Depth of penetration

Due to the exponential nature of the evanescent wave emerging from the IRE, it theoretically continues to infinity, much greater than the depth of material which can meaningfully be sampled. Therefore the depth of penetration, d_p, has been defined as being z when $E = E_0\exp[-1]$. By defining the electric field amplitude decay constant γ as:

$$\gamma = \frac{2\pi}{\lambda_1} \left(\sin^2 \theta_i - n_{21}^2 \right)^{1/2}$$

Equation 3-12

then:

$$E = E_0 \exp[-\gamma z]$$

Equation 3-13

and thus:

$$d_p = \frac{1}{\gamma}$$

Equation 3-14

The electric field amplitude at d_p is ~37% of E_0 so the actual depth sampled, d_s, is

$$d_s \approx 3d_p$$

Equation 3-15

For this work assuming $n_1 = 1.5$, with the IRE mentioned above ($n_2 = 3.4$, $\theta_i = 45°$) and at a frequency of 1600cm^{-1} the depth sampled is therefore ~1.6μm.

Since an LB monolayer of the calixarenes used in this project are of the order of 1-2nm thick, even the very thickest films are entirely sampled by the evanescent wave.

3.5.2.2 Advantages

The main advantage in using ATR over transmission is the enhanced sensitivity obtained. This factor is very important in obtaining good quality spectra of the calixarene LB films under investigation, something which would be difficult to do using the transmission method. Additionally, the sensitivity is even greater with the ATR crystals used in this project due to the large number of reflections obtained. Another benefit is that there are never any interference fringes in spectra obtained by ATR (other than from the beam splitter) which can be a problem in transmission spectra of thin films.

3.5.2.3 Disadvantages

The most common drawback of ATR spectroscopy is that since the evanescent wave samples such a short distance, very good contact is required between crystal and sample. This is not a problem in this case since the LB films analysed are deposited directly onto the IRE, which has been thoroughly cleaned beforehand. A bigger problem is that the crystals used are very thin (0.5mm) in order to obtain a large number of reflections and therefore high sensitivity. However, this means the infrared beam is greatly attenuated and consequently the energy throughput of the system is small in comparison to transmission. This is countered by using many co-added scans for each spectrum. A further related drawback is that there is an increased sensitivity to small changes in water vapour conditions which can mask bands of interest.

3.5.3 Refection-absorption infrared spectroscopy

This method is commonly used to study surfaces and thin films, even sub-monolayers. Also known as grazing angle infrared spectroscopy, RAIRS shows a considerable increase in sensitivity compared to TIR. The sample under investigation must be on a reflective substrate. In this project, aluminium coated glass slides are used. The infrared beam is directed through the film where it is reflected at the substrate and passes back through the sample [Figure 3-9]. In this simple picture it is clear that even at normal incidence the effective amount of material sampled is doubled compared with TIR. Therefore, when performed at grazing incidence a further increase in sensitivity can be expected.

49
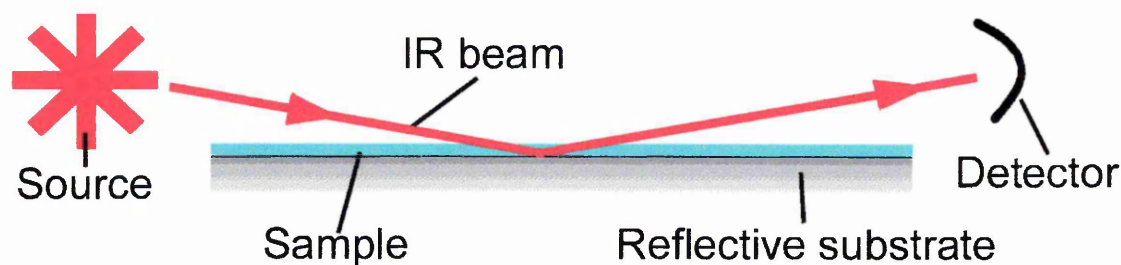
Figure 3-9: RAIRS sampling geometry.

This simple picture is in reality more complicated and the electric fields must be considered in more detail. The system shown in Figure 3-9 is a three layer system consisting of air, a thin film sample and a metal substrate. In order to understand the interaction of the infrared radiation fully, the electric field interactions with the sample and substrate must be calculated. This has been well documented so only the important results will be covered here.

Firstly the absorbance in the sample is heavily dependent on the polarisation of the light and the angle of incidence. For parallel (E_p) polarisation at normal incidence there is no absorbance and this remains the case until around 45°. After this point it increases up to a maximum at 88° before subsequently falling sharply to 0 at 90° [Figure 3-10]. Therefore, the optimum angle for analysis would seem to be 88°. In practice, it is difficult to obtain a good signal to noise ratio at this angle and it is better to conduct the analysis at 85° where good reflectance is achieved together with a much better signal to noise ratio.
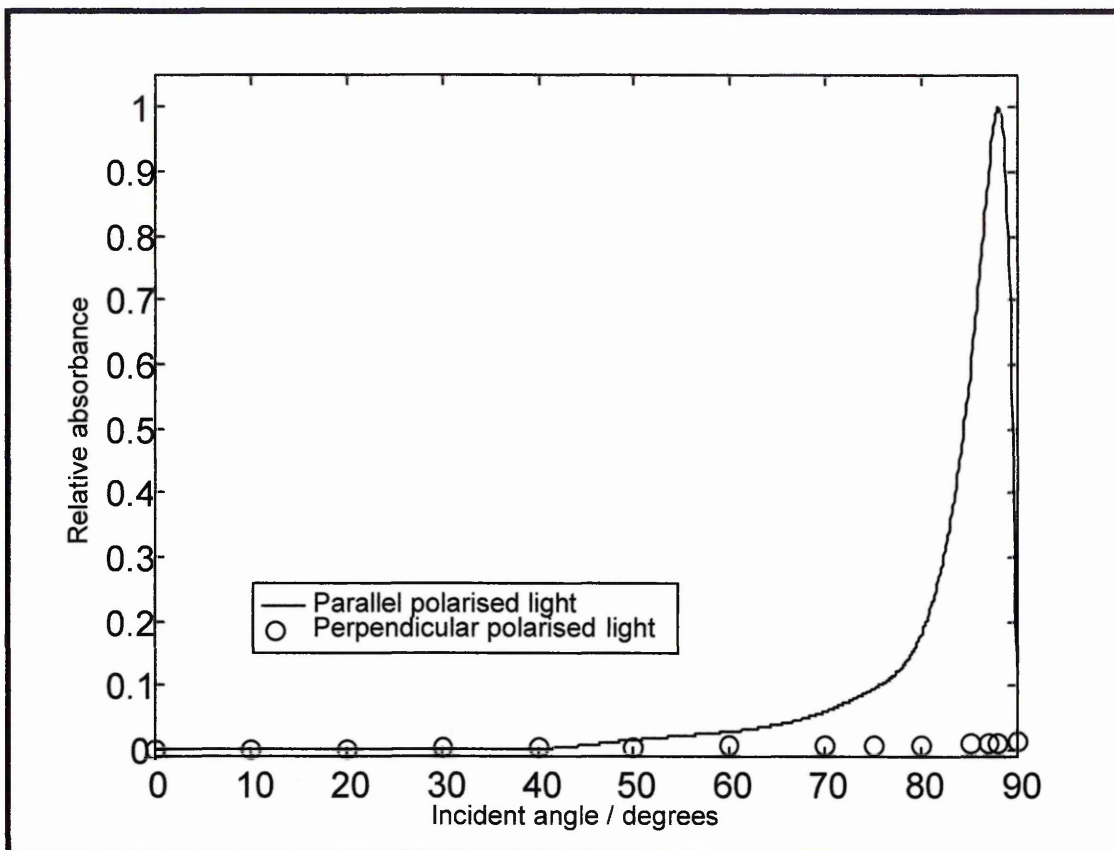
Figure 3-10: The effect of the angle of incidence on the relative absorbance observed during the RAIRS experiment.[18]

For perpendicular (E_s) polarisation there is virtually no absorbance at any angle [Figure 3-10]. Although this polarisation does not contribute to the signal of the spectrum obtained, it adds to the noise.[19] Therefore, the sensitivity of RAIRS is maximised by using E_p polarised radiation only and an 85° angle of incidence.

These reflectance characteristics are not difficult to understand. They arise because, for a reflecting surface (such as a metal), the standing wave formed has a node at the surface in the x and y directions. The result is that, for films which are much thinner than the period of the standing wave, transition dipoles with components parallel to the surface are not sampled. This is known as the surface selection rule [Figure 3-11]. It also explains why there is no reflectance near to normal incidence. In this case both

51

polarisations would sample dipoles in the x and y directions. However, since each polarisation now has a node at the surface, the reflected wave cancels out the incident one and no absorption by the material occurs.

3.5.3.1 Advantages

RAIRS provides an increase in sensitivity compared to transmission which makes it suitable for thin film samples. However the great benefit of this technique is that only transition dipoles with components normal to the substrate surface are sampled. This provides information on the orientation of the molecules in the material studied. Additionally, this information is complementary to that obtained in transmission where dipoles parallel to the surface are sampled [Figure 3-7].

3.5.3.2 Disadvantages

The main disadvantage is that, even though RAIRS is a sensitive technique, long sampling times are required for a good signal to noise ratio. Other disadvantages are ones common to infrared techniques such as water vapour and CO_2 which can be rectified by purging with dry air or nitrogen or by making use of digital subtraction.
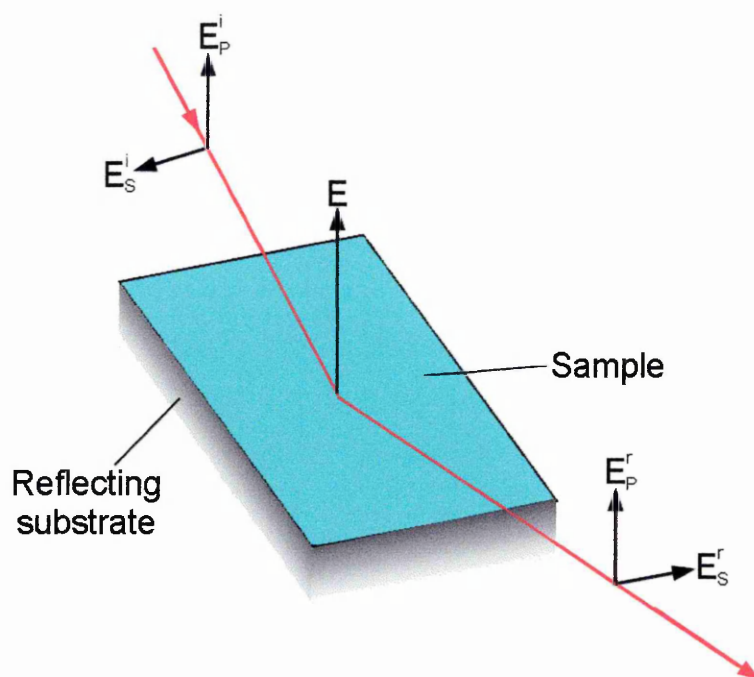
Figure 3-11: The surface selection rule in RAIRS.

3.6 Summary

A general background to infrared spectroscopy has been presented. FT-infrared spectroscopy and the specific techniques of ATR and RAIRS, used in this study, have been described, along with the reasons for choosing them to analyse the Langmuir-Blodgett films of calixarenes under investigation.

3.7 References

[1] C. N. Banwell, Fundamentals of Molecular Spectroscopy, McGraw-Hill, 1966.

[2] B. Schrader, Infrared and Raman Spectroscopy, VCH, 1995.

[3] J. L. McHale, Molecular Spectroscopy, Prentice Hall, 1999.

[4] D. H. Williams, Spectroscopic methods in organic chemistry, McGraw-Hill, 1995.

[5] S. F. Johnston, Fourier transform infrared: a constantly evolving technology, Ellis Horwood, 1991.

[6] P. Fellgett, Multi-Channel Spectrometry, Journal of the Optical Society of America, 1952, 42, 872.

[7] P. Fellgett, Three concepts make a million points, Infrared Physics, 1984, 24, 95-98.

[8] P. Jacquinot, The Luminosity of Spectrometers with Prisms, Gratings or Fabry-Perot Etalons, Journal of the Optical Society of America, 1954, 44, 761-765.

[9] B. C. Smith, Fundamentals of Fourier transform infrared spectroscopy, CRC Press, 1996.

[10] I. Newton, Optiks II book 8, 97, 1817.

[11] N. J. Harrick, Surface chemistry from spectral analysis of totally internally reflected radiation, Journal of Physical Chemistry, 1960, 64, 1110-1114.

[12] J. Fahrenfort, Attenuated total reflection, Spectrochimica Acta, 1961, 17, 698-709.

[13] L. H. Sharpe, Observation of Molecular Interactions in Oriented Monolayers by Infrared Spectroscopy Involving Total Internal Reflection, Proceedings of the Chemical Society, 1961, 461-463.

[14] N. J. Harrick, Internal Reflection Spectroscopy, Harrick Scientific Corporation, New York, 1987.

[15] F. M. Mirabella, Internal Reflection Spectroscopy: Theory and Applications, Marcel-Dekker, 1993.

[16] F. Goos, H. Hänchen, Ein neuer und fundamentaler Versuch zur Totalreflexion, Annalen der Physik, 1947, 1, 333-346, (in German).

[17] F. M. Mirabella, Internal reflection spectroscopy, Applied Spectroscopy Reviews, 1985, 21(1 and 2), 45-178.

[18] C. Sammon, PhD Thesis, Vibrational spectroscopic studies of degradation and diffusion processes in polyethylene terephthalate, Sheffield Hallam University, 1997.

[19] Y. P. Song, M. C. Petty, J. Yarwood, Effects of polarisation of infrared spectra collected in reflection at grazing incidence, Vibrational Spectroscopy, 1991, 1, 305-309.

4. Pyroelectric analysis

4.1 Introduction

It is well known that straight chain[1,2] and other types[3] of molecules containing carboxylic acid and amine groups can be pyroelectric, if deposited as alternate layer LB films [chapter 1]. Additionally, it has been demonstrated that calixarene films show particularly high pyroelectric coefficients.[4,5,6] By studying a family of these systems, an insight into the pyroelectric mechanism can be gained. This knowledge can then be used to obtain further improvements in the pyroelectric properties of LB film systems, such as by chemical modification or in the film manufacture.

The analysis of the pyroelectric properties of the calixarenes under investigation is the subject of this chapter. The manufacture of the pyroelectric LB films is outlined, including a description of the physical properties of the materials as measured by isotherms on the water surface. This is followed by a description of the equipment used to perform the pyroelectric measurements and the results obtained are then presented and analysed.

4.2 Langmuir film formation

All the materials under investigation were treated in the same manner in the formation of the alternate layer LB assemblies. Each was dissolved in chloroform at a concentration of ~0.1mgml^{-1}. The solutions were spread drop by drop, using a Hamilton 250µl syringe, onto the water surface in the Langmuir trough [chapter 2]. The

chloroform was then allowed to evaporate for a period of 15 minutes. The evaporation was assisted by a fan mounted in the trough housing.

4.2.1 Isotherms

Prior to the manufacture of the actual alternate layer systems to be investigated, each material was studied individually. Pressure-Area (Π-A) isotherms were taken for all the materials. After spreading the material and allowing the solvent to evaporate, the barrier of the trough was gradually closed and the resultant variation in surface pressure recorded. The resulting isotherms are shown below [Figure 4-1 - Figure 4-4]. These all have the same scale for ease of comparison. A summary of the measurements appears in Table 4-1.
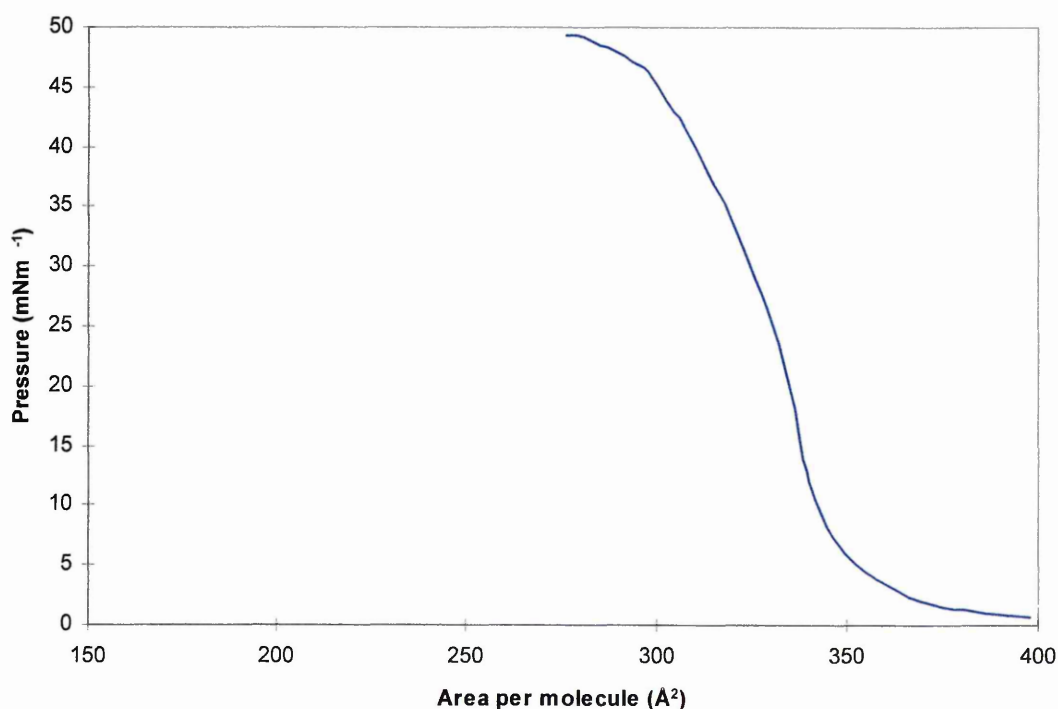
Figure 4-1: Pressure-Area isotherm of C1.
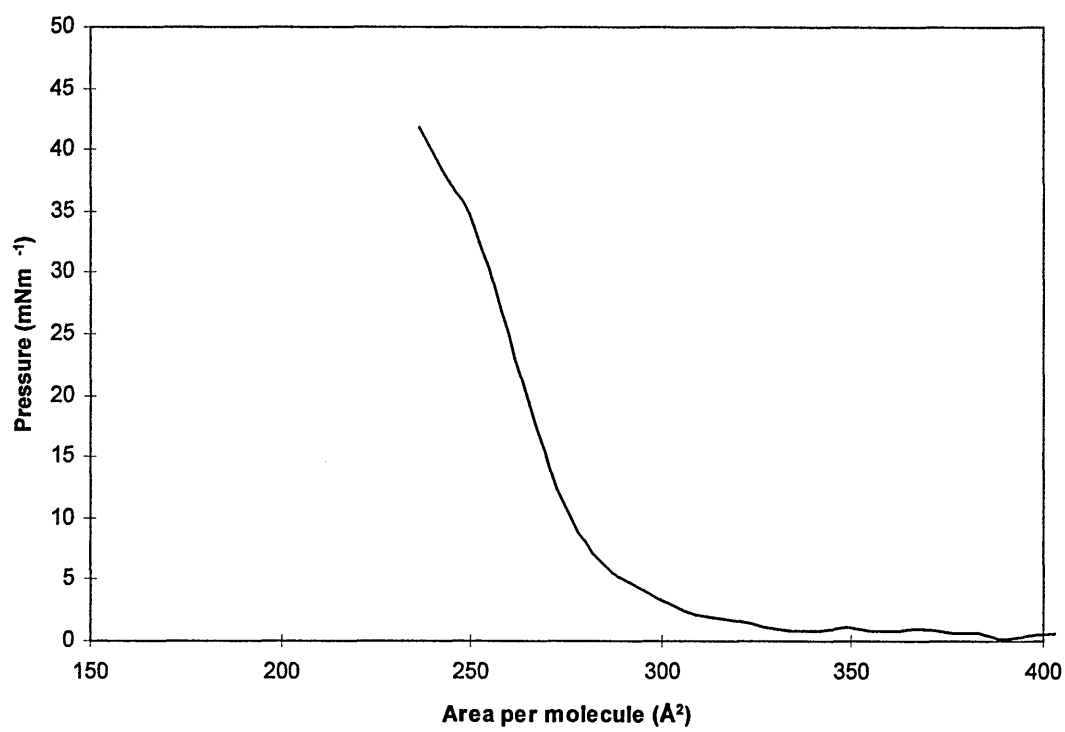
Figure 4-2 Pressure-Area isotherm of C3.
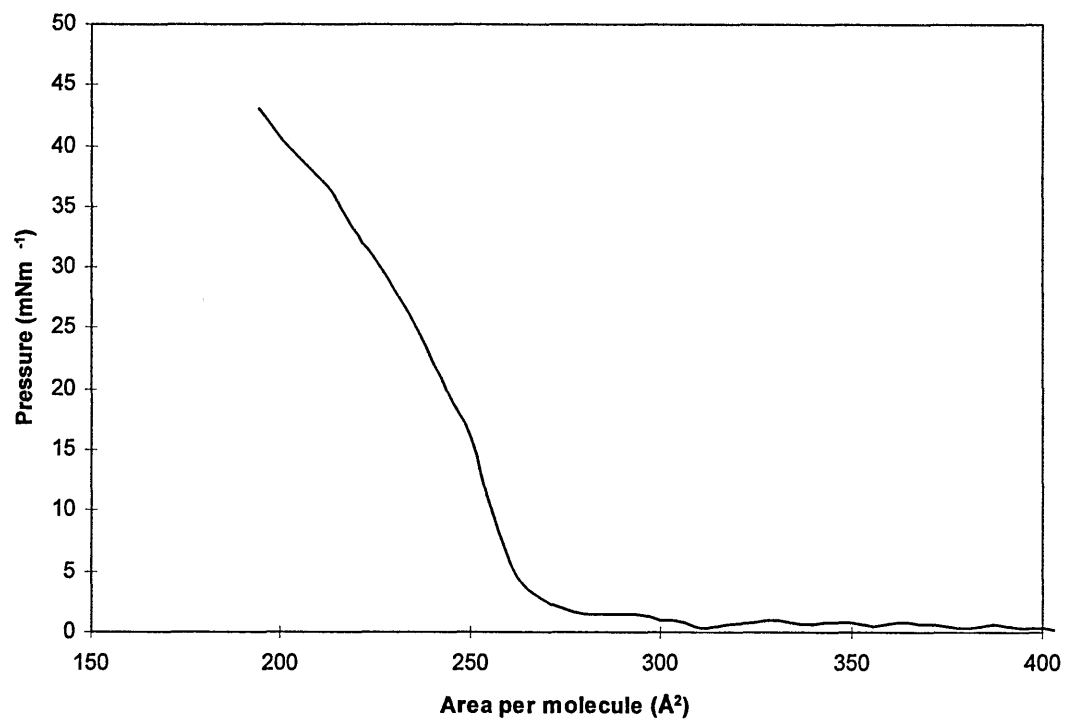
Figure 4-3: Pressure-Area isotherm of C5.

58
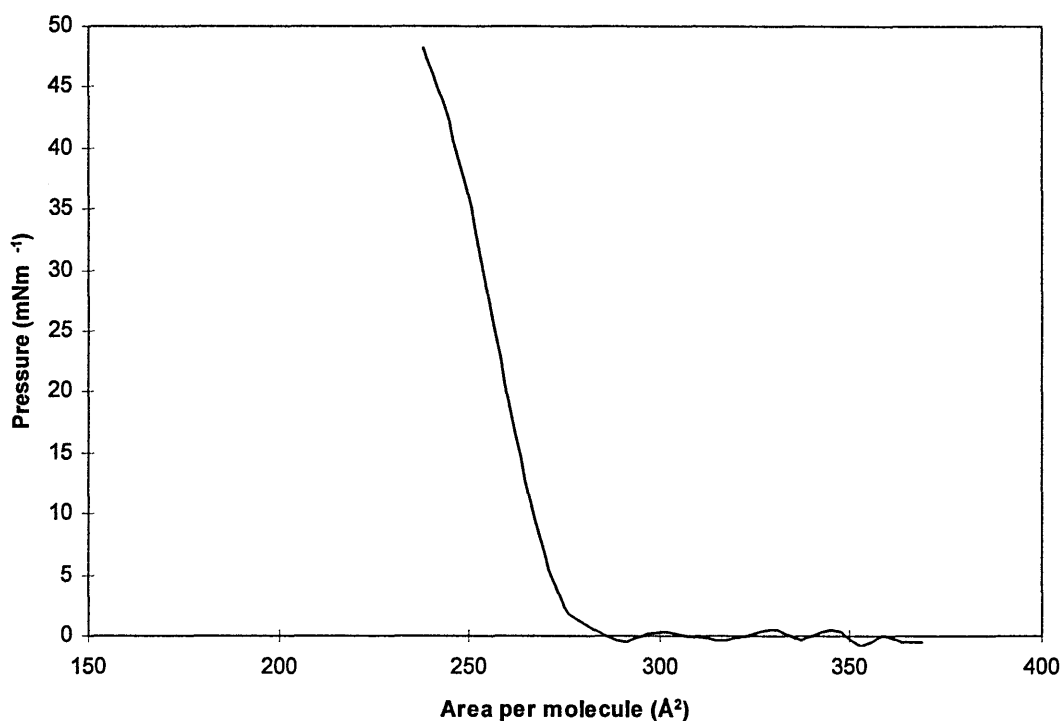
Figure 4-4: Pressure-Area isotherm of AM.

Material	Area per molecule (Å^2)	Compressibility (k)
C1	350±5	0.77
C3	275±5	1.02
C5	255±15	1.72
AM	275±5	0.63

Table 4-1: Area per molecule and compressibility obtained from the isotherms.

In general, these isotherms show that all the materials formed rigid solid phases, thus indicating that there is efficient packing of the molecules on the subphase. Considering the isotherms obtained for the acid-substituted calixarenes, it is clear that the measured area per molecule decreases with increasing substituant chain length. While this may

seem counterintuitive it can be seen from CPK models that the t-butyl part of the molecules form the widest point [Figure 4-5 and Figure 4-6]. The measured area per molecule from the CPK models is ~320Å^2 which is a little smaller than the actual area of the C1 molecule but rather larger than that of the other materials. Therefore it is likely that the longer chains allow the carboxylic acid moieties greater freedom of movement on the water surface.

The compressibility data provide further information on the conformation of the molecules. It shows that the longer the pendant chain length, the "softer" the film formed. This confirms that there is greater flexibility in the molecules with longer pendant chains. The logical conclusion is that for very short chains (C1), the acid groups stay tucked underneath the calix bowl so that this latter and the t-butyl groups form the widest part of the molecule. As the chain length is increased, the pendant groups can no longer fit under the calix bowl, thus causing the molecules to adopt a more cylindrical rather than conic conformation. In turn, this effectively reduces the area occupied by each molecule and increases the compressibility.

Additionally, it can be seen that the amine groups interact differently to the acid groups at the water surface as the compressibility of AM is much less than for the equivalent acid (C3) but the area per molecule is the same.

Figure 4-5: Side view of C1.
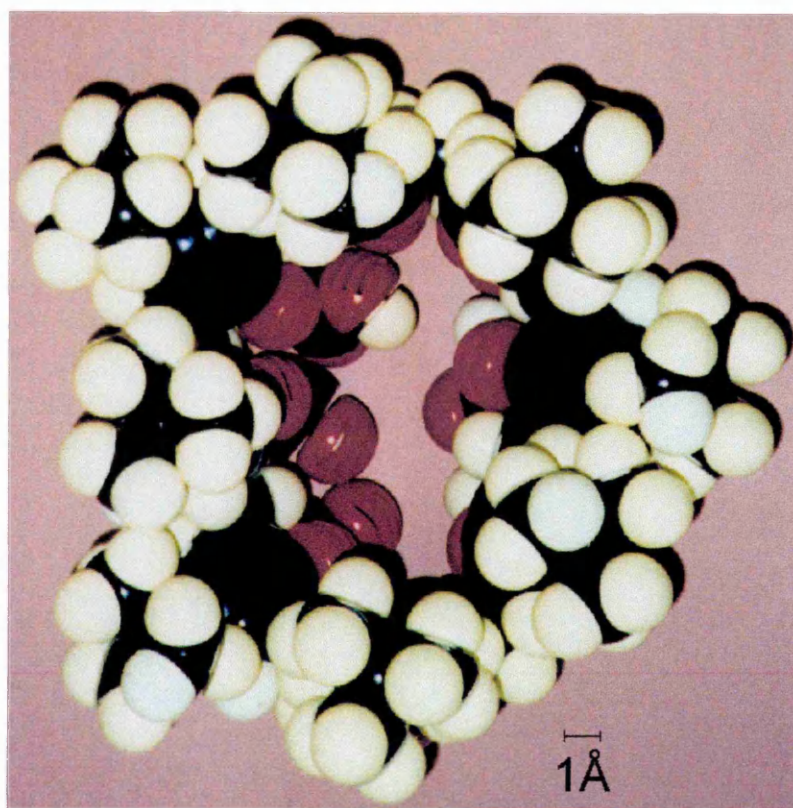
Figure 4-6: Top view of C1.

4.3 Pyroelectric devices

In order that the pyroelectric properties of an LB film can be measured, the sample must be incorporated into a parallel plate capacitor type device. The process by which such a device is manufactured is described below along with the experimental arrangement used to obtain the pyroelectric results.

4.3.1 Device manufacture

The substrates used for the deposition of the pyroelectric LB assemblies were Super Premium Microscope (Merck) glass slides coated with 750Å of thermally evaporated aluminium (99.9%). The glass slides were first thoroughly cleaned by ultrasonification in Decon 90 solution. This was followed by copious rinsing with ultra pure water and then drying using compressed nitrogen gas. They were then loaded into the evaporator which was pumped down to $\sim 10^{-6}$ torr and the aluminium was evaporated at $\sim 5 \text{Ås}^{-1}$. This bottom layer acts as one electrode in the final device. The LB films were then deposited [chapter 2] and the samples returned to the evaporator for the application of the top electrode. This is done in the same manner as for the bottom electrode except that a mask is used to form an electrode of a pre-determined shape. Additionally, to avoid damaging the LB film, the evaporation rate was initially kept at $\sim 0.1 \text{Ås}^{-1}$ for the first 100Å before being increased to $\sim 5 \text{Ås}^{-1}$ for the remaining deposition. The result is a device with the form of a parallel plate capacitor shown in Figure 4-7.

62
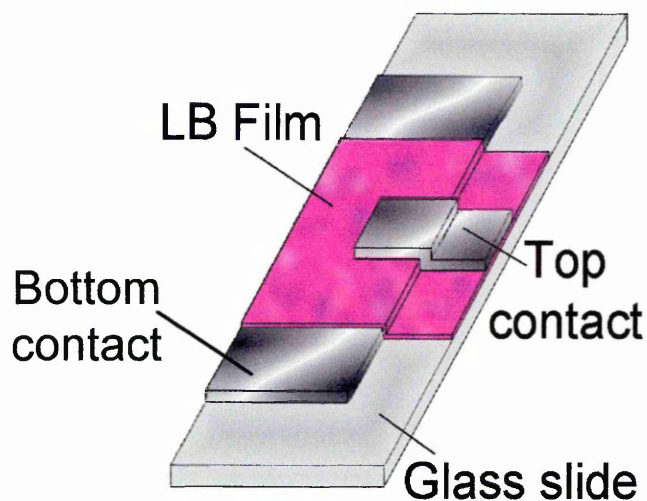
Figure 4-7: Geometry of the LB pyroelectric device.

4.3.2 Pyroelectric measurement

In order to asses the pyroelectric properties of a material, it is necessary to be able to measure the changes in electric polarisation it undergoes when the temperature is altered. There are three ways of doing this: the static method,[7] whereby the temperature is changed and then held constant while the change in polarisation is measured; the dynamic method,[8] in which the sample is heated with chopped infrared radiation and the quasi-static method,[9] used in this research.

In the quasi-static method, the sample is heated and cooled using a non-radiative source. Ideally, this heating and cooling takes the form of a triangular function with a small amplitude. A change of <1°C has been used here. This ensures that any variation in the pyroelectric coefficient with temperature is minimised and thus an accurate value can be obtained. The changing temperature profile causes a variation in the polarisation of the sample. In the case of the LB devices described above, the top and bottom electrodes can be short-circuited. The result is that a current is measured, induced by the changing

polarisation. Rearranging the previously obtained equation for the pyroelectric coefficient, Γ, [chapter 1, section 1.2.1] to include the pyroelectric current, I_P, results in the following expression:

$$I_P = \Gamma A \frac{dT}{dt}$$ **Equation 4-1**

where $\dfrac{dT}{dt}$ is the rate of change of temperature with time

and A is the area of overlap of the electrodes.

Since the sample is alternately heated and cooled in a linear fashion there are two rates

of change of temperature, $\left(\dfrac{dT}{dt}\right)_h$ and $\left(\dfrac{dT}{dt}\right)_c$, of opposite sign. The pyroelectric current

caused by each of these is then:

$$I_{Ph} = \Gamma A \left(\frac{dT}{dt}\right)_h$$ **Equation 4-2**

and

$$I_{Pc} = \Gamma A \left(\frac{dT}{dt}\right)_c$$ **Equation 4-3**

The peak to peak pyroelectric current is defined as $I_{P2P} = \left|I_{Ph}\right| + \left|I_{Pc}\right| = I_{Ph} - I_{Pc}$. This is because the rates of change of temperature for heating and cooling are opposite in sign. The pyroelectric coefficient is therefore given by:

$$\Gamma = \frac{I_{P2P}}{A\left[\left(\dfrac{dT}{dt}\right)_h - \left(\dfrac{dT}{dt}\right)_c\right]}$$ **Equation 4-4**

Therefore, the pyroelectric coefficient can be evaluated by measuring the amplitude of the generated current and the gradient of the temperature variation. This is shown in Figure 4-8.
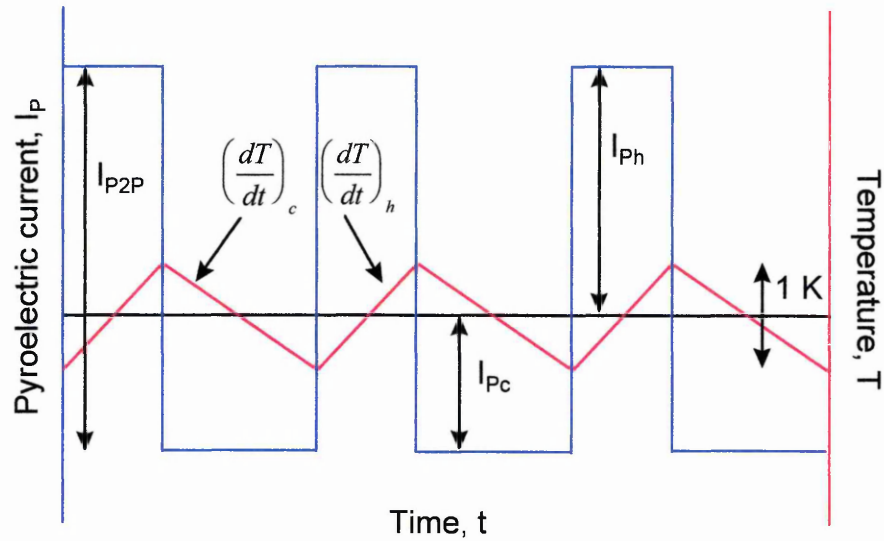
Figure 4-8: Ideal pyroelectric current output.

In reality, the pyroelectric current is rarely exactly a square wave [Figure 4-9]. One source of the variation from the square wave nature arises due to thermal currents induced within the sample. Additional deviations occur due to the finite response times of the measurement equipment, the electrometer and chart recorder. This, however, demonstrates an advantage of the quasi-static method, as non-pyroelectric currents can easily be distinguished by the shape of the current profile.

65
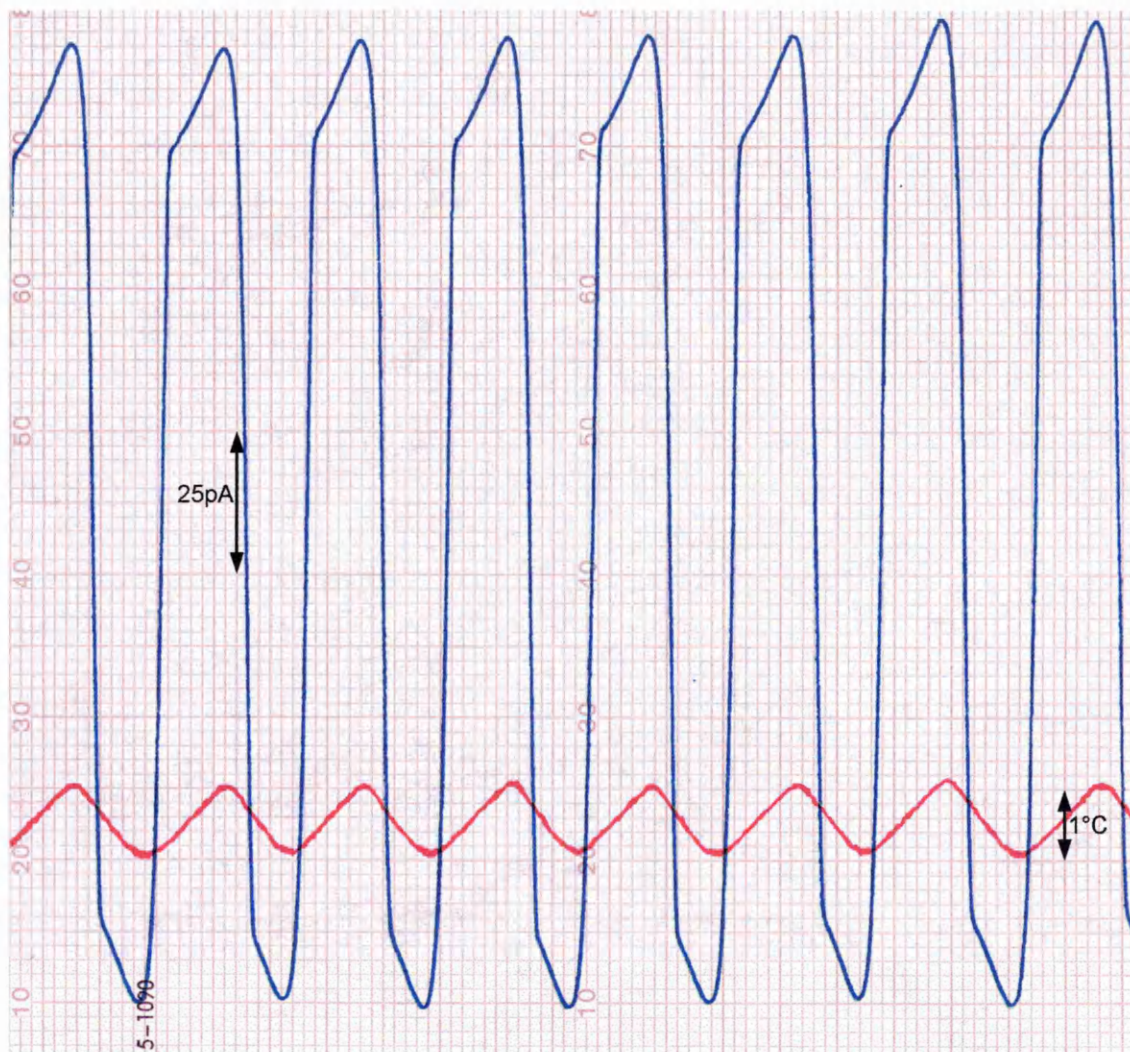
Figure 4-9: Typical pyroelectric trace (C3, 13 alternate LB layers, 22°).

4.3.3 Pyroelectric experiment arrangement

A schematic of the equipment used is shown in Figure 4-10. Linear heating and cooling ramps are obtained using an 18W Peltier device in contact with a copper block, to ensure even heat distribution. The sample is then mounted on top using zinc oxide heat sink paste so that there is good thermal contact. In order to measure the temperature *in situ*, a platinum resistance thermometer is placed in contact with the top of the sample. Finally, the contacts of the pyroelectric device are connected to a pico-ammeter (Keithley 614 electrometer) with gold wire (0.5mm diameter). The connections are

made to the device using silver conductive paste (RS components) to improve electrical contact. The whole system is then allowed to settle for at least one hour.
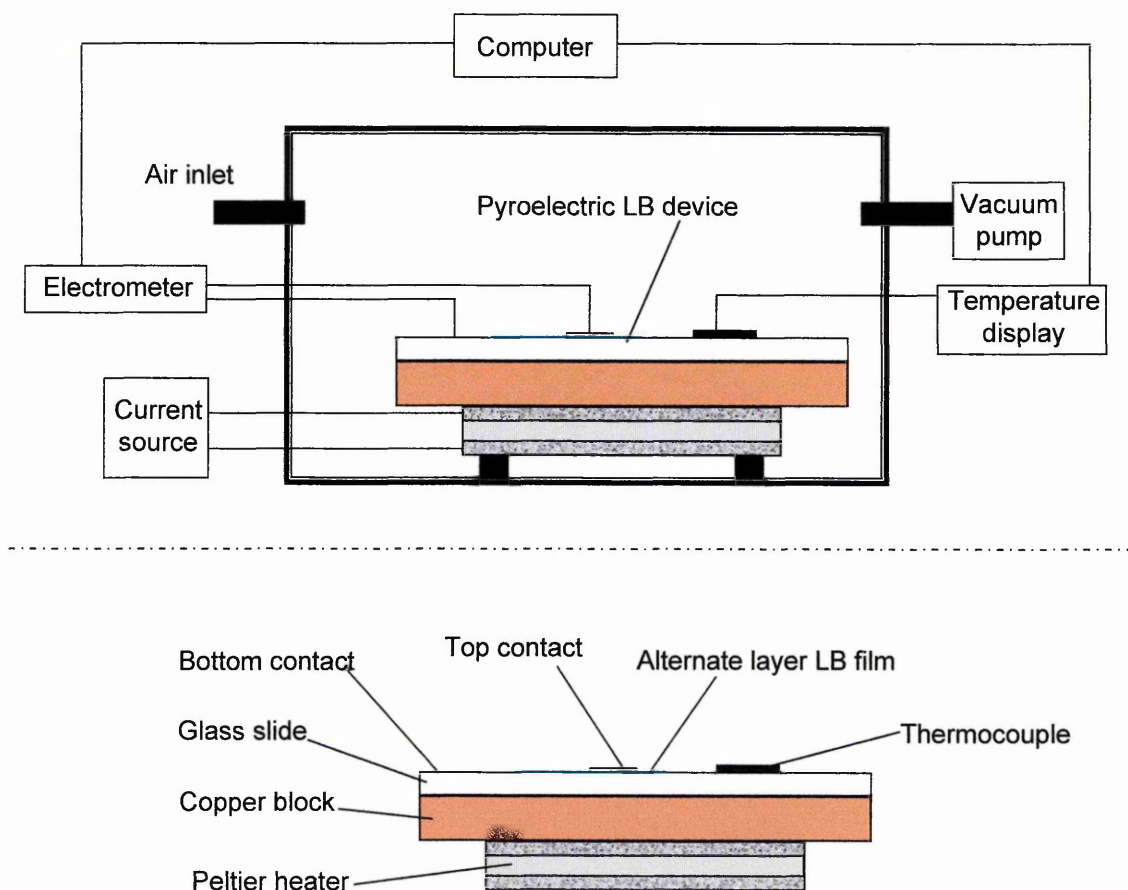
Figure 4-10: Pyroelectric measurement equipment schematic (top) and the heating stage components (bottom).

4.4 Pyroelectric results

The materials used were described in chapter 1. From the four calixarenes available, three sets of pyroelectric samples can be made: C1/AM; C3/AM and C5/AM. Firstly, pyroelectric measurements were attempted on the materials individually, for example 15 LB layers of C3. Only thermal currents were observed in these samples, showing that the acid alone cannot produce a pyroelectric effect in these calixarenes. Subsequent

67

measurements were performed on the pyroelectric samples investigating the effect of the number of LB layers deposited and temperature variations on the pyroelectric coefficients. These results are presented in the following sections.

4.4.1 Variation with number of layers

The total number of LB layers in the devices (i.e. the number of acid layers plus the number of amine layers) was varied from 9 to 23. The total number of layers is always odd as the first and last layers deposited are both of the acid-substituted calixarene. The results obtained are shown in Figure 4-11.

The first observation to make is that the pyroelectric coefficients recorded are large for LB devices, up to $\sim 15 \mu Cm^{-2}K^{-1}$. However, there is a marked decrease in pyroelectric activity with increasing chain length.

The variation in pyroelectric coefficient with the number of deposited layers does not seem to follow any simple relationship. There is a maximum in the coefficient at 13 layers for both C1/AM and C3/AM systems. The reasons for these facts are not yet know but possible explanations are discussed below.
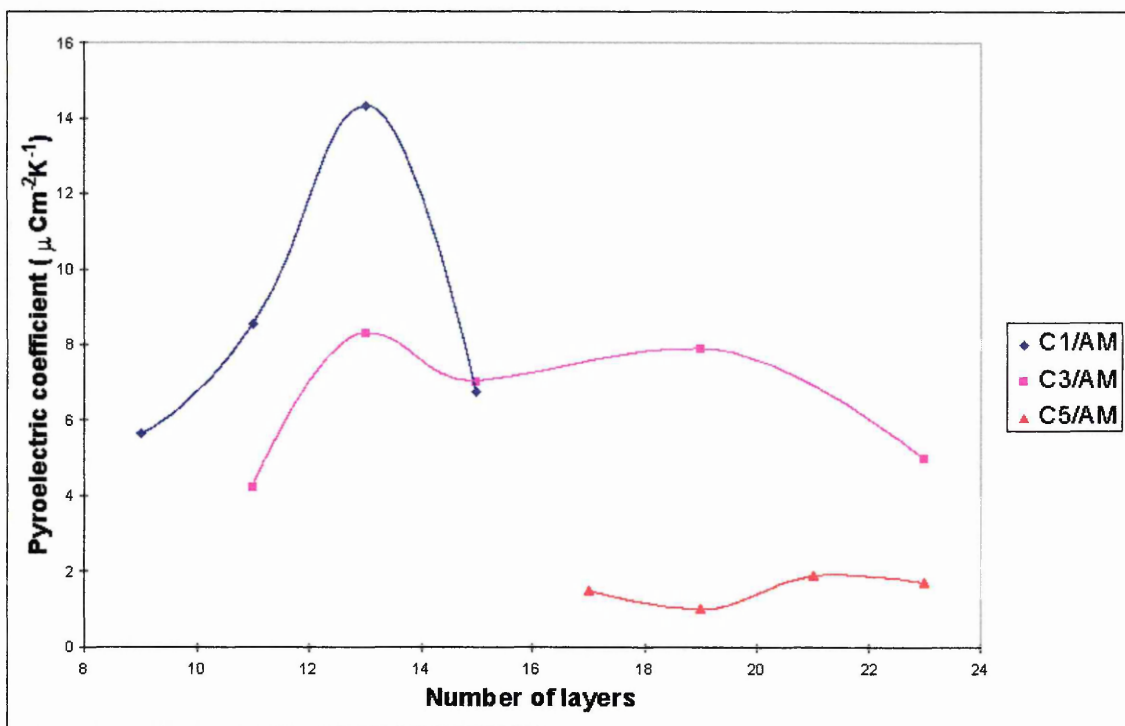
Figure 4-11: The variation of pyroelectric coefficient with total number of LB layers.

4.4.2 Variation with temperature

The number of LB layers which showed the greatest pyroelectric activity were used for the temperature studies. The results of the effects of temperature variation are shown in Figure 4-12. There is a general trend for all samples for the pyroelectric coefficient to gradually decrease with increasing temperature. Normally, pyroelectric coefficients in LB film systems increase dramatically with increasing temperature.[10] This linear variation is an advantage in the manufacture of pyroelectric sensors as it is easier to compensate for. A non-linear dependence requires complex electronic processing, a disadvantage which can outweigh the potential benefit of a higher pyroelectric coefficient at high temperature.
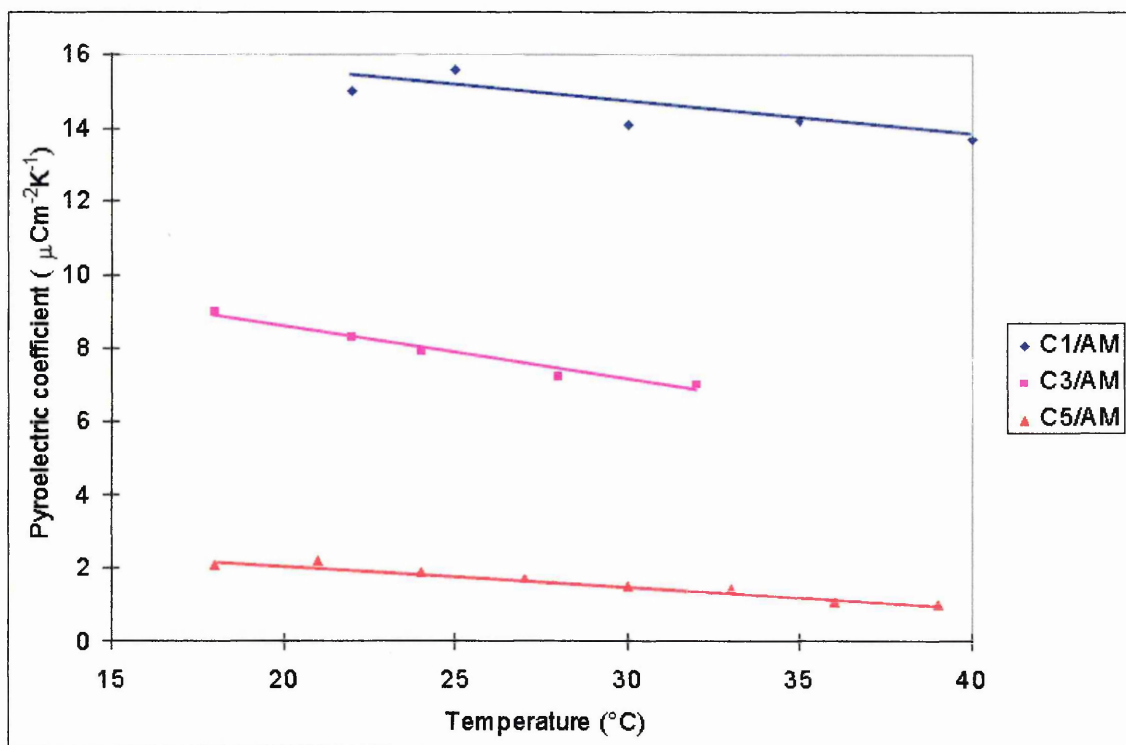
Figure 4-12: The variation of pyroelectric coefficient with temperature.

4.5 Interpretation and summary

This chapter has covered the pyroelectric analysis of the alternate layer calix[8]arene films. A variety of interesting properties have been observed. From the isotherms there is evidence that increasing the substituent chain length can serve to increase the density of acid amine pairs by reducing the area per molecule. However the pyroelectric measurements indicate that the pyroelectric activity in fact decreases. The reason is that as the chain length increases, there is an overall drop in the number of acid/amine pairs per unit volume, despite an increase in the plane of the LB layers. Calix[8]arenes were chosen because they provide a high acid/amine pair density (due to their extreme thinness in the z-direction) and this result seems to confirm that this is the reason for their high pyroelectric coefficient.

70

This is not the full story however, as the increase in chain length from one CH_2 unit (C1) to five CH_2 units (C5) results in approximately a doubling of the size of the molecule but the measured pyroelectric coefficient decreases by approximately an order of magnitude. It would seem that, in the case of these calixarenes, an increase in the flexibility of the molecules, corresponding to greater freedom for the acid and amine moieties, reduces the pyroelectric coefficient. This indicates that there is another mechanism for pyroelectricity.

Furthermore, there is a significant peak in the pyroelectric coefficient at 13 layers as well as an oscillation with number of deposited layers. This points to a long range effect throughout the films which has an influence on the pyroelectricity. One possible explanation is a shift in dipole direction as each bilayer is deposited. Since LB deposition is surface dependent, the dipole of a previously deposited bilayer could affect the deposition of the next bilayer. If this were to result in a change in the dipole direction for the new layer away from normal (the ideal direction) a dilution of the overall polarisation across the film would occur. Therefore, the pyroelectric coefficient would be reduced. However a further bilayer could have a dipole normal to the surface again, thus increasing the pyroelectric coefficient [Figure 4-13]. It is interesting that this sort of variation is not unique to this particular calixarene system; it has been observed in calix(4)arenes[11] and linear polysiloxanes[12] [Figure 4-14].
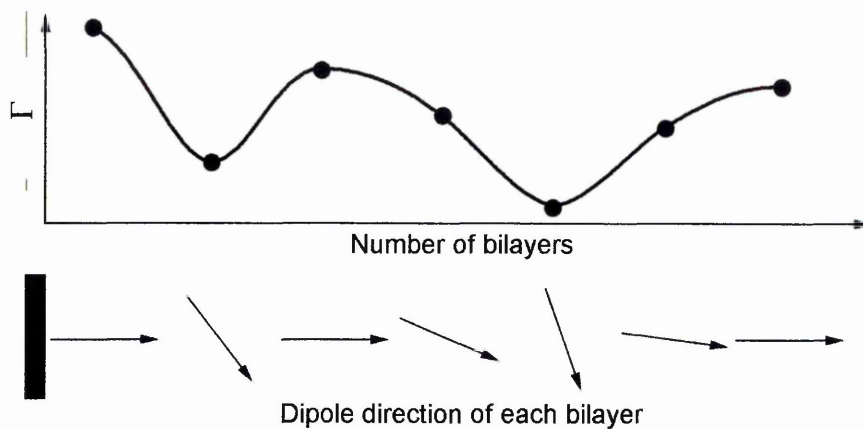
Figure 4-13: Example of the variation in pyroelectric coefficient due to varying dipole direction.
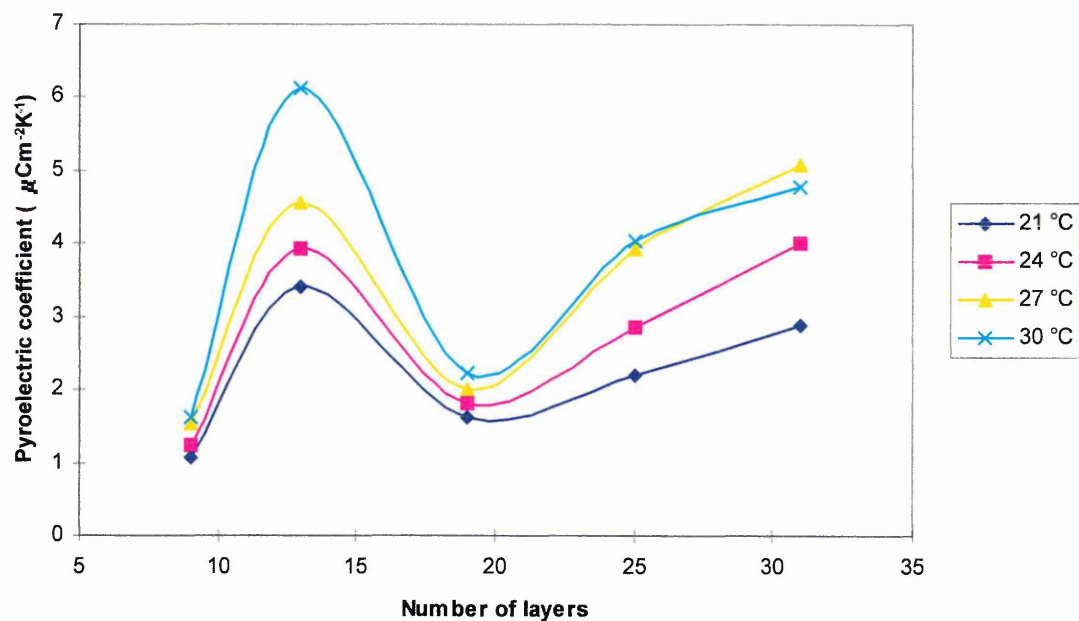
Figure 4-14: Variation of pyroelectric coefficient with temperature and number of layers in polysiloxane/eicosylamine LB system.[12]

The behaviour with respect to temperature is unusual for a pyroelectric material as generally an increase in activity with temperature is observed. The reason for this behaviour is not know but it may be a result of the great thermal stability of these materials.[13] Straight chain systems show increasing pyroelectric activity up to the point of melting.[14,15] The melting points of these calixarenes are greater than 200°C compared to <100°C for straight chain acid/amine systems.[16,17]

Additionally, in fatty acid LB films, disorder induced by chain melting is not recovered on cooling.[18,19] Therefore, these calixarene-based devices offer a more robust product, resilient to temperature variations even far outside their operational range.

Overall, these results show promising signs for the potential of LB film devices as heat sensors. These calixarenes demonstrate that reasonably high pyroelectric coefficients can be achieved along with a good stability of response over a useful temperature range. There is no reason to believe that further improvements cannot be made in related systems as calixarenes can undergo a wide variety of structural modifications and still be suitable for LB deposition.[20] Another alternative would be to make use of novel superstructures.[21]

4.6 References

[1] C. A. Jones, M. C. Petty, G. G. Roberts, G. Davies, J. Yarwood, N. M. Ratcliffe, J. W. Barton, IR studies of pyroelectric Langmuir-Blodgett films, Thin Solid Films, 1987, 155, 187-195.

[2] G. H. Davies, J. Yarwood, M. C. Petty, C. A. Jones, Fourier transform IR studies of alternate layer acid-amine Langmuir-Blodgett films with pyroelectric properties, Thin Solid Films, 1988, 159, 461-467.

[3] W. H. Abd. Majid, T. Richardson, S. Holder, D. Lacey, Pyroelectric activity of aromatic-substituted copolysiloxane eicosylamine alternate-layer Langmuir-Blodgett-films, International Journal of Electronics, 1994, 76, 745-750.

[4] T. Richardson, M. B. Greenwood, F. Davis, C. J. M. Stirling, Pyroelectric molecular baskets: temperature-dependent polarization from substituted calix(8)arene Langmuir-Blodgett films, Langmuir, 1995, 11, 4623-4625.

[5] T. Richardson, M. B. Greenwood, F. Davis, C. J. M. Stirling, Calix(8)arene LB superlattices: Pyroelectric molecular baskets, IEE Proceedings-circuits devices and systems, 1997, 144, No.2, 108-110.

[6] C. M. McCartney, T. Richardson, M. B. Greenwood, N. Cowlam, F. Davis, C. J. M. Stirling, The effect of pendant chain structure on the pyroelectric behaviour of calix(8)arene Langmuir-Blodgett films, Supramolecular Science, 1997, 4, 3-4, 385-390.

[7] I. M. Sil'Vestrova, Iu. N. Sil'Vestrov, An apparatus for measuring pyroelectric polarization of crystals, Soviet Physics. Crystallography, 1958, 3, 53-58.

[8] A. G. Chynoweth, Dynamic Method for Measuring the Pyroelectric Effect with Special Reference to Barium Titanate, Journal of Applied Physics, 1956, 27, 78-84.

[9] N. P. Hartley, P. T. Squire, E. H. Putley, A new method of measuring pyroelectric coefficients, Journal of Physics E, 1972, 5, 787-789.

[10] R. Colbrook, D.Phil thesis, Pyroelectric Langmuir-Blodgett Films, University of Oxford, 1990.

[11] C. M. McCartney, PhD thesis, Electrical and structural properties of calixarenes, University of Sheffield, 1998.

[12] R. Çapan, PhD thesis, The Pyroelectric Effect in Langmuir-Blodgett Films Containing Linear Polysiloxanes, University of Sheffield, 1998.

[13] C. M. McCartney, T. Richardson, M. A. Pavier, F. Davis, C. J. M. Stirling, The temporal and thermal stability of pyroelectric calix[8]arene Langmuir-Blodgett films, Thin Solid Films, 1998, 329, 431-434.

[14] T. Kamata, J. Umemura, T. Takenaka, N. Koizumi, Relationship between Pyroelectricity and Molecular Orientation in Alternate Langmuir-Blodgett Films, Journal of Physical Chemistry, 1991, 95, 4092-4098.

[15] T. Takenaka, J. Umemura, FT-IR study of structure-pyroelectricity relationship in noncentrosymmetric Langmuir-Blodgett Films, New Functionality Materials, Volume C, 1993, 565-570.

[16] T. Gavrilko, M. Drozd, G. Puchkovskaya, A. Naumovets, Z. Tkachenko, L. Viduta, J. Baran, H. Ratajczak, Structural phase transitions in organised organic thin films built of alkali stearates, Journal of Molecular Structure, 1998, 450, 135-139.

[17] S. R. Cohen, R. Naaman, J. Sagiv, Thermally Induced Disorder in Organised Organic Monolayers on Solid Substrates, Journal of Physical Chemistry, 1986, 90, 3054-3056.

[18] D. Vollhardt, A. Seeboth, Surface potential studies of the thermal behaviour of insoluble carboxylic acid monolayers on solid substrates, Thin Solid Films, 1991, 197, 349-356.

[19] Z. Zhang, Y. Liang, Y. Tian, Y. Jiang, Fourier transform infrared transmission spectral study on the thermal stability of multilayer Langmuir-Blodgett film of stearic acid, Spectroscopy Letters, 1996, 29(2), 321-336.

[20] F. Davis, A. J. Lucke, K. A. Smith, C. J. M. Stirling, Order and Structure in Langmuir-Blodgett Mono- and Multilayers of Resorcarenes, Langmuir, 1998, 14, 4180-4185.

[21] S. V. Batty, R. Capan, T. Richardson, T. E. Mann, D. Lacey, Novel superstructures for the enhancement of temperature-dependent polarisation in LB films, Thin Solid Films, 1996, 285, 919-923.

5. Room temperature infrared analysis

5.1 Introduction

The first stage in understanding the behaviour of calixarene films with varying temperature is to have a picture of their infrared characteristics at a single temperature. In this manner the pertinent absorption bands can be identified, that is those which are due to the parts of the molecules expected to be sensitive to changes in temperature. This chapter describes the FTIR-ATR and -RAIRS spectra of the materials studied, taken at room temperature. Firstly, spectra of related but simpler, aliphatic systems in cast film and LB film form are presented. Subsequently spectra of the calixarenes individually and of the pyroelectric alternate layer systems are described.

5.2 Straight chain systems

In order to gain a thorough background knowledge of the acid- and amine-substituted calixarene films under analysis, the much simpler systems of straight chain assemblies were first investigated. Samples of stearic acid (SA) and octadecylamine (ODA) (as described in chapter 1) were made in the form of cast films as well as in LB films. The spectra obtained using ATR and RAIRS are described in the following sections.

5.2.1 Cast films

Films of each material were cast individually, from chloroform solution, directly onto the relevant substrates (silicon for ATR and aluminium-coated glass slides for RAIRS)

in order to obtain randomly oriented samples. To compare with the alternate layer LB devices, mixed cast films were produced. This was done by thoroughly mixing both solutions together and casting the mixture as for the individual samples.

5.2.1.1 Attenuated total reflection infrared spectroscopy

The FTIR-ATR spectra of SA, ODA and a mixture of the two are shown in Figure 5-1. In the SA (blue) spectrum a strong C=O absorption band is seen at $1701cm^{-1}$ indicating carboxylic acid groups are hydrogen bonded as cyclic dimers.[1] Progression bands from the CH_2 wagging mode from 1312 to $1185cm^{-1}$ indicate that the alkyl chains are highly ordered in the crystalline state. Additionally, the CH_2 scissoring band occurs as a doublet at 1472 and $1465cm^{-1}$ which is also due to the high crystalline order of the hydrocarbon chains.[2] The absorption band at $1299cm^{-1}$, assigned to a coupled vibration of the C-O stretch and the OH in-plane bending modes, shows that the carboxylic acid dimers are in the energetically favourable trans configuration.[3]

The most important features of the ODA (green) spectrum are the NH_2 stretching bands at 3330 and $3163cm^{-1}$ and the NH_2 deformation modes at $1611-1566cm^{-1}$. It should also be noted that the CH_2 wagging progression bands are not seen, implying that there is a lower level of crystalline order than in the case of stearic acid. However, there is some splitting in the CH_2 scissoring absorption band, indicating that this material is still, to some degree, in a crystalline state.
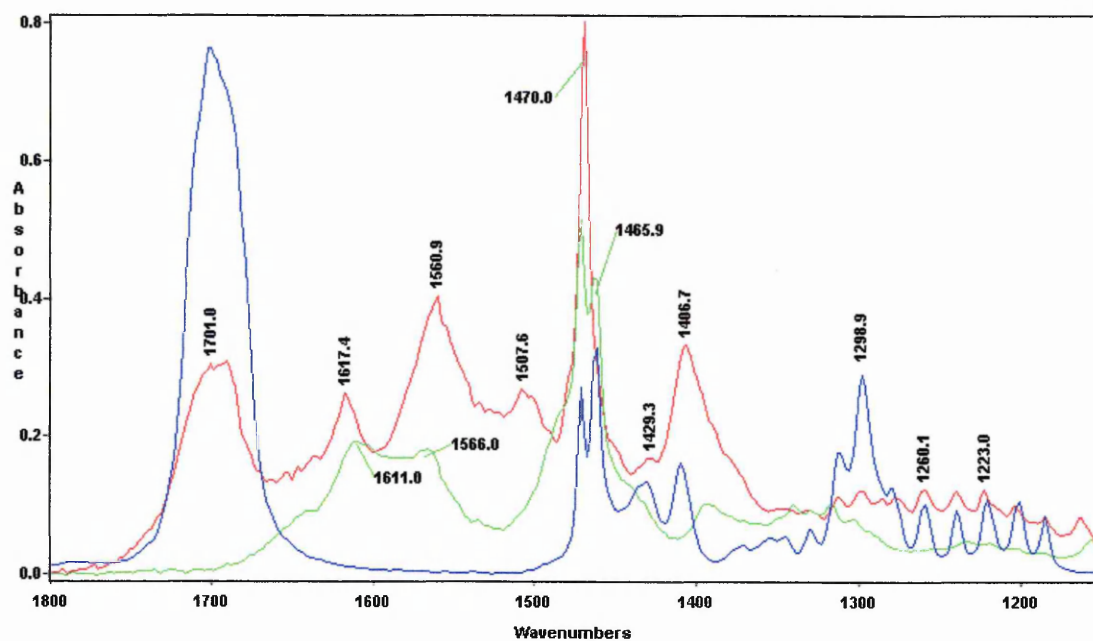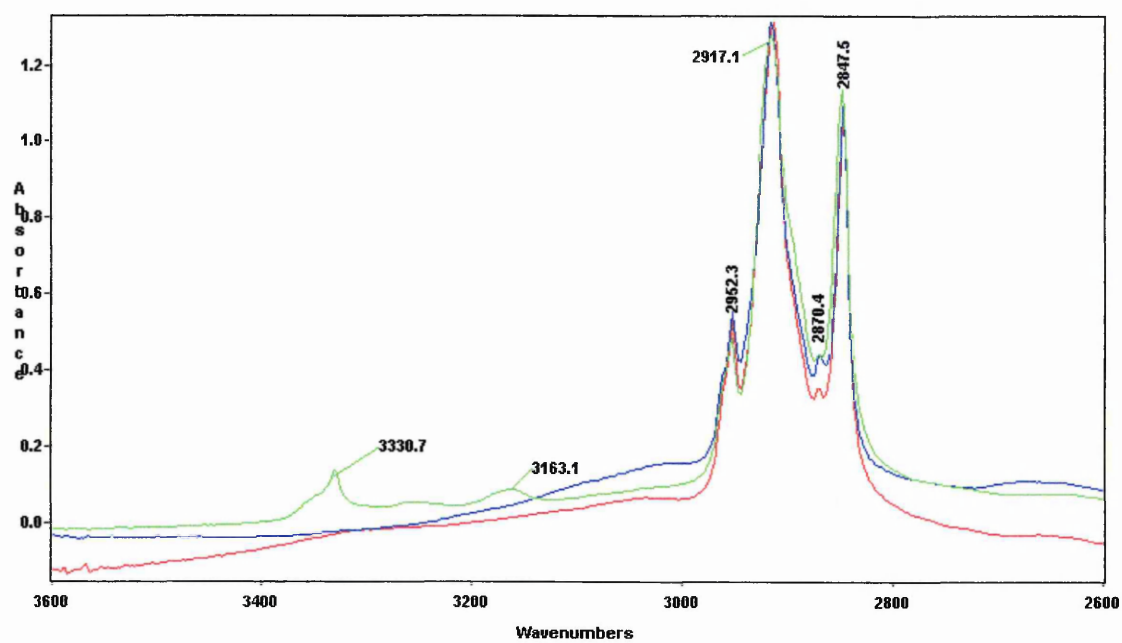
Figure 5-1: FTIR-ATR spectra of SA (blue), ODA (green) and a mixture of the two (red) in cast film form.

The spectrum for the cast mixture of SA and ODA (red) shows signs of deprotonation of the carbonyl moiety. The carbonyl stretching mode at $1701cm^{-1}$ is reduced in intensity and the NH_2 stretching absorption bands at 3330 and $3160cm^{-1}$ are no longer visible. The related NH_2 deformation modes at 1611 and $1566cm^{-1}$ are also reduced in intensity and have been overtaken by a host of new absorption bands. These new bands are at 1617 and $1507cm^{-1}$, assigned to NH_3^+ bending modes, and at 1561 and $1407cm^{-1}$ due to the COO^- antisymmetric and symmetric stretching modes[4] respectively. Additionally, the $1299cm^{-1}$ absorption band is no longer seen. The CH_2 wagging progression, while still present, is weaker than in the case of the acid alone and the CH_2 scissoring band appears as a single absorption. All this shows that the crystal structure is significantly different in this mixture than for either of the components alone.

5.2.1.2 Reflection-Absorption infrared spectroscopy

The FTIR-RAIRS spectra for cast films of SA, ODA and a mixture of the two are shown in Figure 5-2. For the SA (blue) spectrum the same features (as in the ATR spectrum) can be seen. These include the CH_2 wagging progression and the C=O stretching band, now seen at $1706cm^{-1}$, as expected for RAIRS.[5] The important point to note is the variation in the relative intensities of the bands compared with those found in the ATR spectrum. The most obvious differences are the enlargement of the acid C=O stretching band and the CH_2 wagging progression bands in comparison with the other bands. In the case of the ODA (green), the absorption bands due to the NH_2 groups are significantly different. The most prominent mode occurs at $1592cm^{-1}$ with shoulders at either side corresponding to the bands seen in the ATR spectrum.
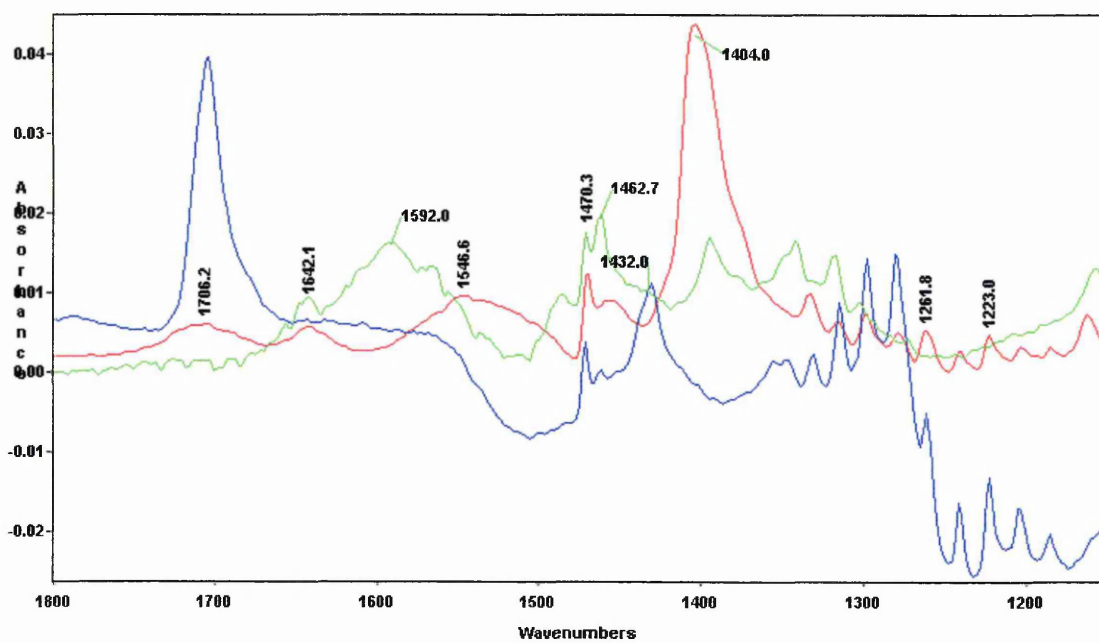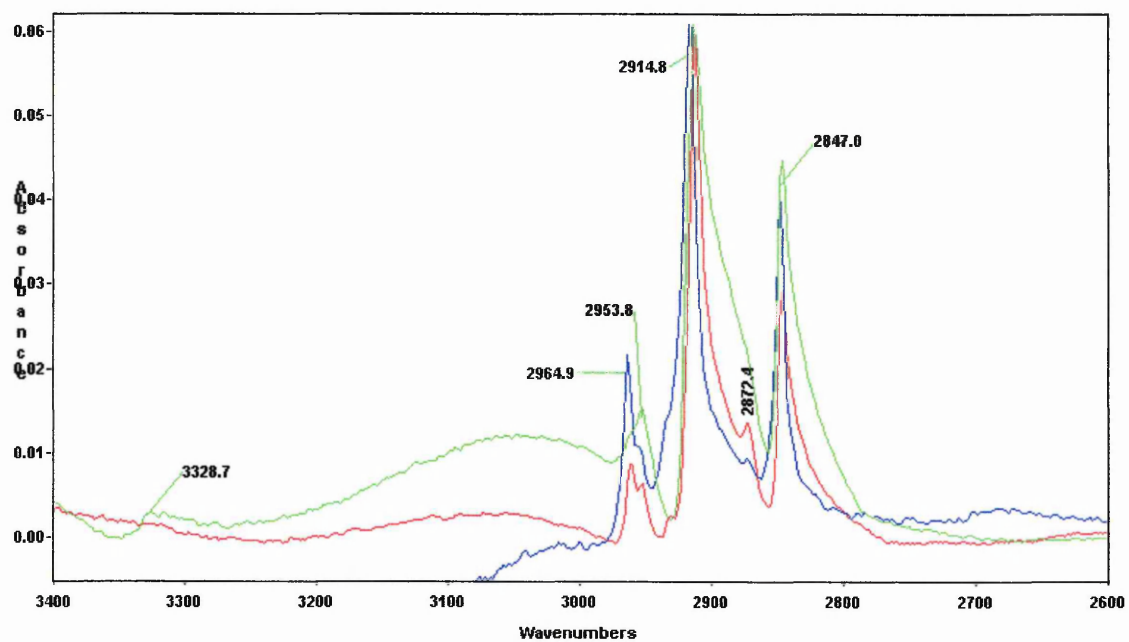
Figure 5-2: FTIR-RAIRS spectra of SA (blue), ODA (green) and a mixture of the two (red) in cast film form.

80

Similarly, an absorption is seen at 1642cm^{-1} in RAIRS which was seen as a shoulder in ATR. These changes arise from the orientational sensitivity of RAIRS as compared to ATR. An interesting feature of the spectrum of the mixture (red) is the very large 1404cm^{-1} band due to the symmetric COO$^-$ stretching mode showing that this transition dipole is close to being perpendicular to the surface. Similarly, it is likely that the remaining C=O groups are aligned nearly parallel to the surface as the 1706cm^{-1} band is now very weak. This results in there being an apparently greater amount of proton transfer, in comparison to that seen in the ATR spectra [Figure 5-1], but the ratios of proton-transferred to hydrogen-bonded species are probably similar in both cases.

5.2.2 Langmuir-Blodgett films

Langmuir-Blodgett film samples were made as described in chapter 2. In the case of the alternate layer samples, the acid monolayer was always deposited first and last. This is in order that the samples analysed by FTIR are as similar as possible to those prepared for the pyroelectric devices, [Chapter 4] which also have one more acid layer than amine layer.
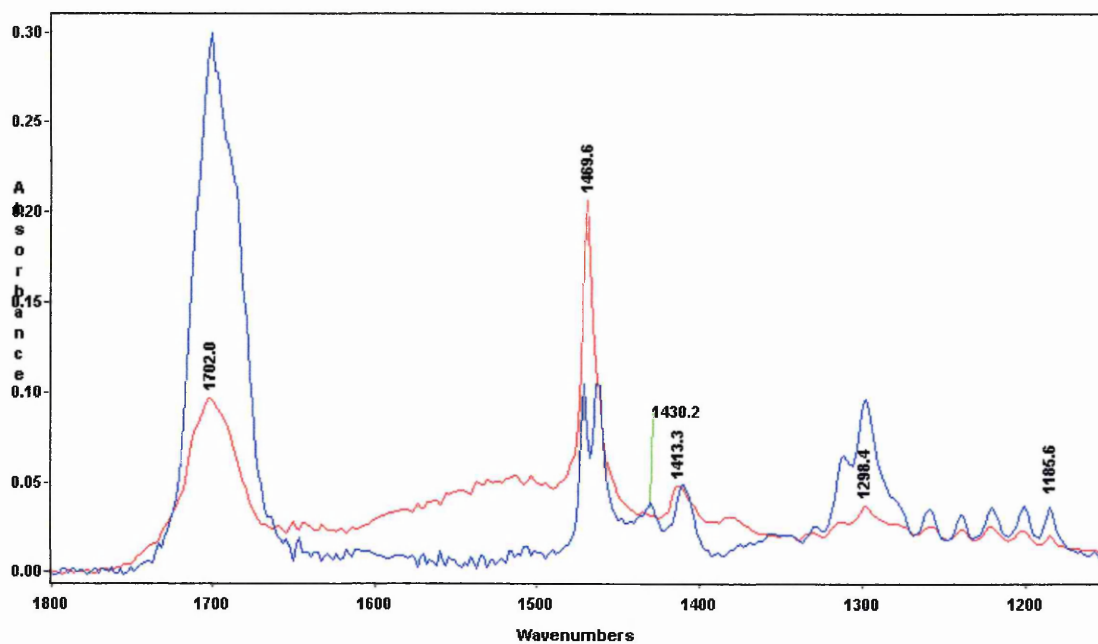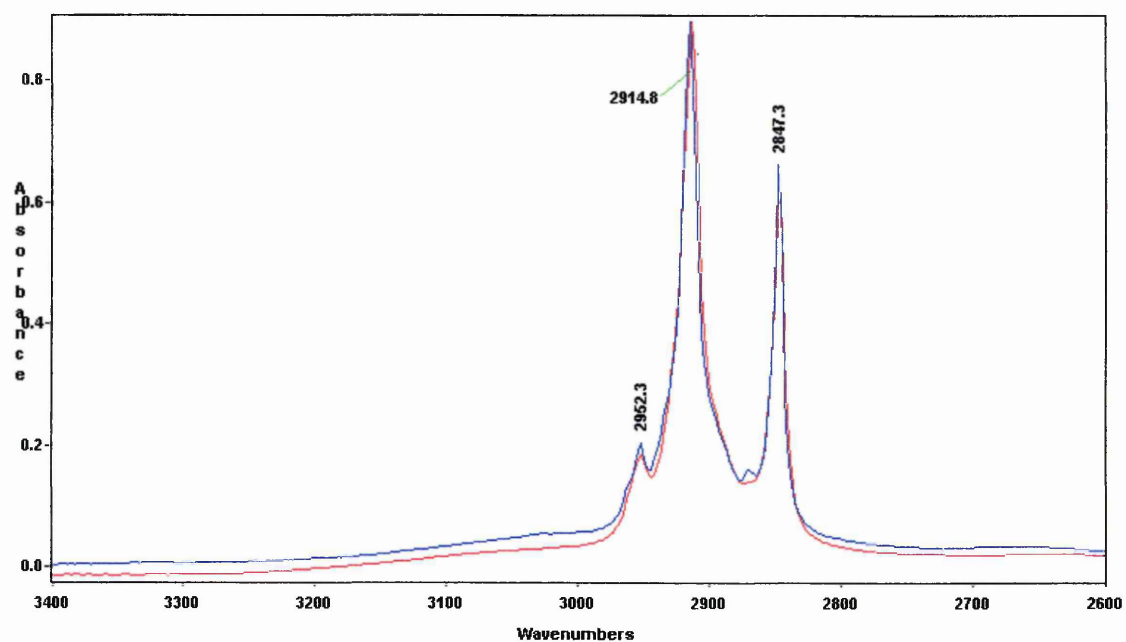
Figure 5-3: FTIR-ATR spectra of SA (blue) and SA/ODA (red) in LB film form.

5.2.2.1 Attenuated total reflection infrared spectroscopy

The FTIR-ATR spectra for LB deposited stearic acid and the alternate layer system are shown in Figure 5-3. For SA (blue) the only real difference, in comparison to the cast film, is in the overall intensity of the spectra. This is simply due to having less material sampled as the LB films are very much thinner than the cast films. In addition, it is reasonable to expect that the molecules in the cast film self-assemble with the carboxylic acid groups at the surface. Since this is the expected conformation in the LB film, and since ATR (in particular) is most sensitive at the interface between crystal and sample, it is not surprising that the spectra of cast and LB films are similar. This also confirms the crystalline order of these straight chain systems when deposited as LB films.

The FTIR-ATR spectrum for 15 alternate layers of SA and ODA is shown in red. The most obvious feature of the ATR spectrum is that there are not as many peaks as in the cast film. The main difference between the two is that the $v(COO^-)$ peaks, which usually show very strong absorption, are ill defined. Only the symmetric stretching mode is really visible at $1380cm^{-1}$. Additionally, there are no well defined NH_2 or NH_3^+ bands. Instead, there is a broad absorption between 1670 and $1350cm^{-1}$ which is probably due to all these overlapping bands. The bands due to the CH_2 wagging progression, although not as strong as for the acid alone, show that the alkyl chains have a reasonably high degree of crystalline ordering.

Octadecylamine does not readily form LB films[6] so no spectrum is shown for it here. However, since the SA and mixed spectra are reasonably similar to their cast versions, it can be safely assumed that there would be no great differences for the case of ODA.

5.2.2.2 Reflection-Absorption infrared spectroscopy

The FTIR-RAIRS spectra for the LB deposited aliphatic systems showed the same bands as in the cast film case. The only real difference was that the CH_2 wagging progression bands (1332-1187cm^{-1}) were particularly strong, especially for the SA. These bands and the alkyl stretching bands indicate that the chains are oriented closer to the surface normal, on average, than in the cast film case. As the main advantage of LB films is the high degree of orientational order which can be obtained, it is confirmation that these films are well deposited.

The band assignments for all the straight chain spectra described above are given in Table 5-1.

Band Position (cm^{-1})	Assignment	Occurrence (ATR, **R**AIRS)
3331	$\nu(NH_2)$	A, R
3163	$\nu(NH_2)$	A
2952	$\nu_a(CH_3)$	A, R
2917	$\nu_a(CH_2)$	A, R
2870	$\nu_s(CH_3)$	A, R
2947	$\nu_s(CH_2)$	A, R
1706	$\nu(C=O)$	R
1701	$\nu(C=O)$	A
1617	$\delta(NH_3^+)$	A
1611	$\delta(NH_2)$	A
1592	$\delta(NH_2)$	R
1566	$\delta(NH_2)$	A
1561	$\nu_a(COO^-)$	A
1507	$\delta(NH_3^+)$	A
1470 + 1466	$\delta(CH_2)$	A, R
1430	$\delta(CH_3)$	A, R
1414	$\delta(CH_3)$	A
1404	$\nu_s(COO^-)$	A, R
1380	$\nu_s(COO^-)$	A, R
1299	$\nu(CO) + OH$ in plane bending[2]	A, R
1312-1185	CH$_2$ wagging progression	A, R

Table 5-1: The assignments of infrared bands for the straight chain materials.

5.3 Calixarene systems

5.3.1 Cast films

The cast films of the C3 set of calixarenes were made in the same way as those of the straight chain systems. Unfortunately, no C1 was available for the manufacture of infrared samples and only limited supplies of C5 were available so cast film samples were not made for it alone or as a mixture.

5.3.1.1 Attenuated total reflection

The FTIR-ATR spectra for cast films of C3, AM and a mixture of these are shown in Figure 5-4. They are clearly very different to the straight chain system spectra. This is due to the structure of the calixarene [Figure 5-5]. The alkyl stretching bands (3100-2800cm^{-1}) highlights the different ratio of CH_3 to CH_2 groups in these molecules, compared to the aliphatic materials [Table 5-2]. The region 1480-1150cm^{-1} contains many bands arising from vibrations of the t-butyl groups and benzene rings.[4] The main bands of interest in this study are those due to the acid and amine groups. In the C3 spectrum (blue) the acid band is prominent, occurring at 1710cm^{-1} with a shoulder at 1735cm^{-1} due to a sideways dimerisation of the acid groups.[7] The AM spectrum (green) has broad NH_2 absorptions at 1638 and 1561cm^{-1}, a slight shift in comparison to ODA.
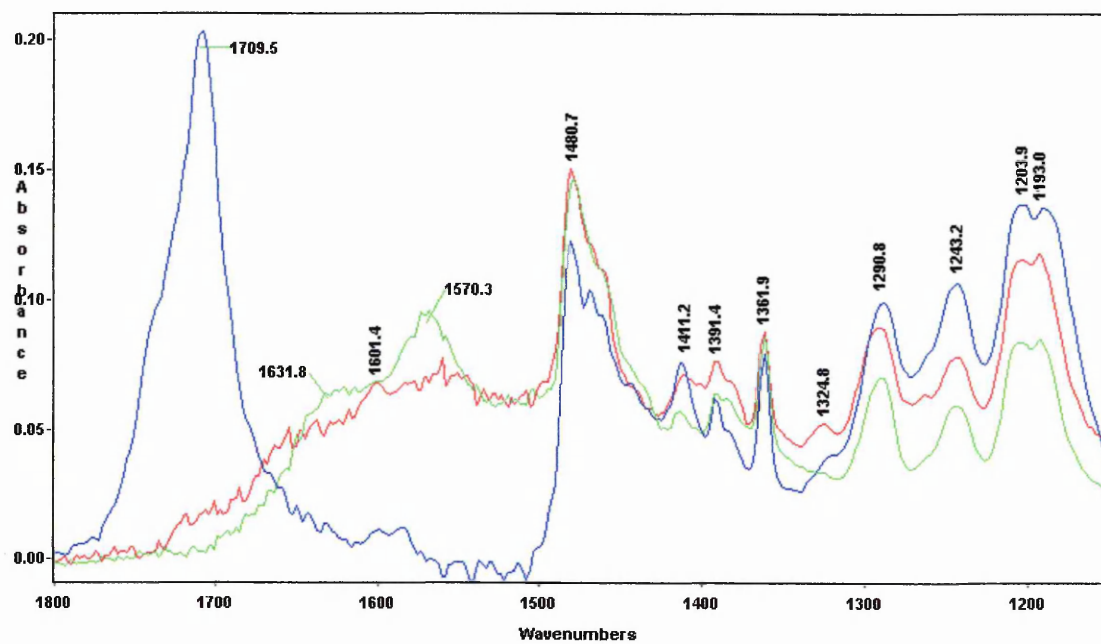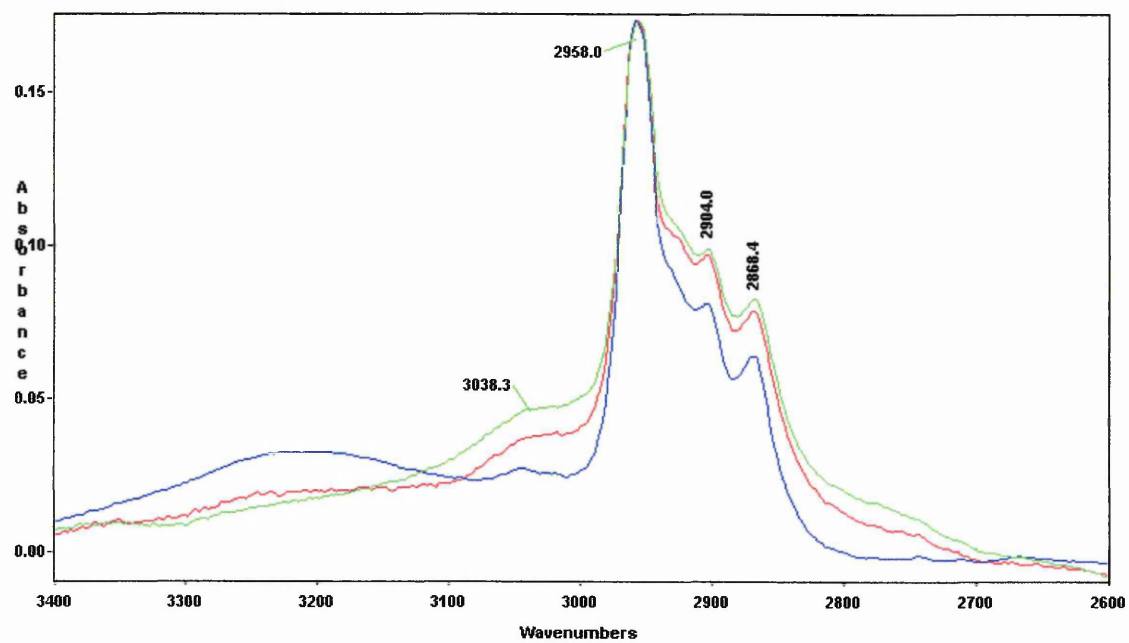
Figure 5-4: FTIR-ATR spectra of C3 (blue), AM (green) and C3/AM (red) in cast film form.

These bands are broad and are complicated by a benzene ring mode at ~1600cm^{-1}. Additionally, the amine stretching modes are not seen. In the case of the mixture (red) the acid band has virtually completely disappeared and there is a broad absorption from 1680-1500cm^{-1}. A point to note is that there do not appear to be any bands due to $\nu(COO^-)$ modes appearing. This is unusual as they can be strong.
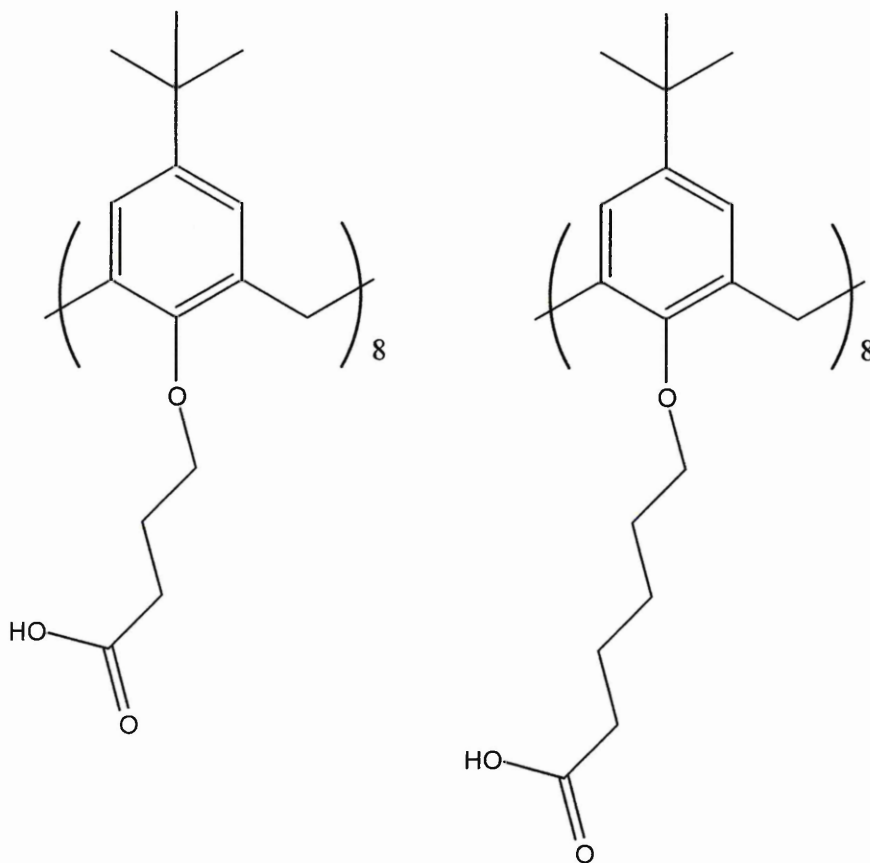
Figure 5-5: The structures of C3 (left) and C5 (right).

Material	Number of CH_2 groups (Number of C-H vibrations)	Number of CH_3 groups (Number of C-H vibrations)	$CH_3:CH_2$ vibrations
SA	15 (30)	1 (3)	1:10
ODA	17 (34)	1 (3)	3:34
C3	4 (8)	3 (9)	9:8
C5	6 (12)	3 (9)	3:4
AM	4 (8)	3 (9)	9:8

Table 5-2: Ratios of the vibrations arising from CH_3 groups to those from CH_2 groups for the materials under analysis.

5.3.1.2 Reflection-absorption infrared spectroscopy

The FTIR-RAIRS spectra for cast films of C3, AM and a mixture of the two are shown in Figure 5-6. In the C3 spectrum (blue), the occurrence of two different states for the acid groups is clear. Other than this, the bands are much the same as for the ATR case, probably because of the disorder in the film. The same is true of the AM spectrum (green) except for the slightly greater prominence of the benzene ring mode at 1600cm^{-1}. The spectrum of the C3/AM mixture does however have an interesting feature. The acid band can still be seen and additionally it now appears as a doublet. This indicates that the acid groups forming sideways dimers undergo significantly less proton transfer with the amine relative to those forming facing dimers. A further point is that there is again very little sign of corresponding bands appearing due to the deprotonation of the acid groups. However, this absence has been previously observed in RAIRS studies of acid-amine LB systems.[8]
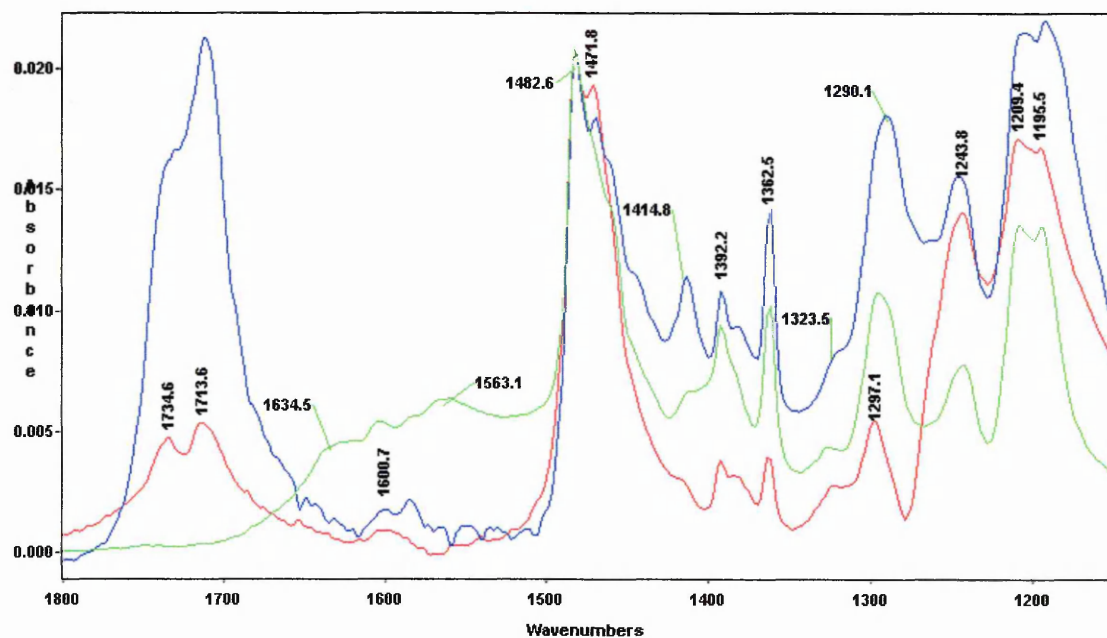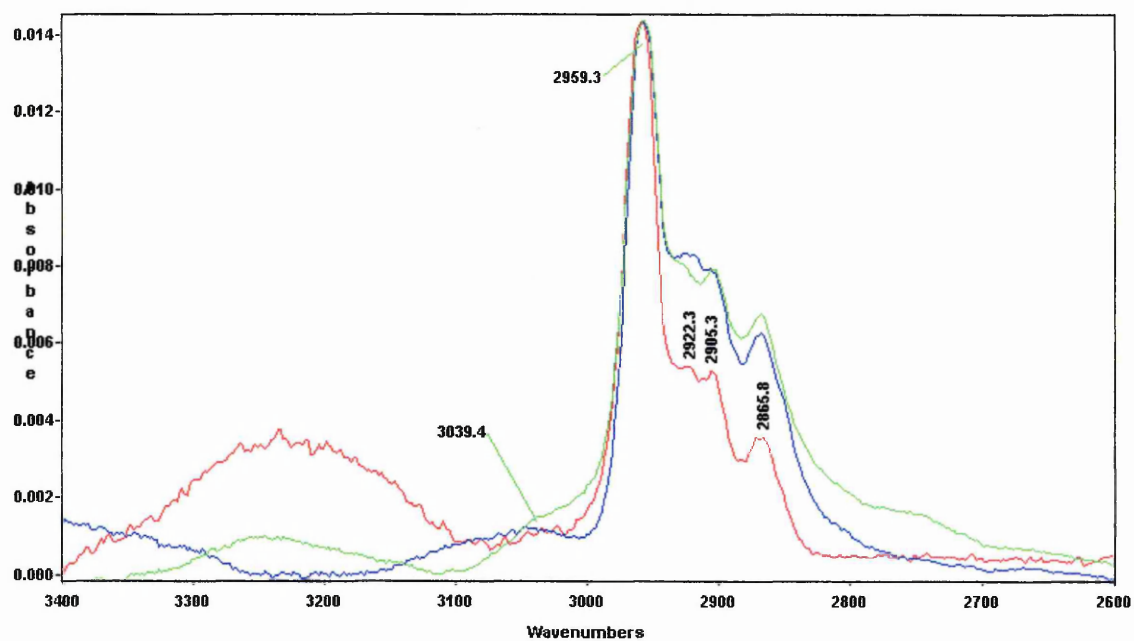
Figure 5-6: FTIR-RAIRS spectra of C3 (blue), AM (green) and C3/AM (red) in cast film form.

5.3.2 Langmuir-Blodgett films

The LB film samples of the calixarenes for FTIR analysis were made in exactly the same way as those destined for the pyroelectric measurements. The only difference was in the silicon substrate used for the ATR measurements as opposed to aluminium-coated glass slides used for both RAIRS and the pyroelectric analysis.

5.3.2.1 Attenuated total reflection

5.3.2.1.1 C3 systems

The FTIR-ATR spectra for LB films of C3, AM and C3/AM alternate layers are shown in Figure 5-7. Looking at the C3 spectrum (blue) the structural bands of the calixarene are very similar to the cast film. The acid band however is shifted slightly to $1708cm^{-1}$ but it still has a shoulder at $\sim1730cm^{-1}$ due to a proportion of the carboxylic acid groups forming sideways dimers. The AM spectrum (green) also shows the same structural absorptions but the amine bands are somewhat less well defined than in the cast film case.

The alternate layer C3/AM spectrum (red) shows the biggest differences from the cast film equivalent. The acid band is still present but is reduced in comparison to in the case of C3 only. Therefore, only partial deprotonation has occurred. Additionally, this band now occurs at $1721cm^{-1}$, confirming the observation made in the case of the cast films RAIRS spectra, that the acid groups forming sideways dimers undergo less deprotonation than those in the facing dimer configuration.
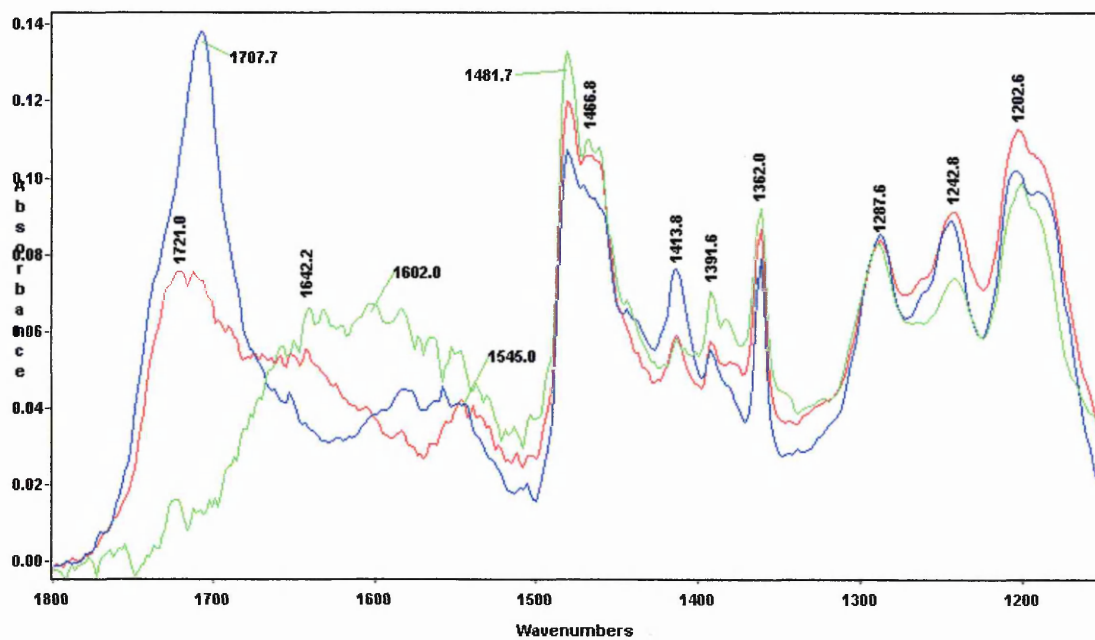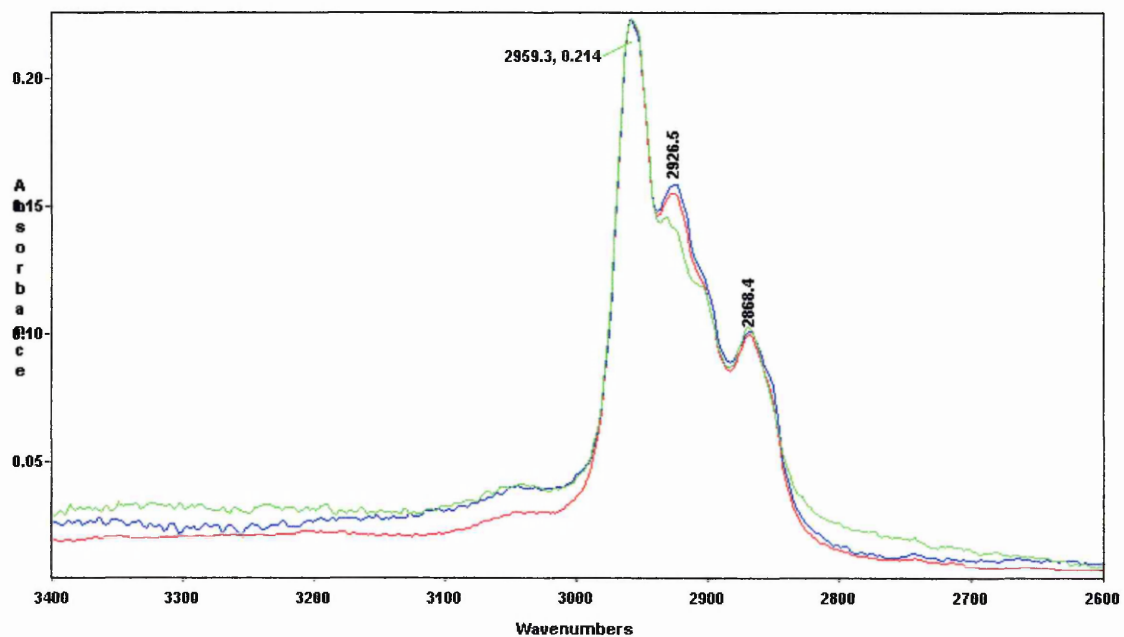
Figure 5-7: FTIR-ATR spectra of C3 (blue), AM (green) and C3/AM (red) in LB film form.

There is also a broad absorption between $1680cm^{-1}$ and $1500cm^{-1}$, due to the presence of NH_3^+ and NH_2 as well as a benzene ring mode. Finally, a band at $1546cm^{-1}$ has appeared which is likely to be the antisymmetric COO^- stretching band.

5.3.2.1.2 C5 systems

The FTIR-ATR spectra of LB films of C5, AM and C5/AM alternate layers systems are shown in Figure 5-8. It is clear that there is very little difference between the C5/AM assembly spectrum (red) and that of the C3/AM (Figure 5-7, red spectrum). Chemically, the only difference between the two systems is a slight increase in the alkyl chain length (two CH_2 groups, see Figure 5-5) of the acid substituted calixarene. Therefore, only small changes in the infrared spectra from one to the other can be expected.

An important observation is that the proportion of deprotonation is somewhat larger in the case of the C5/AM system as compared to the C3/AM case. Related to this, it can also be seen that for the C5/AM alternate layer assembly, the position of the C=O stretching band is only shifted by $3-4cm^{-1}$ from that of the LB film of C5 alone ($1709cm^{-1}$). This is significantly less than the shift observed for the C3 LB systems [Figure 5-7] and means that there is less of a difference in the relative amounts of deprotonation between the groups forming sideways and facing dimers.
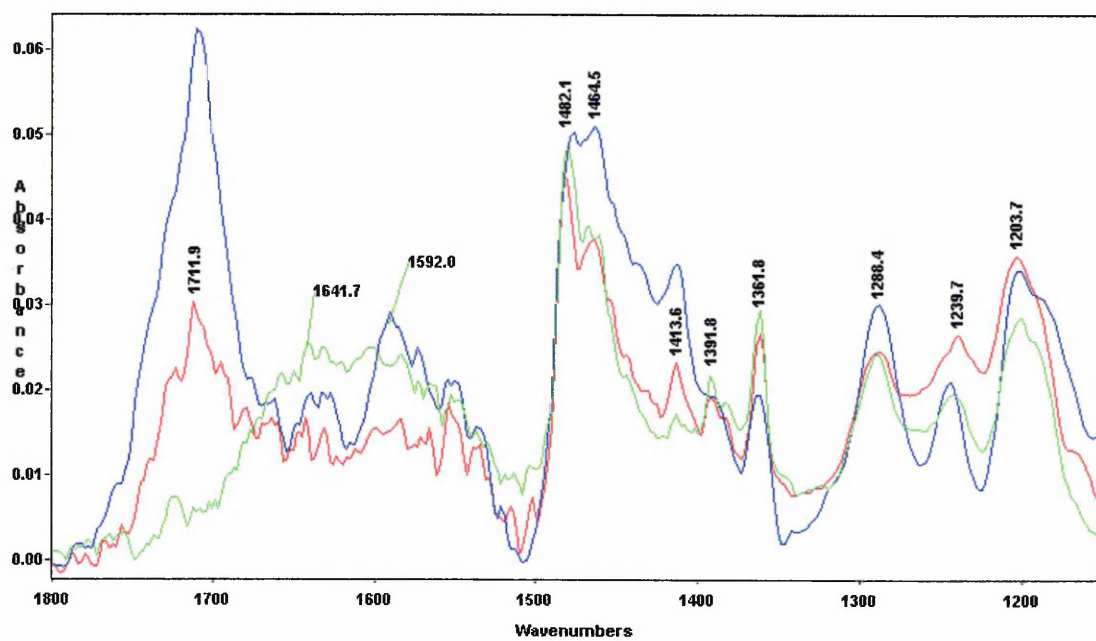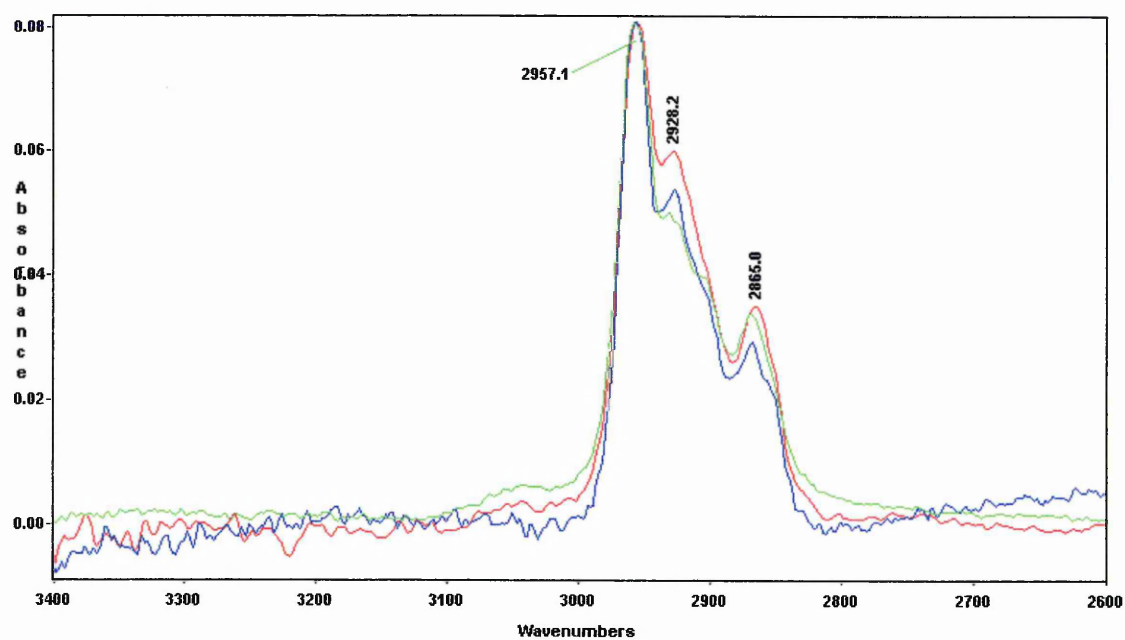
Figure 5-8: FTIR-ATR spectrum of C5 (blue), AM (green) and C5/AM (red) in LB film form.

5.3.2.2 Reflection-absorption infrared spectroscopy

5.3.2.2.1 C5 systems

The FTIR-RAIRS spectra of LB films of C5, AM and C5/AM alternate layer systems are shown in Figure 5-9. In the C5 spectrum (blue) the acid band is again stronger than in the ATR case and there is a slight change in the relative intensities of the CH_2 and CH_3 groups with the latter becoming even more dominant. The amine groups in both the AM (green) and the C5/AM spectra (red) are very weak. The latter however shows that either a high degree of deprotonation of the acid group has occurred or that the acid groups are oriented quite differently in the alternate layer system from when deposited by themselves. Additionally, the band is shifted to $1722cm^{-1}$ indicating that if the carboxylic acid groups form sideways dimers, they are less likely to undergo proton transfer with the amine groups.

The band assignments for all the calixarene systems are shown in Table 5-3.
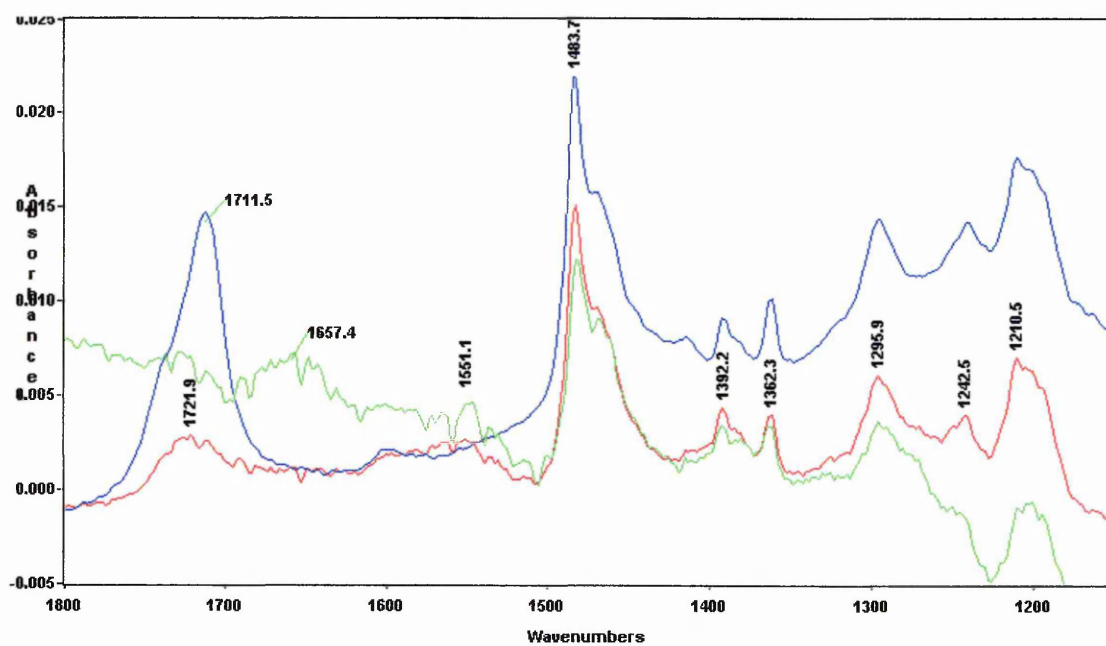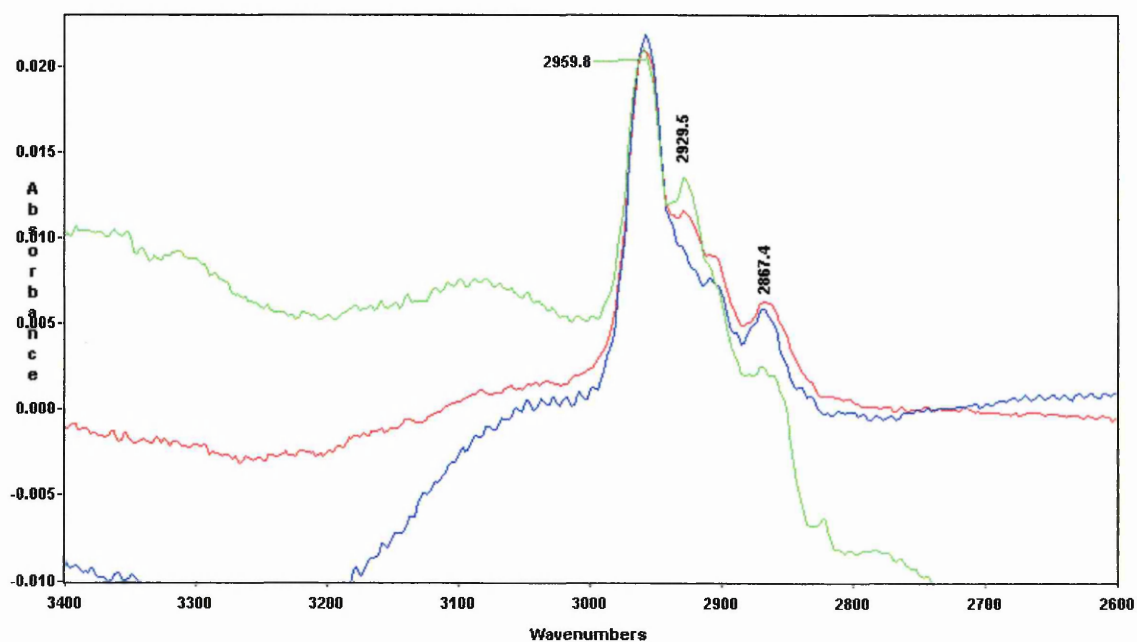
Figure 5-9: FTIR-RAIRS spectra of C5 (blue), AM (green) and C5/AM (red) in LB film form.

Band Position (cm^{-1})	Assignment	Occurrence (**A**TR, **R**AIRS)
3040	$\nu(CH)$	A, R
2958	$\nu_a(CH_3)$	A, R
2927	$\nu_a(CH_2)$	A, R
2904	$\nu_s(CH_3)$	A, R
2868	$\nu_s(CH_2)$	A, R
1735, 1722, 1714, 1711	$\nu(C=O)$	A
1721, 1712-1708	$\nu(C=O)$	R
1642	$\delta(NH_2)$	A, R
1590	ν(benzene ring)	A, R
1545	$\nu_a(COO^-)$	A
1480	$\delta(CH_3)$	A, R
1470	$\delta(CH_2)$	A, R
1460	$\delta(CH_3)$	A, R
1445	ν(benzene ring)	A, R
1414	$\delta(CH_3)$	A, R
1362	ν(benzene ring)	A, R
1391, 1300-1200	t-butyl deformations	A, R

Table 5-3: The assignments of infrared bands for the calix[8]arene systems.

5.4 Summary

A good picture of the structural and packing characteristics of the calix[8]arenes has been obtained. Additionally, some light has been shed on the interaction which occurs between the carboxylic acid and amine moieties. The most basic observation is that proton transfer occurs between these groups. In the cast films this transfer is almost complete but for the LB films this is a long way from being the case.

An important point to note is that the form of the calixarene molecules has a significant influence on the carboxylic acid groups. Firstly, the formation of sideways dimers is encouraged as compared to the straight chain case. Secondly, less proton transfer occurs for the calixarene systems. Further, it can be seen that the longer the substituted chain on the calixarene, the more proton transfer occurs, that is, the system tends more to straight chain behaviour. Finally, it is clear that, on the whole, the carboxylic acid moieties forming sideways dimers are less likely to undergo deprotonation than those forming facing dimers.

5.5 References

[1] G. H. Davies, J. Yarwood, Infrared intensity and band shape studies on LB films of ω-tricosenoic acid on silicon, Spectrochimica Acta, 1987, 43A, 12, 1619-1623.

[2] F. Kimura, J. Umemura, T. Takenaka, FTIR-ATR Studies on Langmuir-Blodgett Films of Stearic Acid with 1-9 Monlayers, Langmuir, 1986, 2, 96-101.

[3] S. Hasyashi, J. Umemura, Infrared spectroscopic evidence for the coexistence of two molecular configurations in crystalline fatty acids, Journal of Physical Chemistry, 1975, 63, 5, 1732-1740.

[4] L. J. Bellamy, The infrared spectra of complex molecules, Chapman and Hall, London, Volume 1, 1975, Volume 2, 1980.

[5] J. Umemura, S. Takeda, T. Hasegawa, T. Takenaka, Thickness and temperature dependence of molecular structure in stearic acid LB films studied by FT-IR reflection-absorption spectroscopy, Journal of Molecular Structure, 1993, 297, 57-62.

[6] M. Puggelli, G. Gabrielli, G. Caminati, Langmuir-Blodgett monolayers and multilayers of stearic acid and stearyl amine, Thin Solid Films, 1994, 244, 1050-1054.

[7] C. A. Jones, M. C. Petty, G. G. Roberts, G. Davies, J. Yarwood, N. M. Ratcliffe, J. W. Barton, IR studies of pyroelectric Langmuir-Blodgett films, Thin Solid Films, 1987, 155, 187-195.

[8] J-X. Li, J. A. Gardella, Jr., P. J. McKeown, A quantitative time-of-flight secondary ion mass spectrometry study of ion formation mechanisms using acid-base alternating Langmuir-Blodgett films, Applied Surface Science, 1995, 90, 205-215.

6. Variable temperature infrared analysis

6.1 Introduction

In order to gain an insight into the important mechanisms of pyroelectric behaviour, an analysis of the calixarene systems at different temperatures is required. The pyroelectric coefficient has been shown to be heavily dependent on the acid/amine pairs [Chapter 4] and these pairs clearly interact, by proton transfer, as seen in their infrared spectra at room temperature [Chapter 5]. Therefore, some change in these groups, related to the pyroelectric properties, can be expected to be seen in infrared spectra taken at various temperatures. This chapter looks at such spectra and then goes on to examine the correlation between the infrared analysis and the pyroelectric effect.

6.2 Variable temperature infrared measurements

Initially, the samples were heated *ex situ* and the infrared spectra taken. Subsequently, a specially designed heating rig [section 6.2.2.1] was constructed to permit *in situ* FTIR-ATR studies.

6.2.1 *Ex situ* temperature variation

For the *ex situ* measurements, samples were placed in an oven at 80°C for 20 minutes. They were then transferred to the spectrometer (at room temperature) and a series of spectra taken. Since the samples are small and not likely to retain heat for long, fewer co-added scans were used than for the room temperature measurements in order to

reduce the scan time. This can only be achieved due to the high sensitivity of the ATR method.

The resulting spectra are shown in Figure 6-1. The spectra are somewhat noisy because of the shorter scan times, but it is clear that no change has occurred in the spectrum between the initial measurement, immediately after removal from the oven, and after a subsequent period of cooling. The collection of the initial spectrum was completed within 2 minutes of removing the sample from the oven and no subsequent change was observed over the next 30 minutes.
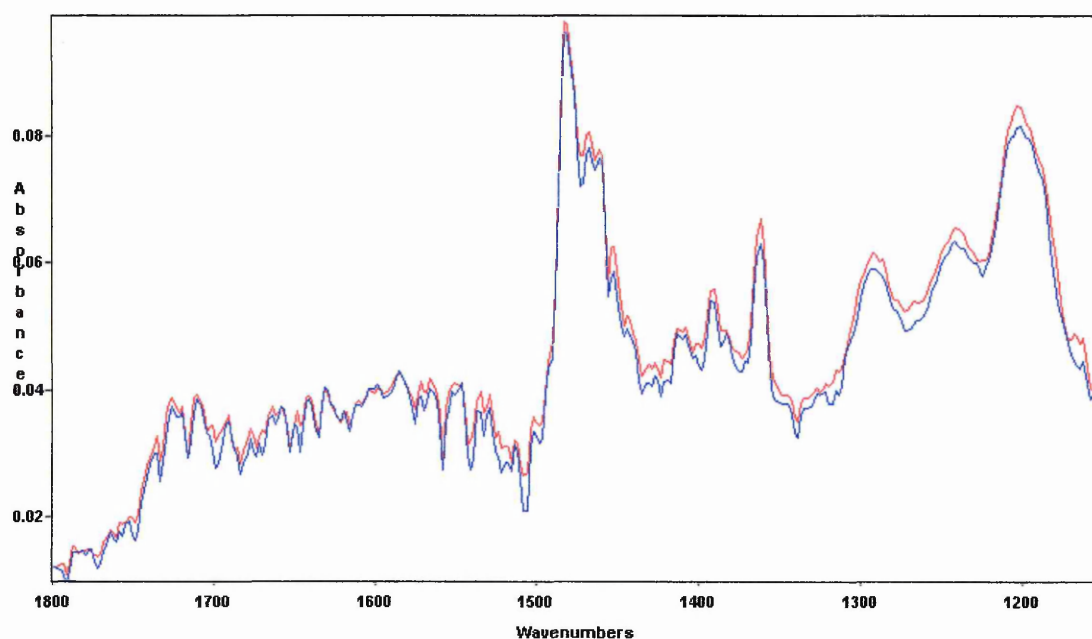
Figure 6-1: FTIR-ATR spectra of a C3/AM LB film immediately after heating to 80°C (red) and after 30 minutes of cooling at room temperature (blue).

There are two possible conclusions; either that the sample cooled completely in the first minute out of the oven, or that no change occurs with temperature for these materials. To ascertain which of these is the case, the sample must be maintained at different temperatures and spectra obtained *in situ*.

101

6.2.2 *In situ* temperature variation

A special heating stage and control system was designed and constructed to allow the collection of ATR spectra while maintaining the sample at a set temperature. The arrangement of this system is described below, followed by the results obtained using it.

6.2.2.1 Experimental arrangement

The heating stage used for the *in situ* measurements is shown in Figure 6-2. The back of the ATR crystal, with the LB film on front side, is placed in direct contact with a Peltier heater/cooler. On the reverse of the heater is a heat sink to assist with the cooling of the sample. A platinum-wire resistance thermometer (PRT) is placed in contact with the LB film to measure the temperature precisely at the sample. The Peltier device is controlled by a feedback mechanism from the thermometer and can maintain a pre-set temperature in the range 0-80±0.2°C.
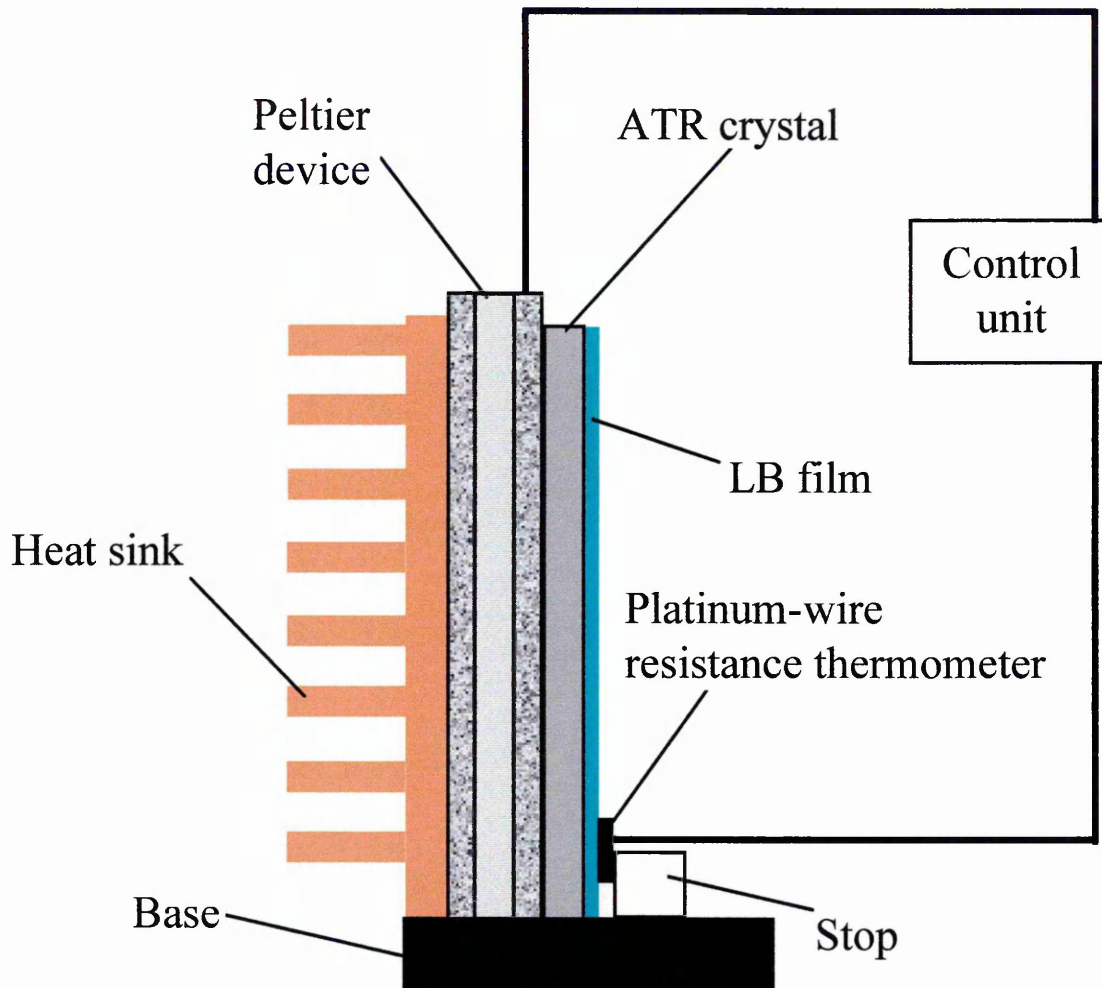
Figure 6-2: The *in situ* temperature variation stage.

6.2.2.2 *In situ* results

FTIR-ATR spectra were taken of both the C3/AM and C5/AM LB films at a range of temperatures. The resulting spectra of the C3/AM system are shown in Figure 6-3 and the C5/AM spectra are shown in Figure 6-4. It is clear that even with a temperature change of 60°C, there is virtually no change in the spectrum, for either type of film.

The changes which are seen at $1362cm^{-1}$ and $1300\text{-}1200cm^{-1}$ may be indicative of some rearrangement in the packing of the calixarene bowls and the t-butyl groups at the upper rim.
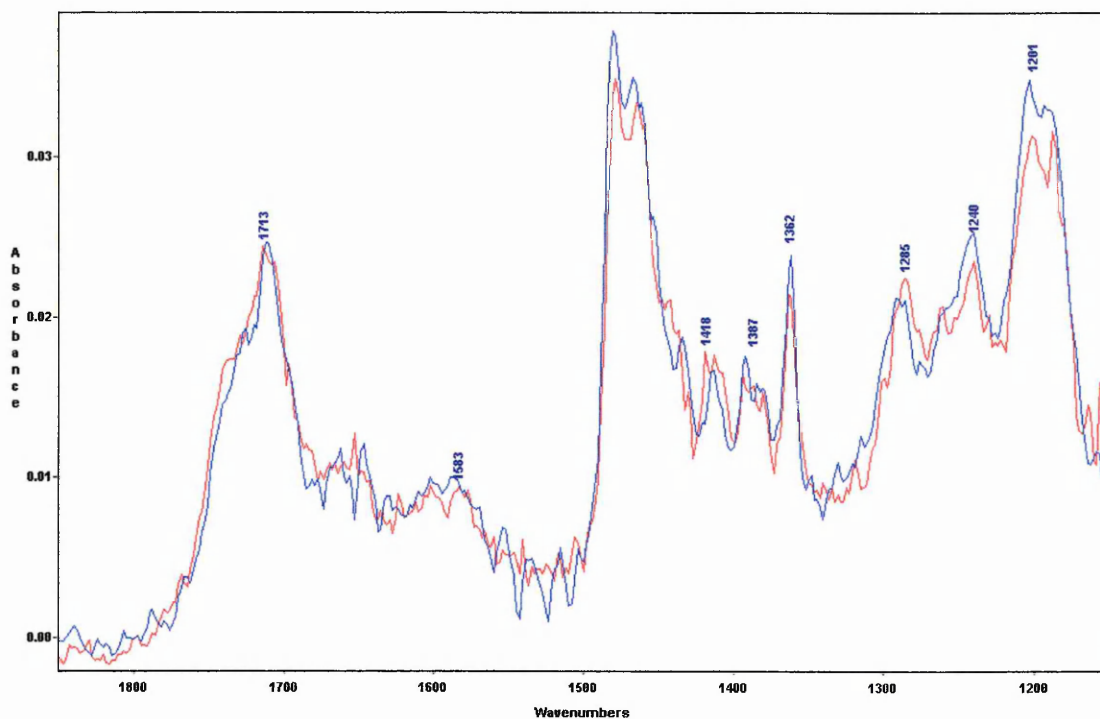
Figure 6-3: FTIR-ATR spectra of a C3/AM LB film at 20°C (blue) and 80°C (red).
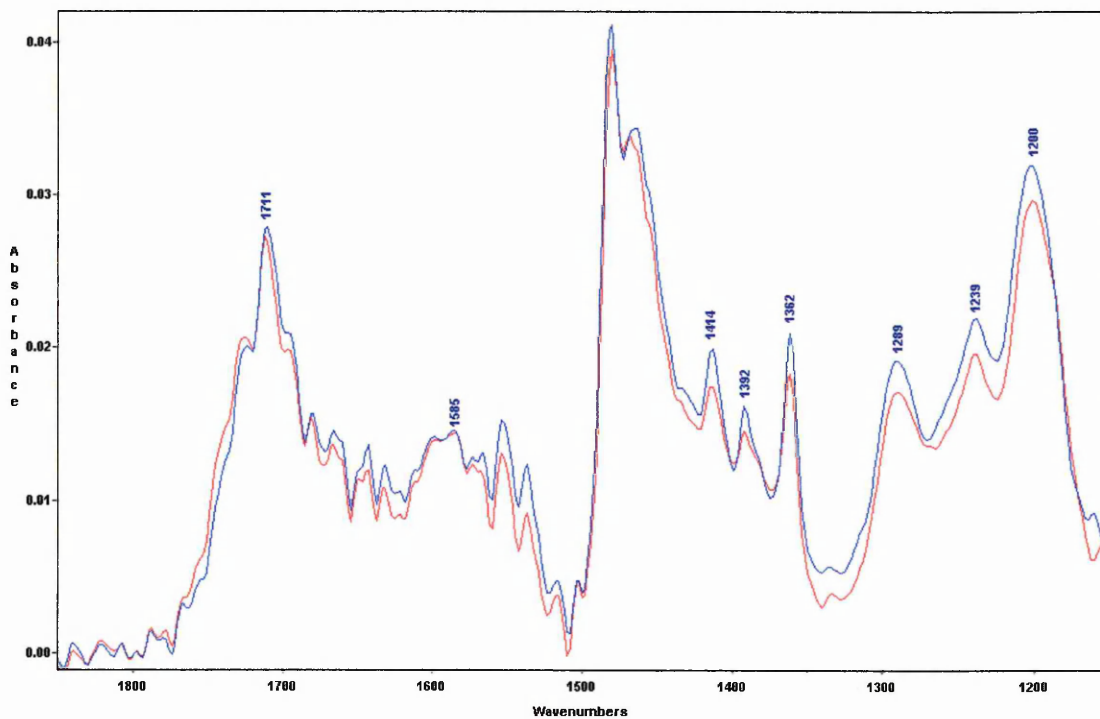
Figure 6-4: FTIR-ATR spectra of a C5/AM LB film at 20°C (blue) and 80°C (red).

104

Some change in the arrangement of the molecules is to be expected in organic thin films exposed to such a large thermal change but the variations are so small that they could feasibly arise from the effect of the temperature change on the ATR experiment itself. Either way, it is clear that these calixarene films display a remarkable resistance to temperature alterations. However, the most important fact regarding these spectra is that they confirm that there is no change in the nature of the acid groups with temperature. That is, there is no change in the amount of proton transfer between the acid and amine moieties.

6.3 Relationship between the pyroelectric effect and the infrared spectra

In order to understand the correlation between the infrared spectra measured above and the observed pyroelectric results [Chapter 4], some theoretical calculations are needed. It is possible to determine the likely changes in the acid and amine groups which would give rise to the measured pyroelectric coefficients. This will then help in the interpretation of the infrared spectra. In the case of the C3/AM system, for a typical pyroelectric coefficient of $6\mu Cm^{-2}K^{-1}$ and looking at a single pair of molecules, the following can be obtained.

The pyroelectric coefficient is defined as the rate of change of polarisation with time:

$$\Gamma = \frac{dP}{dT}$$
<div style="text-align: right">**Equation 6-1**</div>

with:

$$dP = N\Delta\mu$$
<div style="text-align: right">**Equation 6-2**</div>

where N is the number of dipoles per unit volume and $\Delta\mu$ is the change in dipole.

In the ideal case where the molecules in each layer are perfectly aligned [Figure 6-5], then the unit volume is one pair of acid- and amine-substituted calixarenes. Since there are 8 dipoles within this volume:

$$N = \frac{8}{2\delta A_m}$$ **Equation 6-3**

where, A_m is the area per molecule, previously measured from the isotherms of the materials and δ is the molecular thickness, calculated from CPK models.

Therefore the change in dipole is given by:

$$\Delta\mu = \frac{2\Gamma dTA_m\delta}{8}$$ **Equation 6-4**

Applying the figures to this equation, the change required per dipole (in order to obtain a pyroelectric coefficient of $6\mu Cm^{-2}K^{-1}$) is calculated to be:

$$\Delta\mu = \frac{2 \times 6 \times 10^{-6} \times 1 \times 275 \times 10^{-20} \times 1.5 \times 10^{-9}}{8} = 6.2 \times 10^{-33} Cm.$$

Based on this value, an assessment of the physical changes which would give rise to this change in dipole may be made.
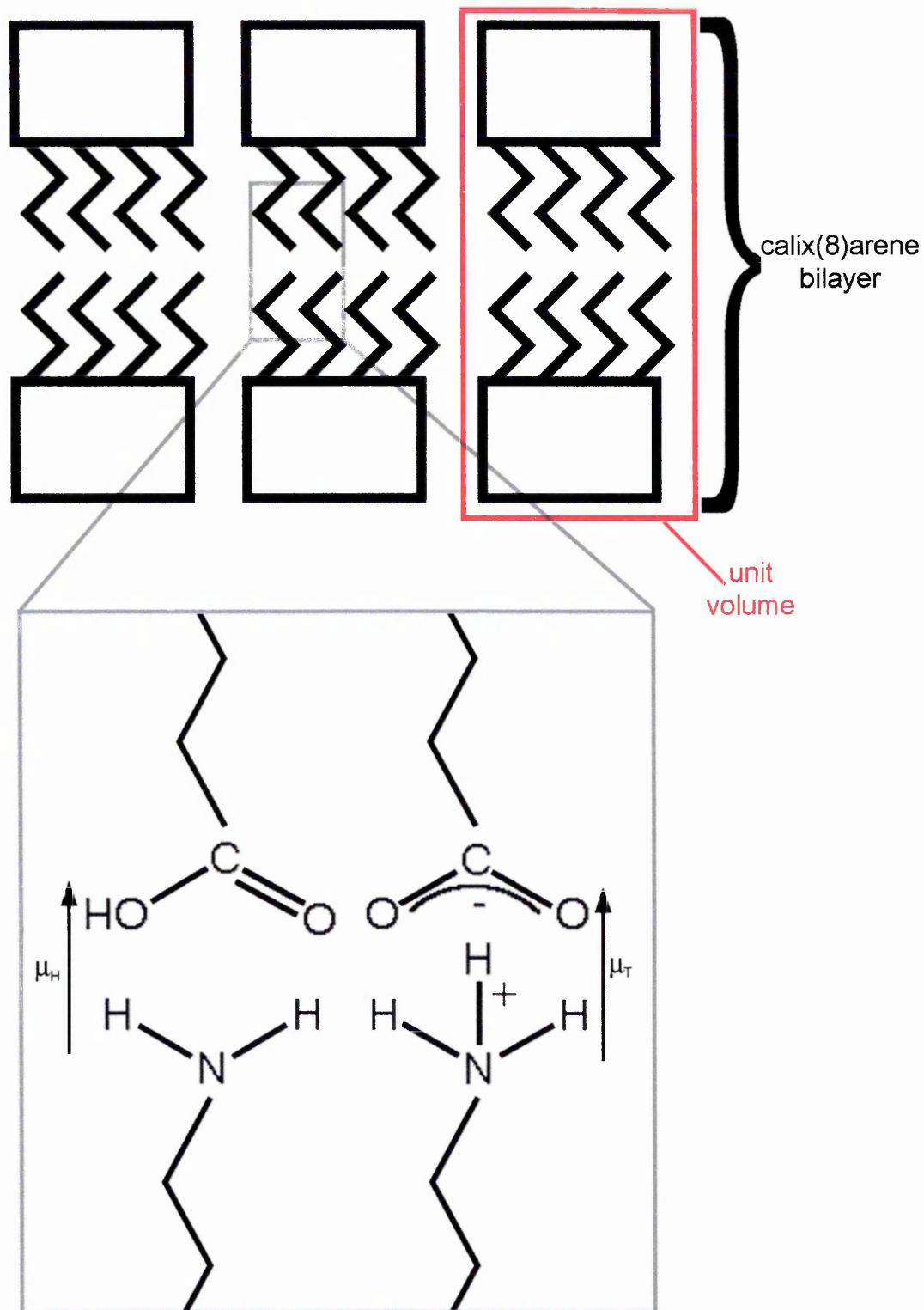
Figure 6-5: Schematic diagram of an ideal calix(8)arene bilayer (top), showing the unit volume (red) and two possible dipoles (bottom), μ_T for the proton-transferred state and μ_H for the hydrogen-bonded state.

a)   b)
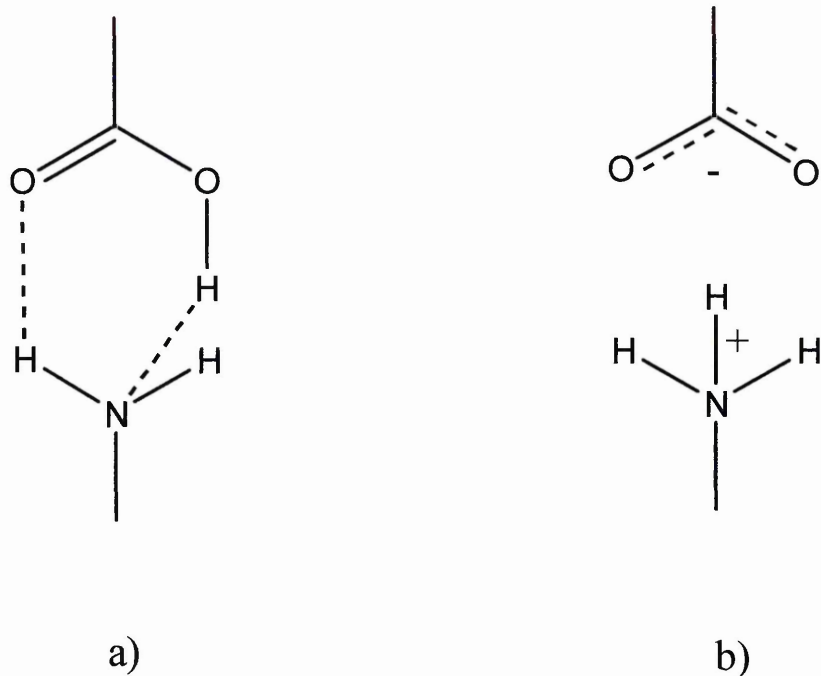
Figure 6-6: (a) The hydrogen-bonded state and (b) the proton-transferred state.

In the case where proton transfer is initially complete [Figure 6-6b], the condition that the electric polarisation can only change as a result of a change in the separation of the acid and amine groups can be imposed. This change in distance, Δd, can then be calculated. The electronic charge of the dipole, q, is that of the transferred proton and is thus known. Hence the change in dipole is simply:

$$\Delta\mu = q\Delta d \hspace{6cm} \textbf{Equation 6-5}$$

Therefore, for the generated pyroelectric coefficient of $6\mu Cm^{-2}K^{-1}$, the change in dipole is 6.2×10^{-33} Cm and $\Delta d = \dfrac{6.1875\times10^{-33}}{1.6\times10^{-19}} = 3.867\times10^{-14}\,m$. This is a tiny amount but it should be noted that the separation of the acid and amine groups is only of the order of $1.5\times10^{-10}m$.

On the other hand, imposing the condition that the length of the dipole is fixed at 1.5×10^{-10}m, the charge flow needed to obtain the same pyroelectric coefficient ($6\mu Cm^{-2}K^{-1}$) can be calculated. The result is that a charge of

$$\Delta q = \frac{6.1875 \times 10^{-33}}{1.5 \times 10^{-10}} = 4.125 \times 10^{-23} C$$ must flow from one group to the other. This is the

equivalent of ~2.5×10^{-4} protons transferred per acid/amine pair.

This analysis applies equally to the case where there is no initial proton transfer [Figure 6-6a]. However, as neither the distances or charges involved in the dipole are known for this state, the results obtained are inevitably less accurate. Even so, it is likely that the distance scale is similar[1] and thus the same result regarding the current flow is obtained. Using a distance of 1.5×10^{-10}m and a previously calculated value of the dipole[2] of 6.9×10^{-30}Cm, the effective charge in the hydrogen bonded system is 4.6×10^{-20}C. Therefore, the change in distance required in the hydrogen-bonded case is

$$\Delta d = \frac{6.1875 \times 10^{-33}}{4.6 \times 10^{-20}} = 1.345 \times 10^{-13} m$$. This is somewhat greater than for the proton-

transferred system.

In the case where the change in polarisation arises solely from a change in distance, this represents an expansion of ~$1 \times 10^{-5}K^{-1}$, a typical value for an organic material (~$4.5 \times 10^{-5}K^{-1}$ for the hydrogen-bonded case, a rather large amount). However, for the case involving proton transfer only, the charge transfer amount calculated (2.5×10^{-4} protons) is equivalent to a current of ~1.0×10^{-23}A which is many orders of magnitude smaller than the measured pyroelectric current (~150pA). This means that the pyroelectric effect cannot be due to the interconversion from a hydrogen-bonded to a proton-transferred state (or vice versa). Therefore, it is solely a change in distance

between the acid and amine moieties which is responsible for the pyroelectric activity in these alternate layer films.

Having established the most likely source of the pyroelectric activity in these calixarene films, it is interesting to consider what the calculated values (of the change in distance required) mean in a real sample. The theoretical model, presented above, assumes that the calixarenes are entirely rigid. Thus the value for the change needed in the distance of the dipole to produce a given pyroelectric coefficient has been translated into an expansion coefficient. However, this is not necessarily an accurate assessment since a variation of this level in the dipole may arise from one of many mechanisms (or several acting together). The first of these possibilities is that the distance between each layer changes uniformly, that is, in the manner assumed in the calculation of the expansion coefficients [Figure 6-7b]. Alternatively, the pendant chains attached to the calixarenes could flex in such a way that the separation of the acid and amine moieties between a pair of molecules was increased [Figure 6-7c and d]. This sort of flexing motion would give rise to much less expansion, if any, across the film as a whole and could explain the excessive value of the expansion coefficient calculated for the hydrogen-bonded system $(\sim 4.5 \times 10^{-5} K^{-1})$.
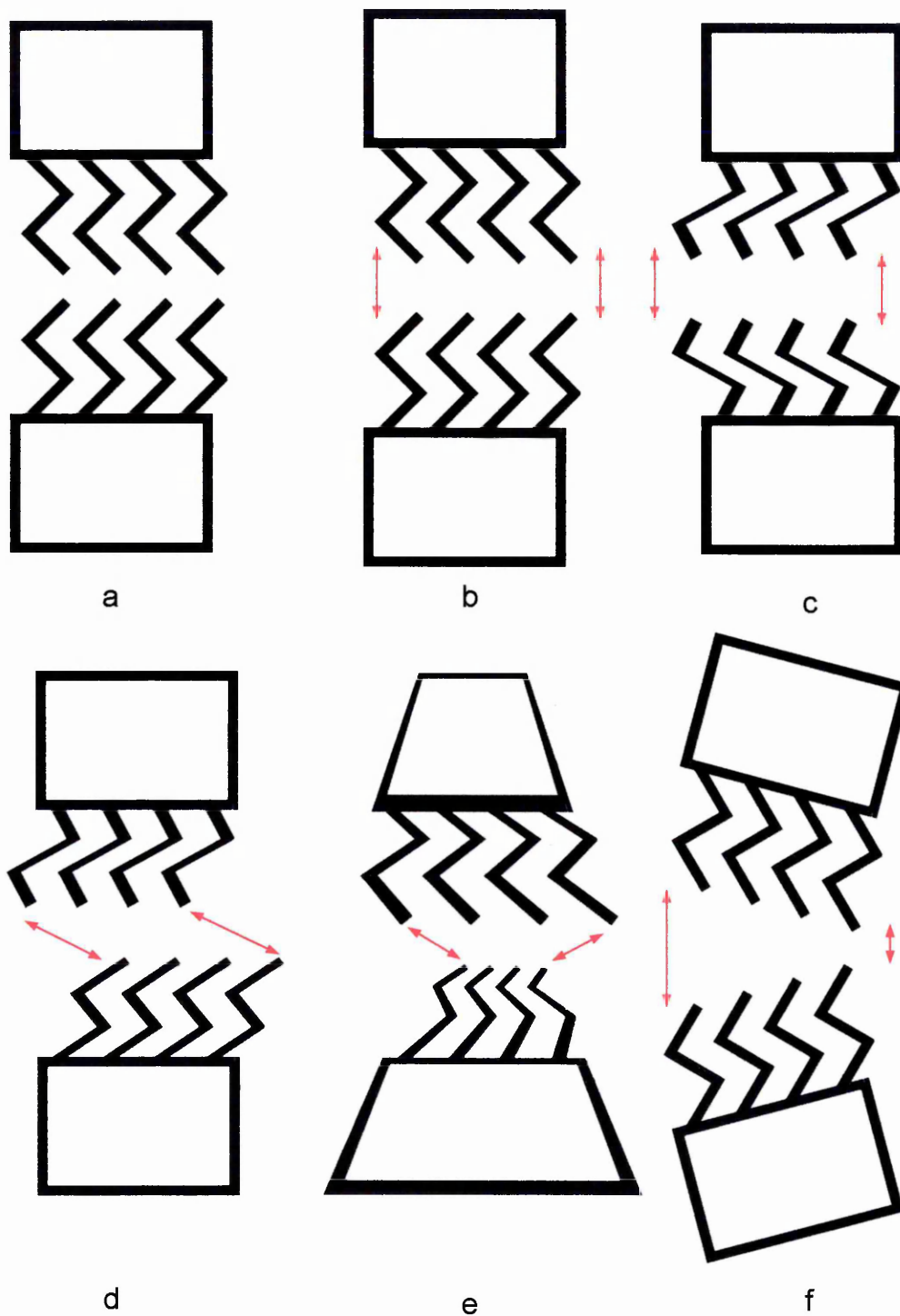
Figure 6-7: Possible changes from the normal state (a) in calixarene LB films giving rise to dipole changes: expansion (b); flexing (c, d and e) and tilting (f). Red arrows indicate the direction of change of the dipole (diagram not to scale).

Another possibility is that the bowl structure of the molecules can itself flex, causing the substituent chains to splay apart or be pinched together [Figure 6-7e]. Finally, the calixarene molecules may tilt in their entirety [Figure 6-7f], resulting in a non-uniform distance change across the dipoles which, on average, amounts to the value predicted by the model.

The hypothesis that a distance change is the source of pyroelectric activity is supported by previous theoretical models. These also show that changes from the hydrogen-bonded to proton-transferred states would result in a much greater change in polarisation than actually occurs.[2] The fact that a change in the ratio of proton-transferred to hydrogen-bonded states is not the mechanism for pyroelectricity explains the lack of noticeable change in the infrared spectra. Indeed, this also leads to further reinterpretation of results already published. In a study of the effects of temperature on straight chain acid/amine systems, the amount of proton-transferred species was seen to decrease with increasing temperature.[3] However, in the case of the calixarenes studied here there is no observed change over a similar temperature range (20-80°C), demonstrating that the ratio of the two states remains steady.

This may seem contradictory, but the answer lies in the variation of the pyroelectric coefficient with temperature. In this analysis of calix[8]arenes the pyroelectric activity was found to be more or less unchanged with increasing temperature, but in the case of straight chain type systems the pyroelectric coefficient generally increases with temperature.[2,4,5] Therefore, it is clear that when the ratio of proton-transferred to hydrogen-bonded species decreases, the pyroelectric effect is enhanced; not because of the change in the ratio itself but due to the greater number of hydrogen-bonded pairs which result.
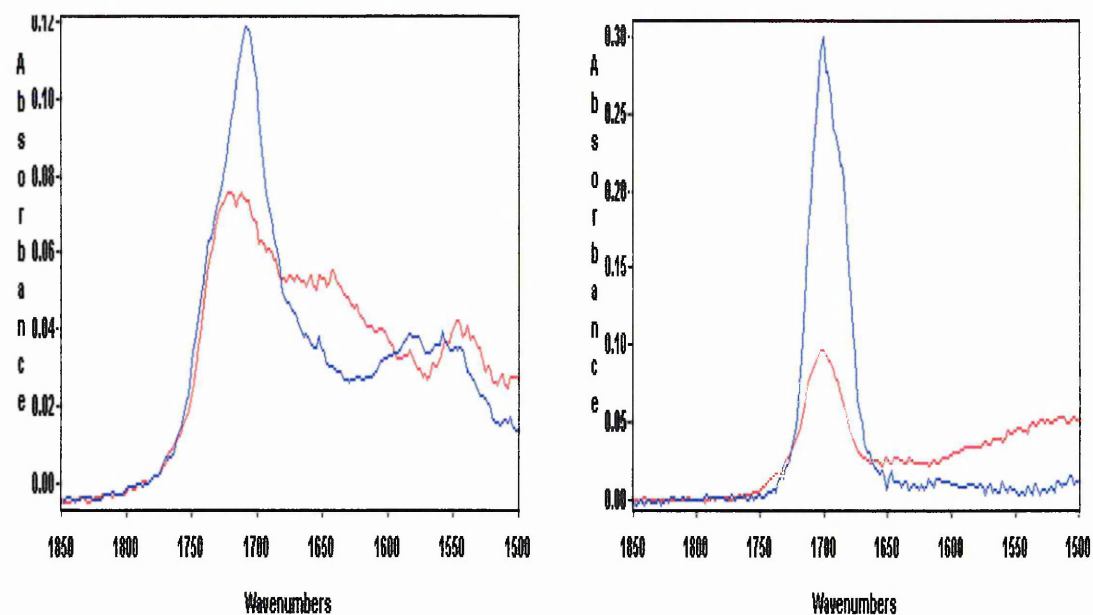
Figure 6-8: The ν(C=O) mode in ATR spectra of LB films. Left, C3 (blue) and C3/AM (red). Right, SA (blue) and SA/ODA (red).
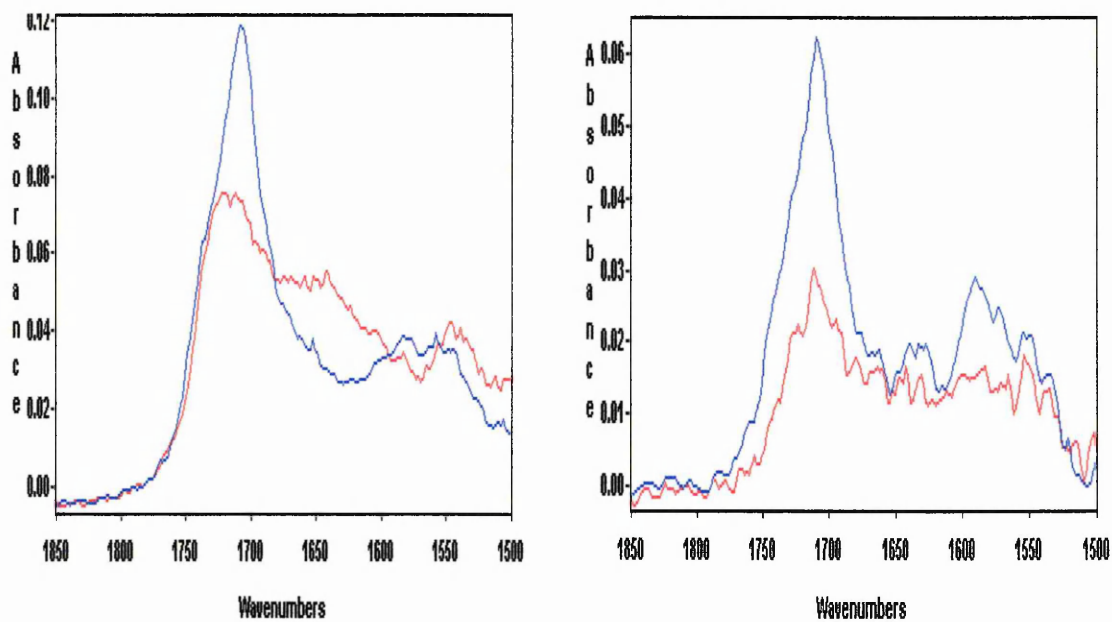
Figure 6-9: The ν(C=O) mode in ATR spectra of LB films. Left C3 (blue) and C3/AM (red). Right C5 (blue) and C5/AM (red).

113

From this, it is now possible to explain why the calixarenes studied here show such large pyroelectric coefficients. The reason is that these calixarene systems have a lower proportion of proton-transferred acid/amine pairs as compared to the straight chain systems. This is clearly seen in the infrared spectra [Figure 6-8] which show that many more carboxylic acid groups remain for the C3/AM system than in the SA/ODA assembly.

Furthermore, the reason for the dramatic decrease in the pyroelectric coefficient as the substituent chain length increases can be elucidated. The infrared spectra reveal that as the substituent chain length is increased (from 3 CH_2 groups in the C3 to 5 in the C5 material), the proportion of proton-transferred groups, in the respective alternate layer systems (C3/AM and C5/AM), increases [Figure 6-9]. In other words, the longer the chain length in the calixarenes, the closer they come to straight chain behaviour. This explains why the reduction in pyroelectric coefficients on going from C3/AM to the C5/AM system is greater than that expected due to the reduction in the acid/amine pair density.

The conclusions which can be drawn from all the above are as follows. Firstly, the results of the calculations show that the pyroelectric effect must arise from a variation in the dipole length scale, rather than from proton transfer. Secondly, empirical observation shows that the greater the amount of acid and amine moieties which are in a hydrogen-bonded state, the higher the pyroelectric coefficient. It is extremely important to note that, while in some systems (e.g. straight chain systems[3]) there may be a temperature-dependent change in the proportion of proton-transferred and hydrogen-bonded nature, this interconversion does not contribute to the pyroelectric activity. It does, however,

114

affect the pyroelectric coefficient since the amount of acid/amine pairs in the hydrogen-bonded state is changed.

a)

b)
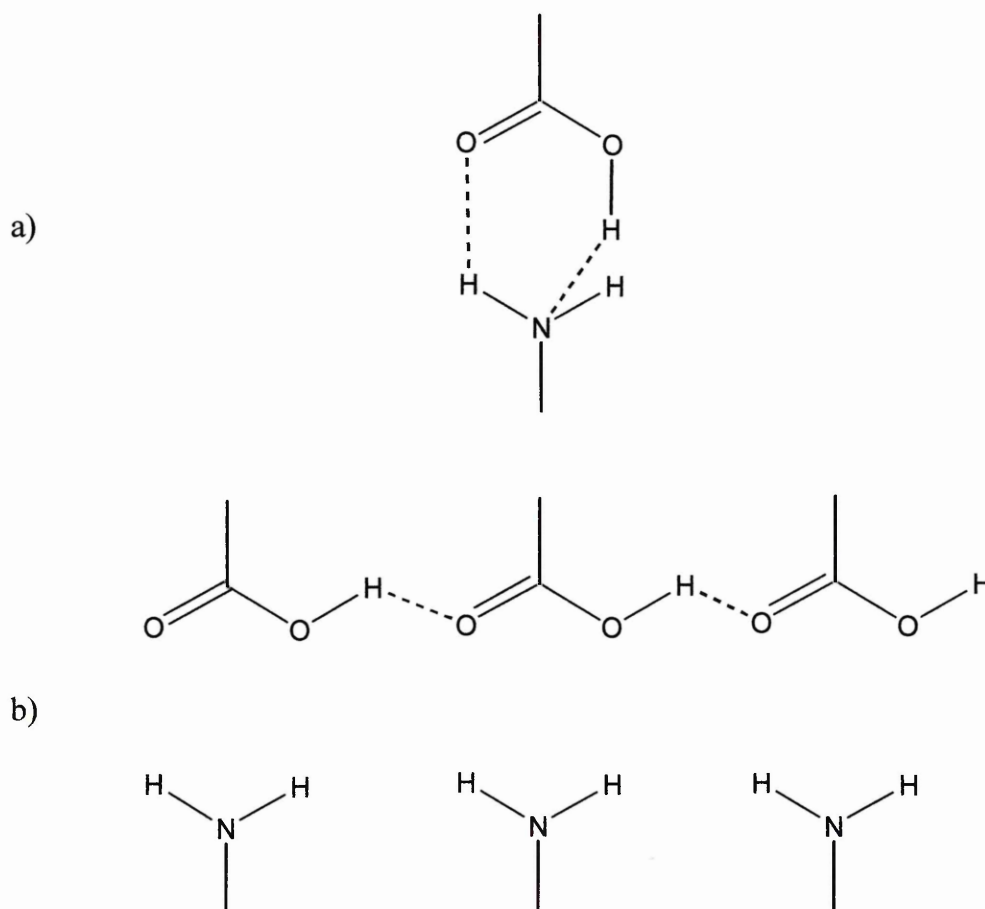
Figure 6-10: (a) Facing and (b) sideways dimers.

The reason for the larger amount of hydrogen-bonded nature in the calixarene systems is twofold. Firstly, a benzene ring in proximity to the carboxylic acid or amine groups withdraws electrons and has the effect of stabilising the hydrogen-bonded state.[2] Secondly, the form of the calixarene molecules favours the formation of sideways dimers [Figure 6-10] of the carboxylic acid. This type of dimer results in the hydrogen atom of the carboxylic acid group in effect being withheld from the amine group, making it less likely for the pair to undergo proton-transfer.

Indeed, it is evident from infrared spectroscopy that deprotonation of carboxylic acid groups in the sideways dimer conformation is hindered [Figure 6-11]. The ν(C=O) stretching band occurs at 1707cm^{-1} in the C3 LB film, with a shoulder at ~1725cm^{-1} indicating that sideways dimers are present. In the C3/AM assembly this same band appears to be formed by two almost even contributions at 1722cm^{-1} and 1710cm^{-1}. The reason for this change is that the 1707cm^{-1} facing dimer mode has undergone proportionally more proton transfer with the amine groups than the sideways dimer mode at 1722cm^{-1}.
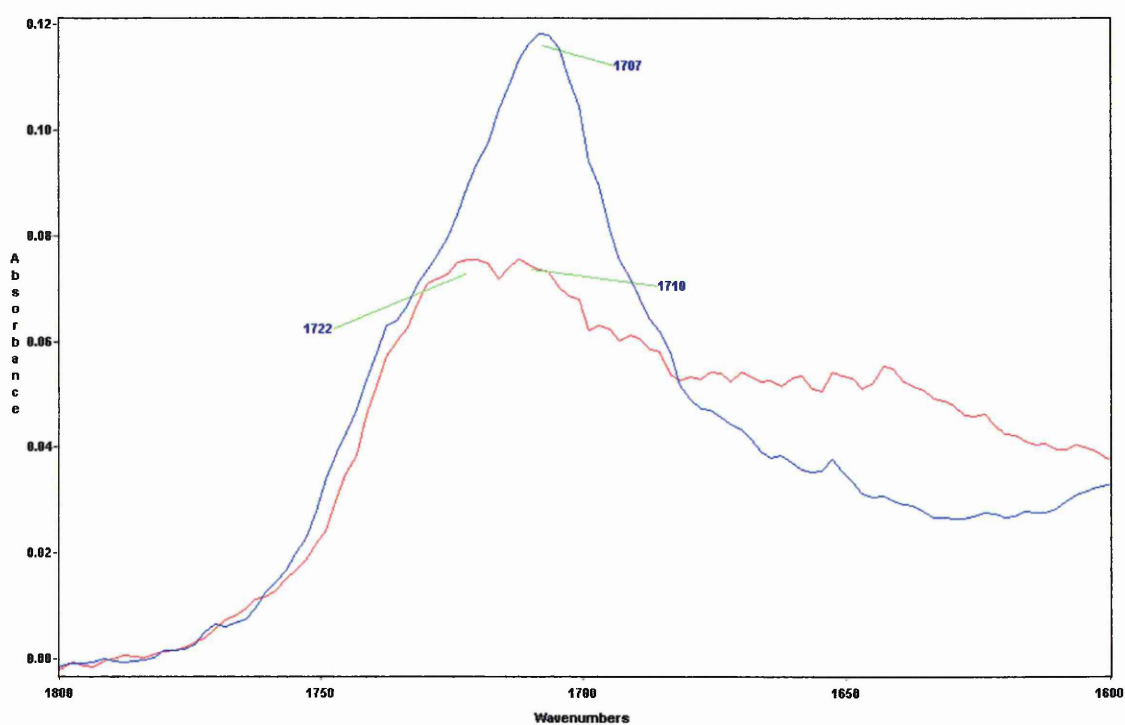
Figure 6-11: The ν(C=O) mode in the ATR spectrum of C3 (blue) and C3/AM (red) LB films.

Further confirmation that it is the hydrogen-bonded state which make the most important contribution to the pyroelectric effect comes from previous studies on a

116

modified straight chain system. Alternate layer 22-tricosenoic acid/4-octadecylaniline systems show more sideways dimers and also display an increased pyroelectric coefficient compared to an entirely aliphatic system.[6]

A more detailed picture of the relationship between the amount of proton transfer and pyroelectric coefficient can be obtained by applying curve fitting techniques to the measured spectra. This allows the intensity of a given band to be assessed. For the spectra shown above [Figure 6-8 and Figure 6-9], curve fitting was performed on the carbonyl stretching band. From this it is possible to ascertain quantitative information regarding the proportion of carboxylic acid moieties in the proton-transferred state. The integrated intensity of the band was calculated and normalised against the CH_3 antisymmetric stretching mode, in order that an accurate comparison may drawn between one spectrum and another. The percentage reduction in the overall C=O stretching mode was then obtained. The results are plotted in Figure 6-12 and show an interesting relationship between the pyroelectric coefficient and amount of proton transfer.

It can be seen that in the region where the proportion of proton-transferred carboxylic acid is greater than 70%, even a relatively large change in the proportion of hydrogen-bonded to proton-transferred species gives rise to only a slight change in the pyroelectric coefficient. This is seen in previous studies, in that the infrared spectra show a large shift towards a more hydrogen-bonded nature but with a relatively small increase in the pyroelectric coefficient.[2,3] Conversely, below 70% even a slight change in the hydrogen-bonded to proton-transferred ratio will result in a significant alteration in the pyroelectric coefficient.
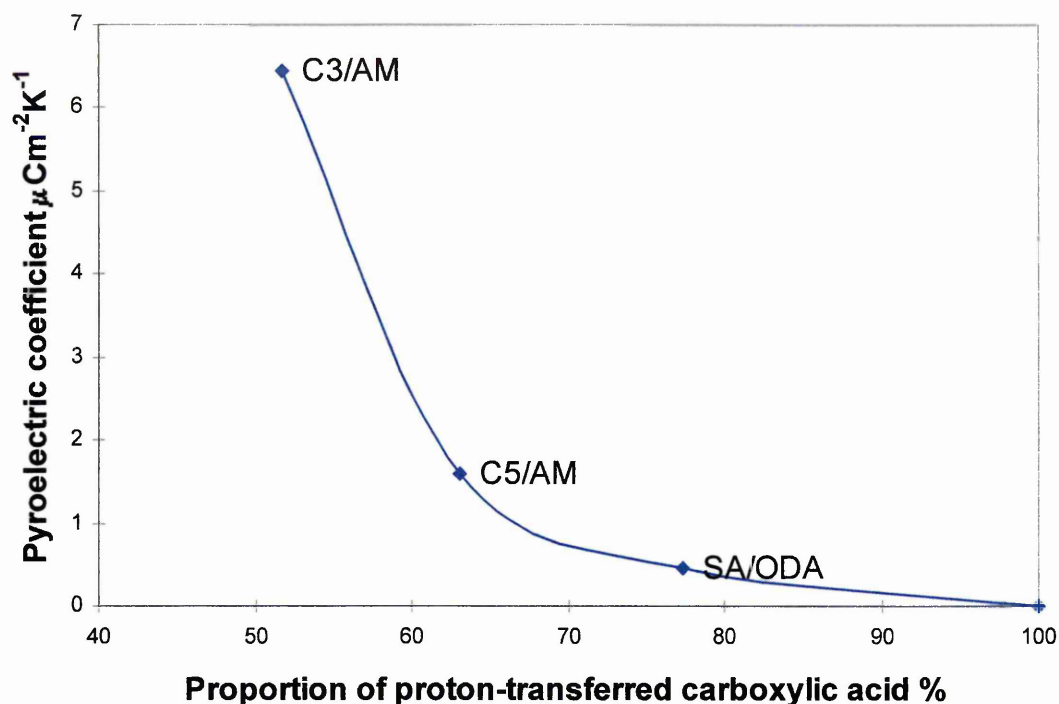
Figure 6-12 The relationship between the amount of proton transfer and

pyroelectric coefficient

It should be made clear that the curve fitting performed to obtain Figure 6-12 results in the measurement of the total amount of the hydrogen-bonded species. This comprises sideways as well as facing dimers. As has previously been shown [Figure 6-11 and Chapter 5] a higher proportion of the pairs which form facing dimers undergo proton transfer. Therefore it is to be expected that a more accurate picture would be obtained by separating these two components. Unfortunately, this has not been possible with the data obtained so far. To do so would require spectra of much better resolution in order to perform the curve fitting with the necessary degree of precision. However, if both sideways and facing dimers in the alternate layer systems contribute to the pyroelectric effect by approximately the same amount, then the results will be much the same as those presented here.

6.4 Summary

No change with temperature is observed in the infrared spectra of these calixarene assemblies. This is a surprising result especially as a significant change occurs over a temperature variation of 1°C in the form of a large pyroelectric current. There are two possible conclusions to draw from this observation; that no change occurs or that the change is not detectable in the infrared. Since there are clearly temperature-dependent changes in these systems, it seems likely that infrared spectroscopy is not sensitive to these minute changes. It should also be noted that the infrared spectra were taken at fixed temperatures. This is potentially very important as the pyroelectric coefficient is effectively zero at any fixed temperature, whether high or low. Infrared is, however, sensitive to the orientation of alkyl chains and can detect their melting or other deformations, in ordered films, so this is not occurring. This is therefore a testament to the thermal stability of these materials in LB film form.

The absence of any great variation in the infrared spectra also provides a valuable insight into the pyroelectric mechanism. It is now clear that proton transfer in acid/amine LB systems makes little or no contribution to the pyroelectric effect. In fact, it a change in the distance between acid and amine groups which causes the change in polarisation responsible for pyroelectric current generation. Indeed, it would seem that the strong dipole formed between proton-transferred species in effect, locks them together. Thus, only the acid and amine pairs which have not undergone proton transfer can move further apart (or closer together) as the temperature changes and are responsible for the pyroelectric activity in these systems. This emphasises the point that

119

it is not the magnitude of the polarisation in a film which is of importance in pyroelectric devices but the dependence of any polarisation on temperature.

A final conclusion which can be drawn from these results is that it should be possible to assess the magnitude of the pyroelectric coefficient of an acid/amine system directly from the infrared spectrum of such a system. In order to achieve this, more work needs to be done on these types of system before this technique of pyroelectric coefficient measurement can be applied. Additionally, the dependence of the pyroelectric coefficient itself on temperature can potentially be measured in the same way.

6.5 References

[1] S. Lifson, A. T. Hagler, P. Dauber, Consistent Force Field Studies of Intermolecular Forces in Hydrogen-Bonded Crystals. 1. Carboxylic Acids, Amides, and the C=O•••H- Hydrogen Bonds, Journal of the American Chemical Society, 1979, 101(18), 5111-5121.

[2] R. Colbrook, D.Phil. Thesis, Pyroelectric Langmuir-Blodgett Films, University of Oxford, 1990.

[3] G. H. Davies, J. Yarwood, M. C. Petty, C. A. Jones, Fourier transform IR studies of alternate layer acid-amine Langmuir-Blodgett films with pyroelectric properties, Thin solid films, 1988, 159, 461-467.

[4] R. Çapan, S. V. Batty, T. Richardson, D. Lacey, S. J. Holder, W. H. Abd. Majid, Optimisation of the pyroelectric figure of merit of polysiloxane/amine superlattices, Thin Solid Films, 1996, 284-285, 915-918.

[5] R. Çapan, T. Richardson, D. Lacey, Cd^{2+} and Mn^{2+} incorporation in copolysiloxane/eicosylamine alternate layer LB films: influence on pyroelectric activity, Thin Solid Films, 1998, 327-329, 369-372.

[6] C. A. Jones, M. C. Petty, G. G. Roberts, G. Davies, J. Yarwood, N. M. Ratcliffe, J. W. Barton, IR studies of pyroelectric Langmuir-Blodgett films, Thin Solid Films, 1987, 155, 187-195.

7. Summary and conclusions

7.1 Summary

The work presented in this thesis concerns research undertaken on pyroelectric calix[8]arene Langmuir-Blodgett (LB) deposited assemblies. The calixarenes were specially synthesised in order to be suitable for both LB deposition and pyroelectric current generation. The latter was achieved by the substitution of the hydroxyl groups, at the lower rim of the calix bowl, with pendant alkyl chains ending in either a carboxylic acid or an amine group. The attachment of these moieties also goes some way to enabling the materials to be deposited using the LB technique. However, the addition of t-butyl groups to the top rim of the calix bowl is also necessary.

Alternate layer LB deposited films of acid- and amine-substituted calixarenes have already been shown to have pyroelectric properties. Of the systems previously analysed, t-butyl substituted calix[8]arenes demonstrated the highest pyroelectric coefficients. Therefore, further investigation has been undertaken into the pyroelectric behaviour of a family of these particular calixarenes. Three different acid-substituted calix[8]arenes were available (C1, C3 and C5), each with different pendant chain lengths, along with one amine-substituted calix[8]arene (AM).

In the first instance, the physical properties of each material, in the form of a Langmuir layer, were investigated. The isotherms taken allowed the area per molecule of each material, as well their compressibility, to be measured. Subsequently, each acid-substituted calixarene was LB deposited in an alternate layer fashion with the amine-substituted calixarene, thus producing systems which exhibit pyroelectric activity. The

122

dependence of the pyroelectric coefficients of these LB films on temperature and number of deposited layers was investigated. This was done for all three of the alternate layer structures.

Fourier transform infrared spectroscopy was used to glean structural information about the pyroelectric assemblies. The techniques of attenuated total reflection (ATR) and reflection-absorption infrared spectroscopy (RAIRS) were used as these are particularly suited to the analysis of thin films samples. Initially, aliphatic systems containing carboxylic acid and amine moieties were examined, both as cast films and LB deposited assemblies. The calixarenes were then studied individually, at room temperature, starting with the materials in cast film form and then as LB films. This was followed by the analysis of the alternate layer systems. For comparison with the ordered samples, cast films of mixtures of the materials were studied as well. After the room temperature analysis, a specially constructed heating stage was designed and built to allow FTIR-ATR spectra to be obtained at various temperatures. This was used to investigate the effect of temperature on the infrared spectra of the pyroelectric systems *in situ*.

Finally, some theoretic calculations regarding the pyroelectric systems were carried out in order to better understand the observed pyroelectric and infrared results.

7.2 Conclusions

The conclusions derived from each part of the project are outlined individually below. This is followed by a discussion of the overall conclusions obtained from this work, drawing the separate aspects together.

7.2.1 Pyroelectric properties

The pyroelectric results obtained show that LB film systems made up of alternate layers of acid- and amine-substituted calix[8]arenes are good candidates for heat sensing applications. This is most clearly demonstrated by the high pyroelectric coefficients measured, particularly in the case of the C1/AM system. Such large coefficients can be obtained because of the extreme thinness of the LB deposited calixarene monolayers. The variation of the pyroelectric coefficient with the different chain lengths emphasises the need for a high density of such pairs per unit volume.

Further improvements with this particular set of materials could potentially be obtained by shortening the pendant chain on the amine substituted material. This can be expected to give rise to a pyroelectric coefficient of approximately $20\mu Cm^{-2}K^{-1}$, considering the improvement obtained by changing the acid material from C3 to C1. However, it should also be possible to make even more progress using related systems.

In addition, it is important to note the added benefit of these calixarenes; their remarkable thermal stability. This is seen, in the pyroelectric sense, by the invariance in their measured coefficients with temperature change. Such stability and linearity of response, in combination with the large pyroelectric coefficients demonstrated, show that calixarenes have the potential to form the basis of practical heat sensing devices.

The acid/amine pair density does not fully explain the large pyroelectric coefficients in these systems. The unique structural characteristics of the calixarenes clearly play a significant role. This was the subject of the infrared investigation.

124

7.2.2 FTIR analysis

The infrared study of the pyroelectric calix[8]arene LB systems was preceded by some background work. Firstly, an analysis at room temperature was conducted of straight chain systems containing the same acid and amine groups as the calixarenes. This, along with the spectra of the cast calixarene films, allowed the pertinent bands to be identified. From these it was clear that the bands arising from the proton-transferred acid and amine moieties in the alternate layer LB systems are particularly weak. Therefore, the main tool in observing the temperature dependent effects is the carboxylic acid absorption band near $1710cm^{-1}$.

Other conclusions drawn from the room temperature infrared study include the high degree of crystalline order in both the cast and LB films. This is especially true of the straight chain systems. Additionally, it is clear that the calixarene molecules are more likely to form sideways dimers than the straight chain systems. These are probably mainly intramolecular hydrogen bonds, arising from the bowl shape of the calixarenes. Finally, and most importantly, the room temperature spectroscopy revealed that the carboxylic acid groups forming sideways were significantly less likely to undergo proton transfer with the amine groups than those forming facing dimers.

The next step was the analysis of the calixarene systems at a variety of temperatures. The most unexpected result was the invariance of the infrared spectra in all the calixarene systems studied. This means that there was no change in proton transfer with temperature. It is also confirmation that the calixarene LB film structure possesses an extremely high thermal stability. Initially, this lack of change in the infrared spectra seemed contradictory to the pyroelectric results obtained for the same samples which clearly show that there must be some great changes occurring in the films to produce such a large pyroelectric effect. A model calculation performed provided the explanation

125

for the lack of observed change. It was found that the fluctuation in the polarisation (which gives rise to the pyroelectric activity) is most likely caused by a change in the intermolecular distances between monolayers in the film, rather than a change in the amount of proton transfer between the acid and amine groups. This change in distance between the acid and amine moieties is far too small to be detected by infrared spectroscopy. However, the FTIR measurements do explain the behaviour of the pyroelectric coefficients with temperature for the calixarene devices. Since the pyroelectric coefficient is more or less constant with temperature over the range studied, the infrared results imply that this is because using calixarenes as vehicles for the acid and amine groups results in an extremely stable structure. This structure is resistant to temperature variations which result in irreparable damage to other (straight chain) systems.

7.2.3 Overall conclusions

The pyroelectric properties of these calix[8]arenes clearly show their great potential for use in pyroelectric detectors. The infrared results are a testament to the great thermal stability of the devices but there is also another very interesting link between the infrared and pyroelectric measurements. The calculations regarding the change in dipole required to obtain the measured pyroelectric coefficients showed that the source is most likely a variation in the distance between the acid and amine groups. However, they do not identify whether or not there is a difference between the contributions arising from the moieties in the hydrogen-bonded or the proton-transferred state. This can be determined by comparing the infrared spectra with the pyroelectric data. By using curve fitting techniques (and with films of the acid-substituted material as a reference), the

126

amount of hydrogen-bonded species in the pyroelectric samples can be calculated. The results show that the greater the amount of hydrogen-bonded species in a sample, the larger the pyroelectric effect. Previously, it was thought that the proton-transferred groups played the main role in pyroelectric activity with other effects making only minor contributions. However, it is now clear that in fact the proton-transferred moieties make only a secondary contribution, if any. One possible explanation is that the proton-transferred moieties become 'locked' together, thus inhibiting any further change in the dipole.

The relationship between the amount of hydrogen-bonded species and the pyroelectric coefficient reveals the reasons behind the superior pyroelectric properties of calixarenes. From the infrared spectra of the LB films of each individual material, it can be seen that the carboxylic acid groups in the calixarenes have a greater tendency to form sideways dimers as compared to those in stearic acid. This is most probably due to the form of the calixarene molecule. Further, the spectra of the alternate layer systems show that the sideways dimers are less likely to undergo proton transfer. Therefore, given that it is the hydrogen-bonded species which are the source of pyroelectric activity, calixarenes will automatically demonstrate high pyroelectric coefficients because of their shape. Additionally, calixarenes are extremely thin and this benefits their pyroelectric behaviour even more, as a high density of acid/amine pairs results in the alternate layer system.

It is interesting to note that while the change from the hydrogen-bonded to proton-transferred states involves a huge change in dipole, in systems where this change occurs with temperature (i.e. straight chain) it is not accompanied by an equivalently large pyroelectric current. Therefore, this change must occur in a different way to the changes which cause the pyroelectric effect in these films.

127

7.3 Future research

There is clearly much more which needs to be done on the subject of calixarene-based LB pyroelectric sensors. Firstly, obtaining a clearer picture of the relationship between the hydrogen-bonded nature of the films and their resultant pyroelectric activity would be immensely useful in producing marketable devices. In order to do this, further analysis must be done on the infrared spectra of the alternate layer systems. The separation of the hydrogen-bonded components, by curve fitting on higher resolution spectra, will reveal how much of a contribution each dimer (sideways or facing) makes to the pyroelectric coefficient. This can be backed up by computer modelling of the dipoles expected from each. Additionally, a fuller study of a similar system, such as straight chain or polysiloxanes, will show whether or not the relationship between the hydrogen-bonded nature and the pyroelectric coefficient of a sample is the same for all systems or if each type of vehicle for the acid and amine moieties modulates the dependence.

Once this has been done, it should then be possible to work on devices with even higher pyroelectric coefficients. This could be achieved by applying knowledge gained thus far to the synthesis of different substituted calixarenes. From the work done so far it seems that the ideal acid material would be one which had the maximum amount of sideways dimerisation of the carboxyl groups. This should then be coupled with an amine material in which the amine group was stabilised by some nearby electron withdrawing structure. These two conditions should result in a maximum amount of acid/amine pairs being in a hydrogen-bonded state. It should be noted that for the amine, care needs to be taken that the material can still be deposited by the LB technique. Additionally, the ideal materials

would deposit as very thin LB layers, thus ensuring a high density of acid/amine pairs per unit volume.

Finally, the mechanism for the change in dipole moment of the hydrogen-bonded groups is as yet unknown. Further work could be done to elucidate the origins of such change. Indeed infrared study at a higher resolution may cast some light on the subject. However, other methods should also be applied. Using different techniques in combination with FTIR would show if the pyroelectric effect arises from large scale changes between the layers, such as the whole films expanding, or smaller molecular changes, like individual molecular tilting.

Some preliminary atomic force microscopy (AFM) measurements were made on the calixarene films studied in this project [Figure 7-1].

The striations due to the dipping direction can clearly be seen as can the domain nature of the LB film. However, due to time restraints it was not possible to pursue the AFM analysis further. It would be very useful to obtain *in situ* AFM images of the pyroelectric films. These would show any changes in the surface roughness associated with temperature change and this may reveal more detail about the type of movement occurring within the films.
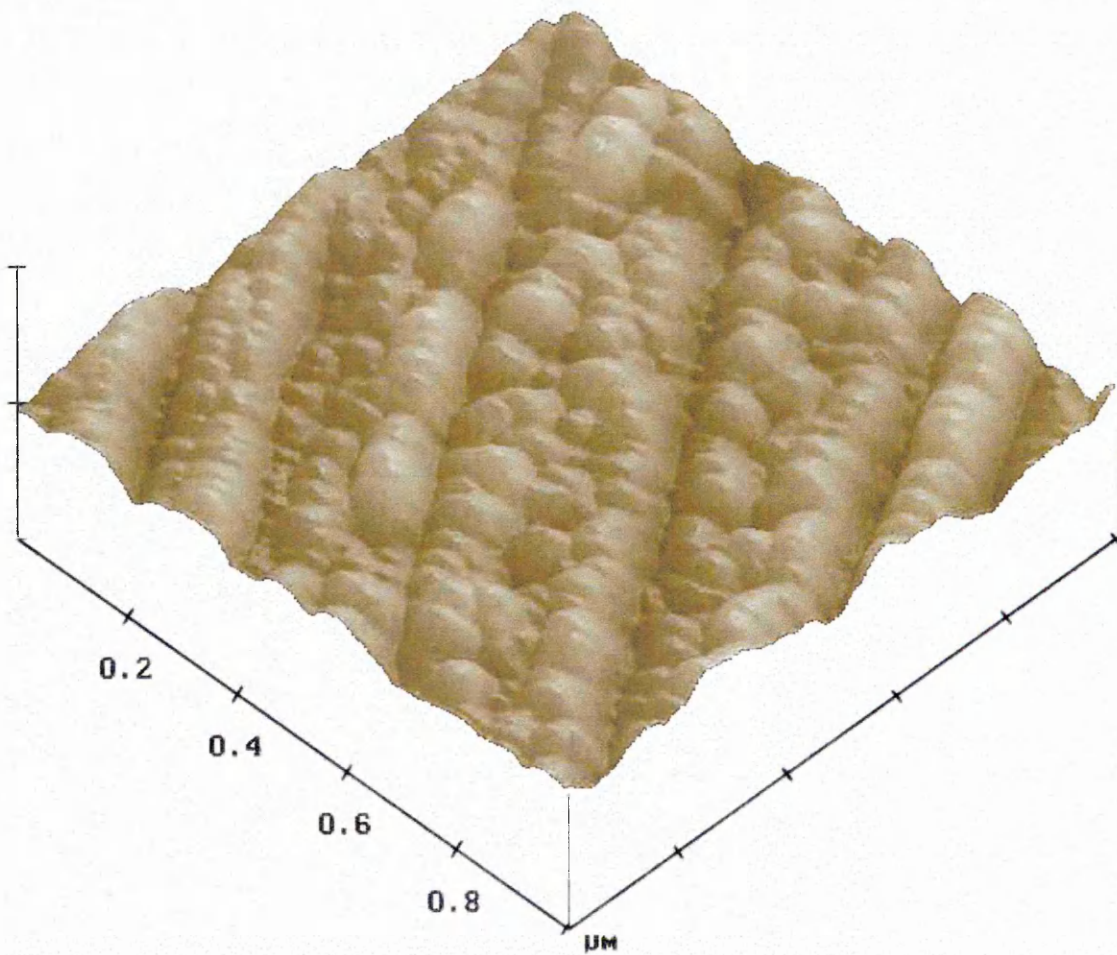
Figure 7-1: AFM image of 3 C3 LB layers on aluminium.

Further information could be obtained from conducting an x-ray analysis of the films. X-ray scattering would provide a further insight into the behaviour of these films as it is capable of detecting changes in the thickness of films as well as variation in the molecular spacing.

7.4 Final comment

The work presented in this thesis represents a significant step forward in furthering the understanding of calix[8]arene pyroelectric LB films. The most important result is that the source of the pyroelectric effect, in these films has been found to be an interaction between acid and amine pairs which have not undergone proton transfer. However, there is still a lot more work to be done in order to fully comprehend this mechanism. There are also many avenues to explore in terms of applying the knowledge gained to produce a functional pyroelectric device based on organic LB films. It is hoped that this thesis may provide a foundation on which to build the future generation of pyroelectric sensors.